



This is a repository copy of *Wave analysis tools*.

White Rose Research Online URL for this paper:

<https://eprints.whiterose.ac.uk/225694/>

Version: Accepted Version

---

**Article:**

Jafarzadeh, S. [orcid.org/0000-0002-7711-5397](https://orcid.org/0000-0002-7711-5397), Jess, D.B. [orcid.org/0000-0002-9155-8039](https://orcid.org/0000-0002-9155-8039), Stangalini, M. [orcid.org/0000-0002-5365-7546](https://orcid.org/0000-0002-5365-7546) et al. (23 more authors) (2025) *Wave analysis tools*. *Nature Reviews Methods Primers*, 5 (1). 21. ISSN 2662-8449

<https://doi.org/10.1038/s43586-025-00392-0>

---

© 2025 The Authors. Except as otherwise noted, this author-accepted version of a journal article published in *Nature Reviews Methods Primers* is made available via the University of Sheffield Research Publications and Copyright Policy under the terms of the Creative Commons Attribution 4.0 International License (CC-BY 4.0), which permits unrestricted use, distribution and reproduction in any medium, provided the original work is properly cited. To view a copy of this licence, visit <http://creativecommons.org/licenses/by/4.0/>

**Reuse**

This article is distributed under the terms of the Creative Commons Attribution (CC BY) licence. This licence allows you to distribute, remix, tweak, and build upon the work, even commercially, as long as you credit the authors for the original work. More information and the full terms of the licence here:

<https://creativecommons.org/licenses/>

**Takedown**

If you consider content in White Rose Research Online to be in breach of UK law, please notify us by emailing [eprints@whiterose.ac.uk](mailto:eprints@whiterose.ac.uk) including the URL of the record and the reason for the withdrawal request.



[eprints@whiterose.ac.uk](mailto:eprints@whiterose.ac.uk)  
<https://eprints.whiterose.ac.uk/>

# Wave analysis tools

Shahin Jafarzadeh<sup>1,2,\*</sup>, David B. Jess<sup>2,3</sup>, Marco Stangalini<sup>4</sup>, Samuel D. T. Grant<sup>2</sup>, Jonathan E. Higham<sup>5</sup>, Martin E. Pessah<sup>6</sup>, Peter H. Keys<sup>2</sup>, Sergey Belov<sup>7</sup>, Daniele Calchetti<sup>1</sup>, Timothy J. Duckenfield<sup>2</sup>, Viktor Fedun<sup>8</sup>, Bernhard Fleck<sup>9</sup>, Ricardo Gafeira<sup>10,11</sup>, Stuart M. Jefferies<sup>12,13</sup>, Elena Khomenko<sup>14,15</sup>, Richard J. Morton<sup>16</sup>, Aimee A. Norton<sup>17</sup>, S. P. Rajaguru<sup>18</sup>, Luiz A. C. A. Schiavo<sup>16</sup>, Rahul Sharma<sup>16</sup>, Suzana S. A. Silva<sup>8</sup>, Sami K. Solanki<sup>1</sup>, Oskar Steiner<sup>19,20</sup>, Gary Verth<sup>21</sup>, Gangadharan Vigeesh<sup>19</sup>, and Nitin Yadav<sup>22</sup>

<sup>1</sup>Max Planck Institute for Solar System Research, Göttingen, Germany

<sup>2</sup>Astrophysics Research Centre, Queen's University Belfast, UK

<sup>3</sup>Department of Physics and Astronomy, California State University Northridge, USA

<sup>4</sup>Italian Space Agency (ASI), Rome, Italy

<sup>5</sup>School of Environmental Sciences, Department of Geography and Planning, University of Liverpool, UK

<sup>6</sup>Niels Bohr International Academy, Niels Bohr Institute, Denmark

<sup>7</sup>Centre for Fusion, Space and Astrophysics University of Warwick, UK

<sup>8</sup>Plasma Dynamics Group, Department of Automatic Control and Systems Eng., The University of Sheffield, UK

<sup>9</sup>ESA Directorate of Science, Operations Department, Greenbelt, USA

<sup>10</sup>Geophysical and Astronomical Observatory, Faculty of Science and Technology, University of Coimbra, Portugal

<sup>11</sup>Instituto de Astrofísica e Ciências do Espaço, Department of Physics, University of Coimbra, Portugal

<sup>12</sup>Department of Physics and Astronomy, Georgia State University, USA

<sup>13</sup>Institute for Astronomy, University of Hawaii, USA

<sup>14</sup>Instituto de Astrofísica de Canarias, La Laguna, Spain

<sup>15</sup>Departamento de Astrofísica de la Universidad de La Laguna, Tenerife, Spain

<sup>16</sup>Department of Mathematics, Physics and Electrical Engineering, Northumbria University, UK

<sup>17</sup>Stanford University, Hansen Experimental Physics Laboratory, Stanford, USA

<sup>18</sup>Indian Institute of Astrophysics, Bangalore, India

<sup>19</sup>Institute for Solar Physics (KIS), Freiburg, Germany

<sup>20</sup>Istituto ricerche solari Aldo e Cele Daccò (IRSOL), Locarno, Switzerland

<sup>21</sup>Plasma Dynamics Group, School of Mathematics and Statistics, The University of Sheffield, UK

<sup>22</sup>Department of Physics, Indian Institute of Science Education and Research Thiruvananthapuram, India

\*e-mail: shahin.jafarzadeh@mps.mpg.de

## ABSTRACT

This Primer provides an overview of a comprehensive set of analysis methods for studying waves, vibrations, and related oscillatory phenomena – including instabilities, turbulence, and shocks – across diverse scientific fields. From astrophysical domains to complex systems in terrestrial environments, such phenomena are ubiquitous. Understanding their nature requires careful selection of techniques, as the misapplication of analysis tools can introduce misleading results. We first review the fundamental principles of various wave analysis methods, along with adaptations to address complexities like non-linear, non-stationary, and transient signal behaviour. To offer unique insights and guide informed choices, we apply these techniques to identical synthetic datasets, providing a quantitative comparison of their strengths and limitations. These experiments facilitate the selection of the most appropriate analysis tools based on specific data characteristics and scientific goals, promoting reliable interpretations and ensuring reproducibility. This Primer highlights best ethical practices for data deposition and the importance of open-code sharing. Finally, we explore the broad applications of these techniques in various research fields, address current challenges in wave analysis, offer an outlook on future directions, and emphasise the potential for transformative discoveries through the optimisation and development of cutting-edge analysis methods.

# 1 Introduction

The study of waves and oscillations is essential for understanding the dynamic universe, from the smallest scales to the most immense<sup>1-3</sup>. Such examples include a simple harmonic wave-form generated in a laboratory plasma<sup>4</sup>, sound waves<sup>5</sup>, oscillations of a guitar string<sup>6</sup>, ocean waves<sup>7</sup>, cosmic gravitational waves in the galactic medium<sup>8</sup>, and those excited by a multitude of restoring forces (e.g., pressure, gravity, and magnetic fields) propagating through complex plasma environments (such as magnetohydrodynamic waves observed in the extreme conditions of the Sun's atmosphere)<sup>9-11</sup>, to name but a few. Oscillatory phenomena go beyond periodic waves. They encompass shocks, instabilities, turbulence, and more. These events shape environments across the cosmos, from the churning plasma of stars to the vast interstellar medium, exhibiting a wide array of behaviours. Figure 1 outlines the typical steps involved in wave analyses, beginning with data collection and culminating in scientific interpretation.

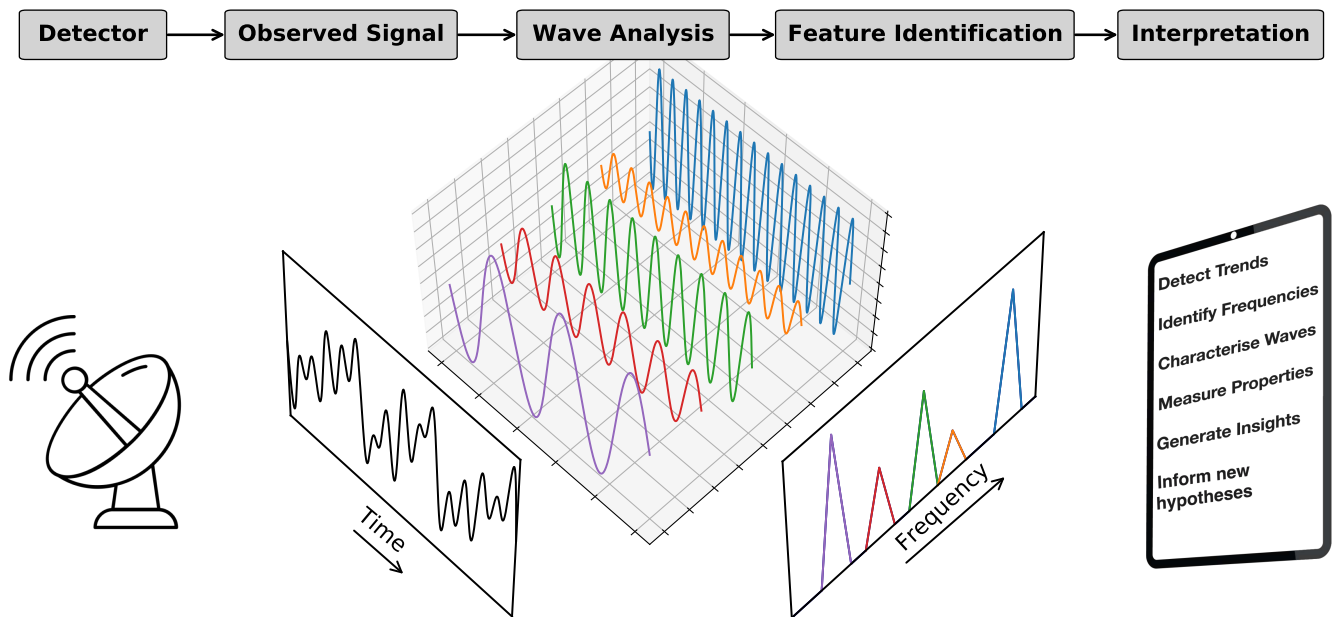


Fig. 1 | **Unveiling wave phenomena: a visual guide to wave analysis.** This schematic diagram illustrates the key steps in wave analysis, showcasing the journey from raw data to scientific insight. A detector captures a wave signal, transforming it into an observable time series. This signal is then decomposed through wave analysis techniques (e.g., Fourier transform) to reveal its constituent frequency components and identify various features, as represented by a 3D cube. The power spectrum displays the relative power of each component as distinct peaks. Ultimately, this analysis, which relies on careful method selection tailored to the data and research goals, enables us to detect trends, identify frequencies, characterise waves, measure properties, generate comprehensive scientific insights, and give rise to new hypotheses.

The research topic of *seismology*<sup>12,13</sup> is founded in the scientific study of the generation and propagation of elastic waves through the Earth, with an emphasis on determining their crucial role in identifying earthquake sources<sup>14</sup> and linking these to the subsequent atmospheric response<sup>15</sup>. Hence, in this field, seismology enables the type of elastic wave mode to be identified (e.g., body and surface modes of oscillation that propagate through the interior and along the surface, respectively, of the Earth) through a quantitative understanding of the embedded wave amplitudes<sup>16</sup>, phase lags<sup>17</sup>, and propagation speeds<sup>18</sup>. Other research fields have adopted the term 'seismology' as a way of highlighting the use of wave and/or oscillatory phenomena to uncover information about the background environment that would otherwise be impossible to measure directly. Such examples include magneto-seismology<sup>19-22</sup>, where waves linked to astrophysical oscillations enable indirect diagnostics of plasma parameters to be inferred, and fibre-optic seismology<sup>23,24</sup>, where phase changes in optical light enable fine-scale studies of challenging areas to be made over multi-km distances. Therefore, analysing oscillatory processes not only reveals their underlying properties (such as the amount of energy they carry) but also provides important information about the medium in

which they propagate<sup>25</sup>.

Propagating waves, of various kinds, can also interact with each other, and may change their nature or characteristics while travelling through different media<sup>26,27</sup>. As such, the applications of traditional analysis techniques, like the Fourier transform<sup>28</sup>, are not always alone capable of uncovering all information contained, particularly in complex systems where superposition of several wave modes may coexist within the same structure<sup>29,30</sup>. In addition to such complexities and non-harmonic behaviour, oscillations observed in the real world often pose limitations for which most theoretical analysis methods, designed for simpler scenarios, are not directly applicable. Examples of such imperfections are large noise levels, finite (sometimes too small) durations of oscillatory signals, low temporal and/or spatial resolutions, embedded non-linear and non-stationary trends, transient oscillations, weak signals, quasi-periodic signatures, or missing data points resulting in the recorded time series being unevenly sampled<sup>31–34</sup>. In order to overcome such challenges, extensive developments have taken place in advancing the wave analysis techniques over the past two decades<sup>35–41</sup>. These advances include techniques specifically designed to handle noisy data, non-linear patterns, complicated wave interactions, and the types of shocks, instabilities, and turbulence found in various environments<sup>42</sup>. However, the huge range of available methods and codes, often designed for specific purposes (e.g., linked to specifics of the datasets employed and/or science cases), can sometimes be inappropriately applied within the science communities<sup>43</sup>. This also includes coding issues in some of the well-used and publicly available packages<sup>44</sup>. As a result, some of the scientific studies are difficult or impossible to reproduce<sup>45,46</sup>.

The sheer variety of wave analysis tools underscores the importance of careful technique selection. The best method for a given task depends on the nature of the oscillatory signal, the characteristics of the environment, and the specific scientific question being asked<sup>47</sup>. For example, analysing the complex three-dimensional wave interactions within a turbulent plasma requires different approaches than identifying a faint, periodic signal in noisy one-dimensional time series. Alternatively, using a tool designed for simple harmonic waves on a dataset containing shocks or instabilities can lead to misleading or incorrect conclusions. Hence, choosing the right technique is crucial not only for accuracy, but also for the physical interpretation of results<sup>48–50</sup>. This Primer aims to guide researchers in selecting appropriate analysis methods from among those commonly used, empowering them to gain reliable insights into the complex world of waves and oscillations. To address these issues, a number of mainstream wave analysis tools are detailed and summarised in this Primer, where their applications to identical synthetic datasets are also demonstrated and compared. Importantly, the computer codes we employ are extensively tested and cross-checked between different packages and programming languages to ensure consistency for future users.

This Primer offers, in *Experimentation* (Section 2), a holistic perspective of the wave analysis field by reviewing a wide range of key methods in analysing oscillatory signals (of different nature and properties) as well as highlighting a number of advanced techniques that support identification of, and disentangling, various wave types/modes. Specific outcomes for these advanced analysis approaches, applied on examples of synthetic datasets with known parameters, as well as their interpretations and comparisons are provided in *Results* (Section 3). The advances in the wave analysis tools reviewed here provide a wide range of science communities and research areas with a diverse set of methods to tackle various challenges in different oscillatory environments (see *Applications*; Section 4). To facilitate *Reproducibility* and set field standards in *Data Deposition* (Section 5), we further describe an ever-expanding publicly-available and open-source repository – WaLSAtools – that we introduce in this Primer. Furthermore, in *Limitations and Optimisations* (Section 6), we discuss the importance of selecting the right tools for various scientific cases and how different choices can impact results. Finally, we address, in *Outlook* (Section 7), some of the future directions in improving the methods making them suitable for outstanding challenges in wave studies across a wide range of research areas.

## 2 Experimentation

This section introduces essential techniques for analysing oscillatory signals across various scientific disciplines, which builds upon previous historical publications that documented pioneering digital signal processing techniques<sup>51–63</sup>. The analysis tools are divided into two categories: (a) those focusing on the characteristics of oscillations within single time series (Sections 2.2 and 2.3), and (b) those examining correlations between oscillations in two

(or more) distinct time series (Section 2.4). We cover methods applicable to one-dimensional (1D) time series, for example representing fluctuations in a measured quantity as a function of time, and three-dimensional (3D) spatio-temporal datacubes, which capture the evolution of oscillations across both space and time. A research methodology flowchart linked to the analysis of wave activity in a variety of data sequences is schematically outlined in Supplementary Figure S1.

It is worth noting that time series analysis often benefits from additional complementary approaches<sup>64</sup>. Whether empirical, analytical, or statistical, these techniques, designed for tasks such as noise reduction, pattern identification, or trend analysis, help uncover important information within complex signals, potentially affected by noise<sup>65</sup>. For instance, scaling properties of fluctuations or irregularities within a signal or turbulence can be characterised by Structure Function Analysis<sup>66–68</sup>, a method that examines how differences in signal values change with increasing time lags. Furthermore, all real-world oscillatory signals must be pre-processed before applying wave analysis techniques (see Box 1).

### Box 1 | Preprocessing of oscillatory signals

Real-world signals often exhibit characteristics that require preprocessing to mitigate unwanted effects prior to the application of spectral analysis.

- **Detrending:** removing long-term trends to isolate the oscillatory component<sup>69</sup>. Common techniques include subtracting a fitted polynomial, applying a high-pass filter, or calculating a moving average and subtracting it from the signal<sup>70,71</sup>. The choice of detrending method depends on the nature of the underlying trend<sup>72</sup>. Incorrect detrending can affect the results<sup>73</sup>.
- **Apodization:** Finite-length time series introduces an abrupt start and end, resulting in artificial frequencies, whose effects can be mitigated by apodization, i.e., apply a windowing function that smoothly tapers the signal to zero at its edges<sup>64</sup>. Common choices include the Hann (Hanning)<sup>74</sup>, Hamming<sup>75</sup>, and Tukey<sup>76</sup> windows. While apodization reduces spectral leakage, it also slightly broadens frequency peaks, decreasing resolution<sup>77</sup>. Hence, the choice of the windowing function involves a trade-off between spectral leakage reduction and frequency resolution.

Additional preprocessing:

- **Zero padding:** adding zeros to the beginning and end of a signal to increase its length, sometimes done to improve the visual clarity of spectral peaks in certain analysis techniques<sup>78</sup>. Zero padding interpolates between the existing frequency points in a spectral analysis. This makes the spectrum look smoother and can make peaks appear sharper, although without improving the true frequency resolution<sup>79,80</sup>.
- **Interpolation:** replacing an irregularly sampled time series with regularly sampled one, if the method is designed for evenly sampled data<sup>81–83</sup>.
- **Normalisation:** ensuring datasets have comparable amplitudes for cross-correlation studies<sup>84</sup>. Alternatively, coherence examination methods (see Section 2.4.2) are able to identify correlations with incomparable amplitudes.
- **Filtering:** isolating specific frequency intervals before analysis<sup>85</sup>, which may involve the use of, e.g., low-pass, high-pass and/or band-pass filters. This step is primarily tied to the science case of interest, where a priori knowledge may enable the investigative team to pre-select frequency windows of interest using a combination of optical hardware and/or computational software<sup>86–90</sup>.

## 2.1 Worked examples

To rigorously test and compare wave analysis techniques, we employ synthetic datasets containing a variety of oscillatory signals with known parameters. These datasets, shown in Figure 2, provide a controlled environment where we can assess how well each method identifies different oscillations (or wave modes), handles non-linearities, and responds to varying noise levels. By comparing analysis results against this ‘ground truth’, we gain clear insights into the strengths, limitations, and appropriate use cases for each method. This is essential for the reliable

interpretation of complex oscillations in real-world scientific data. The results of the analyses and comparisons are presented in Section 3.

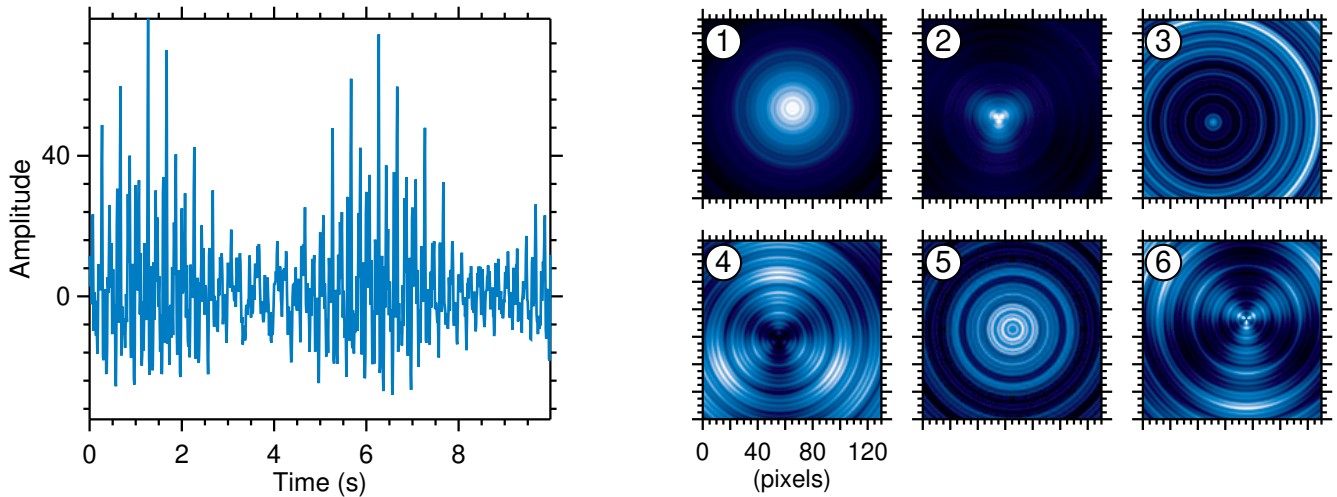


Fig. 2 | **Synthetic datasets.** Left: synthetic 1D time series with various oscillatory components (see main text for details). Right: First six frames of the synthetic spatio-temporal datacube illustrating the temporal evolution of the concentric wave patterns. A movie of the time series is shown in [Supplementary Video 1](#).

### 2.1.1 Synthetic 1D time series

This dataset is constructed by combining five sinusoidal waves with distinct frequencies (5, 12, 15, 18, and 25 Hz) and amplitudes (1.0, 0.5, 0.8, 0.3, and 0.2), respectively (see Supplementary Table S1). To introduce realistic variability, we modulate the amplitudes of these individual waves with an envelope function. We then superimpose features common in real-world data: a short-lived transient oscillation (for a duration of 2 sec), a weak high-frequency signal (33 Hz; 0.1 amplitude), and a quasi-periodic signature with a slightly varying frequency (modulation frequency of 0.2 Hz). Non-linearity is introduced through a mathematical transformation that distorts the waveform (with a non-linear factor equal to 0.1). Finally, we add random noise (with an amplitude of 0.2, corresponding to 20% of the strongest oscillatory amplitude, while being twice the amplitude of the weak high-frequency signal) to simulate measurement imperfections. The sampling rate is 100 Hz, and the signal duration is 10 sec.

In addition to this synthetic time series, and to test cross-correlation methods, we generate another nearly identical signal, but with adjusted phases for the main wave, quasi-periodic signature, and weak signal components. This simulates observing the signal at a later time or different location. The specific phase shifts, listed in Supplementary Table S1, represent propagating waves in both directions.

### 2.1.2 Synthetic spatio-temporal datacube

This datacube comprises 200 frames, each with a resolution of  $130 \times 130$  pixels<sup>2</sup>, representing a time span of 99.5 sec with a cadence of 0.5 sec between frames. The core structure consists of 50 concentric circular regions, each containing ten sinusoidal waves with distinct frequencies, amplitudes, and phases, dynamically selected based on the region's index (see Supplementary Table S2). We further enhance complexity by superimposing a transient cubic polynomial signal (coefficients [0.01, -0.02, 0.03]), a simulated transverse motion with varying amplitudes in  $x$  and  $y$  directions, a fluting-like instability (wavenumber 3), a quasi-periodic signal, and added noise.

## 2.2 Methods for wave studies of single 1D time series

This section presents a range of techniques for spectral analysis within single 1D time series. While all these methods aim to reveal the underlying frequency content of a signal, they employ diverse strategies for decomposition. This diversity is crucial, providing the flexibility to address different data characteristics and scientific questions. Careful consideration of these factors guides the selection of the most appropriate technique for a given investigation.

### 2.2.1 Fast Fourier Transform

The Fast Fourier Transform<sup>91–95</sup> (FFT) is a cornerstone of spectral analysis. As a computationally efficient implementation of the Discrete Fourier Transform (DFT)<sup>96,97</sup>, it decomposes a signal into a superposition of sinusoidal and/or cosinusoidal functions with distinct frequencies, amplitudes, and phases. The core equation underlying FFT calculations is the Discrete Fourier Transform:

$$X(f) = \sum_{n=0}^{N-1} x(n)e^{-i2\pi fn/N},$$

where  $x(n)$  is the discrete input signal (time series),  $X(f)$  is the complex-valued Fourier spectrum,  $N$  is the number of samples in the signal, and  $f$  represents the frequency index. FFT reveals the frequency content of the signal, where each value  $X(f)$  represents the amplitude and phase of the corresponding frequency component. The squared magnitude of  $X(f)$  yields the power spectrum, which, when normalised by the frequency resolution, is known as the power spectral density (PSD; see Box 2 for further details).

FFT excels in analysing evenly sampled, infinite, and stationary signals, and its clear interpretation makes it a frequent starting point for investigations. However, prerequisites like an even sampling, infinite duration, and stationarity should be considered before application.

#### Box 2 | Power spectra and power spectral density

Wave analysis methods often begin by computing the complex-valued frequency representation of a signal, denoted as  $X(f)$ , where  $f$  represents frequency. This representation encompasses both the amplitude and phase information of the signal at each frequency.

The power spectrum provides a broad overview of how power is distributed across frequencies within a signal. It is obtained by squaring the magnitude of the complex frequency representation,  $|X(f)|^2$ , which represents the power at each frequency  $f$ . The magnitude  $|X(f)|$  corresponds to the amplitude of the signal at that frequency. The power spectral density (PSD) refines this concept by normalising the power spectrum by the frequency resolution of the analysis,  $\Delta f$ , typically defined as the inverse of the signal duration. The PSD is calculated as:

$$\text{PSD} = \frac{|X(f)|^2}{\Delta f},$$

However, in wavelet analysis (Section 2.2.3), the frequency resolution varies across frequencies, depending on the scale of the wavelet. Hence, to facilitate comparisons across different frequencies and with other techniques like FFT, the wavelet power spectrum may be interpolated onto a uniform frequency array using methods such as cubic spline interpolation, before calculating the PSD.

Normalising by frequency resolution ensures that PSDs from signals with different sampling rates or durations can be directly compared, facilitating meaningful assessments of power distribution. The PSD often has a direct physical interpretation related to the energy or variance of the signal at different frequencies. For real-valued signals, PSDs are typically presented in a single-sided format, folding power from negative frequencies into the positive domain.

### 2.2.2 Lomb-Scargle technique

Lomb–Scargle<sup>98,99</sup> is a statistical approach for irregularly sampled time series, a common occurrence in many scientific fields. At its core, the Lomb-Scargle method involves fitting sinusoids of different frequencies to the irregularly sampled data and determining the power associated with each tested frequency. The fitting process employs a least-squares approach to find the best-fit parameters for each frequency. The normalised Lomb-Scargle periodogram, often used to represent the spectral power, is given by:

$$P_N(\omega) = \frac{1}{2\sigma^2} \left\{ \frac{[\sum_j (x_j - \bar{x}) \cos \omega(t_j - \tau)]^2}{\sum_j \cos^2 \omega(t_j - \tau)} + \frac{[\sum_j (x_j - \bar{x}) \sin \omega(t_j - \tau)]^2}{\sum_j \sin^2 \omega(t_j - \tau)} \right\},$$

where  $x_j$  is the data value at time  $t_j$ ,  $\bar{x}$  and  $\sigma^2$  are, respectively, the mean and variance of the data,  $\omega$  is the angular frequency being tested,  $\tau$  is an offset that makes the periodogram independent of shifting the time origin. The Lomb-Scargle method effectively handles gaps and missing data points, making it the preferred choice when the data points are unequally spaced<sup>100–102</sup>. It can be generalised<sup>103</sup> and extended to incorporate high-order Fourier models, non-stationary signals, and a Bayesian approach<sup>104–106</sup>. However, it can be computationally expensive for large datasets, and alternative implementations or optimisations might be necessary. While interpolation techniques can be used to fill gaps for other methods like FFT, choosing the right interpolation method is not always straightforward and likely introduces artefacts<sup>107</sup>.

### 2.2.3 Wavelet analysis

Wavelet analysis<sup>108–112</sup> localises spectral power in both time and frequency domains simultaneously, offering unique insights into the temporal evolution of oscillatory patterns. In principle, it reveals the frequency components just like FFT, but it also uncovers any variation of frequencies in the temporal domain<sup>113</sup>. The foundation of wavelet analysis is the Continuous Wavelet Transform (CWT)<sup>114</sup>. It involves convolving the signal with a ‘mother wavelet’ function, whose adjustable width and amplitude capture high/low frequencies and short/long durations simultaneously:

$$W(a, b) = \frac{1}{\sqrt{|a|}} \int_{-\infty}^{\infty} x(t) \psi^* \left( \frac{t-b}{a} \right) dt ,$$

where  $x(t)$  is the input signal,  $\psi^*$  is the complex conjugate of the mother wavelet function,  $a$  is the scaling factor (controls wavelet width), and  $b$  is the translation factor (shifts the wavelet in time). The coefficients  $W(a, b)$  represent the similarity between the signal and the scaled/translated wavelet at each point in time-frequency space. High values indicate a strong correlation between the signal and the wavelet at that specific time and frequency.

The choice of the mother wavelet function is important for optimal results<sup>120</sup> and it should be chosen based on how its characteristics match to the expected oscillatory patterns in the data, and whether time or frequency localisation, or both, are important based on the scientific goals. The ‘Morlet’ wavelet is often used as a default choice due to its balanced time-frequency localisation. However, as demonstrated in our analysis (Section 3.1), the Morlet wavelet may not be sensitive enough to detect certain wave signatures, such as weak or high-frequency oscillations. Therefore, it is important to consider alternative wavelets which might be better suited for specific cases. Table 1 lists the most common wavelet functions suitable for analysing waves, oscillations, and phenomena such as instabilities and turbulence. The shapes and overall characteristics of these wavelet functions are also given.

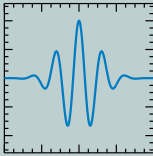
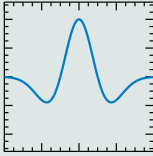
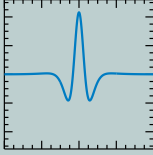
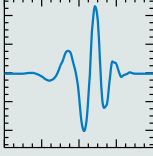
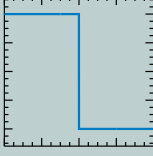
The time-frequency plot also enables one to identify parts of the signal that are subject to the edge effect (that is introduced due to the convolution of the wavelet function close to the edges of the finite time series). Such regions are marked with the so-called Cone of Influence (CoI), identifying unreliable areas of the 2D power spectrum.

The wavelet transform is particularly suitable for studying transient oscillations, weak signals, or quasi-periodic signatures. In addition to the 2D time-frequency spectrum, a 1D spectrum (known as the ‘‘global’’ wavelet spectrum; GWS) can be computed by averaging the power along the entire time domain. However, this traditional approach includes power subject to edge effects, potentially causing misinterpretations.

To address these limitations, we introduce the refined global wavelet spectrum (RGWS), a modification of the traditional GWS. This refinement involves integrating the wavelet power over time, while excluding contributions from the CoI and areas below a given confidence level (e.g., 95%). This ensures that the resulting spectrum focuses on reliable, significant power variations in the signal, encompassing both periodic oscillations and non-oscillatory fluctuations such as those found in turbulence. Thus, RGWS offers a power-weighted frequency distribution of the oscillatory signal, enhancing the identification of significant features. For more details on determining confidence levels, see Supplementary Section S3.

While both GWS and RGWS act as counterparts to the classic Fourier power spectrum, they offer advantages when dealing with time series that exhibit non-stationary behaviour. However, the time averaging or integration processes inherent to their calculation results in smoother spectra compared to the FFT, which in turn may be beneficial in reducing noise and highlighting broader trends. One should also be aware of the frequency resolution limitations

Table 1 | **Wavelet mother functions**

Wavelet Function	Visual Representation	Characteristics	Typical Applications
Morlet <sup>115</sup>		Complex-valued, modulated Gaussian; Balanced time-frequency localisation, but poor spatial localisation	Well-suited for analysing wave-like signals and transient oscillations
Mexican Hat <sup>116</sup> (DOG $m=2$ )		Second derivative of a Gaussian; High time resolution	Useful for detecting transient events, turbulence, and instabilities
Paul <sup>117</sup>		Derivative of a Gaussian; Higher orders provide better frequency localisation	Suitable for analysing brief events or oscillations with distinct frequencies
Daubechies <sup>118</sup> (Db5)		Real-valued, moderate smoothness & support size; Db5 is one example of Daubechies wavelet family	Useful for analysing oscillations with some degree of regularity; can analyse signals at different scales (multi-resolution)
Haar <sup>119</sup> (Db1)		Simplest wavelet, discontinuous	Excellent for detecting sudden changes or discontinuities, such as shocks

intrinsic to wavelet analysis. At smaller wavelet scales (higher frequencies), broad frequency smoothing can mask spectral peaks, while at larger scales, those peaks might appear sharper with artificially increased amplitudes<sup>121</sup>.

### 2.2.4 Empirical Mode Decomposition

Empirical Mode Decomposition (EMD)<sup>122, 123</sup> is a data-driven technique for decomposing a complex signal into its constituent oscillatory components, known as Intrinsic Mode Functions (IMFs). Unlike Fourier-based methods that assume predefined basis functions (sines and cosines), EMD adaptively extracts IMFs based on the local characteristics of the signal itself. This data-driven and adaptive nature makes EMD particularly well-suited for analysing non-linear and non-stationary signals, which are common in many natural phenomena. The EMD process involves identifying local maxima and minima within the signal and then constructing upper and lower envelopes by connecting the extrema with cubic splines. The mean of these envelopes is subtracted from the original signal resulting in the first IMF. This sifting process is repeated on the residual signal to extract subsequent IMFs, and the process is iterated until a stopping criterion is met. Each IMF represents a distinct oscillatory mode within the original signal, and analysing these IMFs reveals the time-varying amplitudes and frequencies, extracted directly from the data.

However, a major limitation of EMD is its sensitivity to noise, which can lead to mode mixing, where a single IMF contains components from different oscillatory modes. To overcome this, Ensemble Empirical Mode Decomposition (EEMD) was introduced<sup>124</sup>. EEMD enhances the robustness of EMD by adding noise to the signal and performing

multiple EMDs. Averaging the resulting IMFs reduces the impact of noise and improves the separation of modes, especially for real-world noisy signals.

The success of EMD and EEMD relies on proper selection of stopping criteria and spline fitting parameters, as these choices can affect the quality of the decomposition and the information contained in each component of the decomposition itself. For example, different stopping criteria can result in varying numbers of IMFs, potentially under- or over-representing the true oscillatory modes present in the signal. Additionally, the choice of spline type and smoothing parameters can influence the shapes and frequencies of the extracted IMFs. Therefore, it is essential to carefully evaluate the appropriateness of these parameters based on the specific characteristics of the data and the research questions. In addition, it is worth noting that the IMFs are only locally orthogonal, meaning that in contrast to, e.g. FFT, each IMF may represent more than one single frequency present in the original signal at the same time. To ensure the reliability of EMD and EEMD results, significance testing plays a crucial role<sup>125</sup>. By assessing the statistical significance of each extracted IMF, researchers can distinguish genuine oscillatory components from noise-induced artefacts. This ensures that subsequent analysis focuses on meaningful oscillations, leading to more accurate interpretations and robust scientific conclusions.

### 2.2.5 Hilbert-Huang Transform

Hilbert-Huang Transform (HHT<sup>32, 126, 127</sup>) is an empirical approach designed to handle non-linear and non-stationary signals. It operates in two primary stages: first, the signal is decomposed into IMFs using either EMD or EEMD. Next, Hilbert Transform is applied to IMFs to calculate instantaneous frequencies and amplitudes. The Hilbert Transform ( $H[x(t)]$ ) of a signal  $x(t)$  is given by:

$$H[x(t)] = \frac{1}{\pi} P \int_{-\infty}^{\infty} \frac{x(\tau)}{t - \tau} d\tau,$$

where  $\tau$  is an integration variable representing time,  $t$  is the specific time point where the Hilbert Transform is being evaluated.  $P$  denotes the Cauchy Principal Value which ensures the integral converges even when there is a singularity at  $t = \tau$  (i.e., if the signal has sudden spikes or discontinuities). Instantaneous frequencies provide insights into how the dominant frequencies of oscillations evolve over time, however, it is important to be aware of potential uncertainties associated with them at particular times. The integration of the 2D Hilbert spectrum across time, known as the ‘marginal’ spectrum, can be useful for visualising the overall frequency distribution, especially for identifying low-amplitude, high-frequency oscillations. Finally, the success of HHT depends on careful selection of parameters for the EMD (or EEMD) decomposition.

### 2.2.6 Welch method

The Welch method<sup>128</sup> is a refined approach for calculating power spectra, or PSD (see Box 2), designed to reduce noise, especially in datasets where noise reduction takes priority over fine frequency resolution. It operates by splitting a signal into overlapping segments, detrending and apodizing each segment, and computing their individual frequency spectra (often using FFT). The resulting spectra are then averaged, resulting in a smoother final spectrum with reduced noise (see Supplementary Section S4 for details on various noise models).

The Welch method is a specialised implementation of the **Short-Time Fourier Transform (STFT)**<sup>129</sup>. The key idea of STFT is to divide the signal into shorter segments and calculate the Fourier Transform of each. Applying a windowing function (e.g., Hann, Gaussian) to each segment before the transformation helps minimise spectral leakage<sup>130</sup>. This process generates a series of spectra representing the frequency content of the signal over time. STFT provides a visual and analytical framework for understanding signals with time-evolving frequency characteristics and is the foundation for various other time-frequency analysis techniques.

### 2.2.7 Specialised time-frequency methods

While FFT, Lomb-Scargle, and Welch (or STFT) are fundamental tools for analysing the frequency content of signals, wavelet transforms, along with EMD and HHT, offer a powerful way to study signals with time-varying frequency content. However, these fundamental methods can be further extended and refined to address specific challenges, or uncover additional insights, within complex datasets, particularly when dealing with, for instance, non-stationary or

noisy data in some specialised areas. This section explores a selection of such advanced time-frequency methods, highlighting their potential to complement the core techniques predominantly covered in this Primer.

One such method is the **Wigner-Ville distribution** (WVD)<sup>131–133</sup>, which offers high-resolution time-frequency representations. It involves calculating the instantaneous frequency and amplitude of the analytic signal corresponding to the input signal, constructing a weighted kernel function, and then analysing this kernel using DFT<sup>134</sup>. It is defined as:

$$W_x(t, f) = \int_{-\infty}^{\infty} x\left(t + \frac{\tau}{2}\right) x^*\left(t - \frac{\tau}{2}\right) e^{-i2\pi f\tau} d\tau \quad (1)$$

where  $x(t)$  is the input signal and  $x^*(t)$  is its complex conjugate. While WVD excels at resolving non-stationary signals, it can introduce artifacts or “cross-terms” when multiple frequency components are present in the signal. These cross-terms can sometimes be mitigated using wavelet-based filtering techniques<sup>135</sup>, potentially improving the WVD’s interpretability. While WVD has proven valuable in various fields, such as quantum physics, recent advancements in signal processing have further enhanced its accuracy and broadened its applications<sup>136</sup>.

Another approach is the **Synchrosqueezing transform** (SST)<sup>137</sup>, which enhances the traditional wavelet transform, or STFT, by “squeezing” the wavelet or Fourier coefficients in the frequency direction, leading to sharper time-frequency representations; particularly useful for signals with closely spaced, or overlapping frequencies. However, this method, originally developed for audio signal processing<sup>138</sup>, may not be able to directly handle signals with a rapidly changing instantaneous frequency<sup>139</sup>.

The **S-transform**<sup>140</sup> combines elements of the STFT and wavelet transforms. It uses a Gaussian window whose width varies with frequency, providing a balance between time and frequency resolution, much like wavelet analysis, but with Fourier-based calculations. While computationally efficient, it may not be, due to its fixed Gaussian window shape, as flexible or adaptable as wavelet transforms (through its various mother functions) for highly non-stationary signals.

Finally, the **Gabor transform**<sup>141</sup> is yet another approach for analysing signals using Gaussian windows, offering good time-frequency localisation. However, its fixed Gaussian window might not be optimal for all types of signals. These additional time-frequency methods, along with many others such as the Choi-Williams distribution<sup>142</sup> and the Zhao-Atlas-Marks distribution<sup>143</sup>, to name but a few, while valuable, represent only a small fraction of the vast array of techniques often developed for specialised applications and/or analysing complex oscillatory signals. Their detailed descriptions and analyses are beyond the scope of this Primer, which focuses on a core set of fundamental methods.

## 2.3 Methods for spatial wave analysis

Understanding the interplay between oscillatory phenomena and their spatial distribution is crucial for identifying and interpreting wave modes. This section introduces analytical techniques designed to reveal such relationships within spatio-temporal datasets. Several strategies exist for analysing how the power of oscillations varies across a spatial domain. Averaging temporal power over regions of similar scale highlights the frequencies dominant at specific spatial locations. We can extend this concept by filtering oscillations based on various physical properties (e.g., magnetic field strength, temperature), or other relevant parameters depending on the field of study. Furthermore, depending on the scientific question, a spatially-averaged power spectrum over the entire field of view may reveal global oscillations, while examining the distribution of dominant frequencies can pinpoint localised phenomena. These techniques are complemented by powerful data-driven methods like Proper Orthogonal Decomposition (POD) which identify coherent patterns and their evolution across both space and time, applicable across various scientific disciplines.

### 2.3.1 Mean power spectrum

The spatially-averaged power spectrum offers a global perspective on oscillatory behaviour within a field of view<sup>144</sup>. Calculated by averaging the power spectra of individual pixels across the region of interest in the frequency domain, it highlights the overall power distribution across frequencies, revealing dominant oscillatory modes. The mean

power spectrum can identify frequencies where oscillations are most pronounced, potentially uncovering global modes or characteristic frequencies. Comparing mean power spectra across different regions or datasets can unveil changes in dominant oscillatory behaviour. In complex datasets, this technique can serve as a baseline for filtering out dominant global contributions, allowing for the study of localised phenomena or weaker oscillations. Applicable to 1D power spectra generated from various methods (FFT, Lomb-Scargle, Wavelets, HHT, or Welch), it is a flexible tool for diverse scientific questions.

### 2.3.2 $k - \omega$ analysis

The  $k - \omega$  diagram provides a powerful way to analyse oscillatory phenomena, revealing how they are distributed across spatial scales (represented by wavenumber,  $k$ ) and temporal frequencies ( $\omega$ )<sup>145, 146</sup>. While often constructed from azimuthally averaging the spatial frequencies (i.e., the wavenumbers  $k_x$  and  $k_y$ ) of the Fourier transform (FFT) power spectra of a 3D spatio-temporal datacube,  $k - \omega$  diagrams can also be generated from phase differences between two oscillatory signals to reveal phase relationships and potential wave propagation directions<sup>147, 148</sup>.

Analysing the relationships within the  $k - \omega$  diagram illuminates dispersion relations, helping identify distinct wave modes and their properties. A key feature of  $k - \omega$  analysis is the ability to filter oscillations selectively within specific ranges of wavenumbers and/or frequencies. Applying an inverse Fourier transform to the filtered data allows us to isolate these oscillations in the original dataset, enabling targeted studies of complex wave phenomena. An example is isolating oscillations with relatively small amplitudes that might be masked by macroscopic flows or dominant wave modes with considerably larger power<sup>37</sup>. This makes  $k - \omega$  analysis a versatile tool across disciplines investigating wave phenomena, fluid dynamics, and other intricate systems where spatio-temporal oscillations are fundamental. While  $k - \omega$  analysis primarily focuses on the relationship between spatial and temporal frequencies, it can be extended to incorporate other relevant properties within the data. This extension, called Property-Frequency Analysis (PFA), allows for a detailed exploration of wave behaviour by filtering oscillations based on specific characteristics, such as magnetic field strength, temperature, or other parameters (See Supplementary Section S6).

### 2.3.3 Proper Orthogonal Decomposition

Proper Orthogonal Decomposition (POD)<sup>149, 150</sup> is a powerful data analysis technique used to identify spatially orthogonal (unique dominant) patterns within complex datasets, often referred to as “spatial modes”. Similar to the more familiar Principal Component Analysis (PCA)<sup>151, 152</sup>, POD extracts these modes based on their contribution to the overall variance in the data. While other approaches exist, such as the classical method (or spatial POD) and the snapshot method<sup>153</sup>, we focus here on the Singular Value Decomposition (SVD)<sup>154</sup> as the primary approach for computation. SVD is a mathematical factorisation that decomposes a matrix into three distinct components which, when combined, describe the original data input in full. For POD, the input data cube is column vectorized into an input matrix such that each row contains the value relating to each spatial coordinate and each column represents each snapshot in time. In this method we express the POD as a singular value decomposition. Therefore the POD modes are expressed components of the SVD.

The POD analysis decomposes the data ( $\mathbf{X}$ ) into a set of Spatial POD modes ( $\mathbf{U}$ ), a set of Eigenvectors (temporal coefficients) ( $\mathbf{V}$ ), and a set of singular values ( $\mathbf{S}$ ). The squares of the singular values, which in this context are referred to as Eigenvalues, are the measures of variance, which, in real-world applications, are seen to be analogous to total energy contribution,

$$\mathbf{X} = \mathbf{USV}^T .$$

Here  $(\cdot)^T$  denotes a transpose. The POD spatial modes and Eigenvectors are ranked by the Eigenvalues from the largest to smallest, i.e., spatial modes and temporal coefficients each descend from the largest contribution to the smallest and in this order can be recombined to describe the original dataset. In most cases, the top few modes capture the majority of variability within the dataset, making POD a valuable data-driven tool for dimensional reduction. The spatial modes provide spatial insights into “coherent” spatial patterns which propagate through the datasets, with the temporal coefficients mapping these contributions through time, showing their variability and repeatability throughout the data; this is often further interpreted using Fourier-based methods<sup>155, 156</sup>, and these temporal coefficients can likewise be used to further decompose the modes by filtering the temporal coefficients<sup>157</sup>.

In short, POD is an invaluable data-driven tool for dimensional reduction<sup>158</sup> and elucidating underlying coherent patterns and temporal behaviours. It can also be extended to multi-variable datasets by applying a weighting procedure<sup>159–161</sup>.

### 2.3.4 Dominant frequency

The dominant frequency, generally defined as the frequency associated with the highest power in a spectrum, offers insights into the most prevalent oscillation within a signal. However, caution is needed when interpreting this metric, particularly in signals with multiple strong spectral peaks. If multiple peaks share the maximum power, the method will typically return the lowest frequency among them, potentially under-representing the true complexity of the oscillatory behaviour.

Calculating dominant frequencies is compatible with 1D power spectra generated using various methods. Maps of dominant frequencies, determined pixel by pixel in spatio-temporal data, provide a visual representation of how these frequencies vary across a spatial region. While potentially biased due to the possibility of multiple strong peaks, these maps offer a statistical overview of the oscillatory landscape, revealing spatial patterns and potential correlations with other physical properties.

Table 2 provides a comparative overview of the wave analysis tools discussed, serving as a guide for researchers to select the most suitable methods for their specific investigations.

## 2.4 Cross correlations between two datasets

Investigating the connections between two time series is crucial for untangling the interplay of phenomena<sup>162</sup>. Whether exploring relationships between different physical parameters, signals across spatial locations, or even between distinct datasets, cross-correlation analysis offers a powerful toolkit. Parameters like the cross-spectrum, coherence, and phase difference quantify the shared frequencies, strength of relationships, and relative timing of oscillations between two signals. These insights are essential for revealing hidden connections, tracing the propagation of disturbances, or identifying common drivers of oscillatory behaviour in diverse scientific fields. Importantly, these cross-correlation parameters can be calculated using the diverse analysis methods we have reviewed in Section 2.2. The dimensions of the output visualisation depend on the chosen method: 1D representations are common for FFT, Lomb-Scargle, and HHT-based power spectra of one-dimensional time series, while wavelet analysis offers time-frequency insights through 2D representations.

### 2.4.1 Cross spectrum

The cross spectrum offers a powerful tool for identifying frequencies where oscillations in two different time series exhibit common power<sup>163</sup>. This provides valuable clues about potential connections or shared drivers influencing the signals. In general, the analysis begins by transforming each time series from the time domain into a representation that highlights its frequency content. This could be achieved through various techniques, such as the FFT for evenly sampled data or wavelet transforms for analysing time-varying frequency content. For unevenly sampled data, the Lomb-Scargle cannot be directly used to calculate the cross-spectrum. However, the smoothed Lomb-Scargle, a variation of the standard method, allows for cross-spectral analysis between two irregularly sampled time series<sup>164</sup>. The cross spectrum is then computed by multiplying the frequency representation of one signal by the complex conjugate of the frequency representation of the other signal, mathematically expressed as:

$$S_{xy}(f) = X^*(f)Y(f) ,$$

where  $X(f)$  and  $Y(f)$  are, e.g., the Fourier transforms of the two time series  $x(t)$  and  $y(t)$ , respectively, and  $X^*(f)$  denotes the complex conjugate of  $X(f)$ . This highlights frequencies where both signals display strong power. The inherently complex-valued nature of the cross spectrum  $S_{xy}(f)$  carries both magnitude and phase information at each frequency. The real part, known as the co-spectrum, and given by:

$$Co_{xy}(f) = \Re[S_{xy}(f)] ,$$

provides a direct measure of the shared power between signals at different frequencies, with high values suggesting a strong link between the oscillations.

Table 2 | **Comparison of various wave analysis methods**

Method	Data Assumptions/Capabilities	Pros and Cons
FFT	Stationary, infinite/long signals, evenly-sampled data	Fast, efficient, clear interpretation. Limited to stationary signals, requires even sampling. May result in biased estimations of the real spectral density.
Lomb-Scargle	Unevenly-sampled data	Handles gaps and missing data well. Less straightforward interpretation, computationally intensive for large datasets.
Wavelet	Transient signals, non-stationary data, weak or quasi-periodic signals	Localises power in time and frequency, good for feature detection, multi-scale analysis. Requires careful wavelet selection, can be computationally intensive.
EMD / EEMD & HHT	Non-stationary, non-linear signals	Data-driven, handles non-linearity well. Sensitive to parameter choices. EMD can be sensitive to noise and mode mixing
Welch	Noisy data	Reduces noise in spectra by segmenting. Reduces spectral leakage. Comes at the cost of slightly reduced frequency resolution.
$k - \omega$	Spatio-temporal datasets	Reveals dispersion relations, filtering in wavenumber and frequency. Requires spatio-temporal data.
PFA	Time series or spatio-temporal data, associated parameter of interest	Isolates oscillations in specific regimes defined by the parameter of interest. Requires auxiliary data.
POD	Complex datasets with dominant spatial patterns	Identifies coherent modes, excellent for dimensionality reduction. Assumes linear superposition of modes.
Mean Power	Time series or spatio-temporal data	Provides global view, reveals characteristic frequencies. Averages out localised behaviour.
Dominant Frequency	Time series or spatio-temporal data	Offers spatial maps or statistical picture. Interpretation requires caution (multiple peaks, etc.).

### 2.4.2 Coherence

While the cross spectrum highlights frequencies with shared oscillatory power, coherence provides a complementary tool for investigating the strength of the relationship between two time series across different frequencies. This is particularly valuable when one or both of the individual power spectra might lack strong, distinct peaks (e.g., signals embedded in noise or with incomparable amplitudes), potentially masking correlations in the cross spectrum. The coherence  $\gamma_{xy}^2(f)$  is defined as the squared absolute value of the complex cross spectrum  $S_{xy}(f)$ , normalised by the product of the individual power spectra  $|X(f)|^2$  and  $|Y(f)|^2$ :

$$\gamma_{xy}^2(f) = \frac{|S_{xy}(f)|^2}{|X(f)|^2|Y(f)|^2} .$$

This normalisation is crucial<sup>36,165</sup>, ensuring that coherence values range between ‘0’ (no correlation) and ‘1’ (perfect correlation). High coherence values at a specific frequency indicate that the oscillations in the two time series are linearly related at that frequency, even if the individual power spectra do not exhibit strong peaks. This makes coherence a powerful tool for uncovering hidden relationships, tracing wave propagation across spatial locations, and investigating connections between oscillations in different physical parameters, even if their amplitude is small.

### 2.4.3 Phase difference

Phase difference (or phase lag) provides a crucial measure of the relative timing of oscillations in two time series. It is calculated from the phase angle of the complex cross spectrum and offers insights into whether oscillations are in phase, or if one signal systematically leads or lags the other. A zero phase difference indicates that the oscillations are in phase, meaning their peaks and troughs align in time. Values between  $-180$  and  $180$  degrees reveal a phase shift and a phase difference of  $\pm 180$  degrees represents an anti-phase relationship, where the oscillations are perfectly out of step (one’s peaks align with the other’s troughs). The phase lag ( $\phi$ ) can be easily translated into a time lag ( $\tau$ ) at a specific frequency ( $f$ ) using the relationship:  $\tau = \phi / (2\pi f)$ . This conversion provides a more intuitive understanding of the temporal offset between the oscillatory signals. Phase difference analysis is valuable for determining the direction and speed of wave travel, exploring potential cause-and-effect connections between phenomena, and investigating the degree of synchronisation between oscillating systems<sup>146,166</sup>.

## 3 Results

This section presents the results of applying the diverse analysis methods introduced in Section 2 to our carefully crafted synthetic datasets. By utilising signals with known ground truth, we thoroughly evaluate the capabilities of each method in identifying specific wave modes, handling complex wave components, and assessing their robustness in the presence of noise. It is important to note that these comparisons and insights are based on the specific characteristics of our synthetic datasets, which are designed to represent a wide range of oscillatory behaviours but may not fully encompass all the complexities present in real-world data. Therefore, researchers should carefully consider the specific properties of their data (such as noise levels, non-linearity, non-stationarity, length, cadence, and other relevant parameters) and the specific aims of their study when selecting the most appropriate method or combination of methods. To aid reproducibility and understanding of the analysis process, all codes used in this section, along with the synthetic datasets, are available in a publicly accessible repository (see Section 5). This evaluation provides a valuable framework for understanding the strengths, limitations, and complementarity of different techniques, ultimately guiding the interpretation of results obtained from the analysis of real observational data.

### 3.1 Synthetic 1D signal: method performance evaluation

Figure 3 showcases a systematic assessment of various wave analysis methods applied to the synthetic 1D signal plotted in Figure 2 and described in Section 2.1.1. Before analysis, the signal was linearly detrended by subtracting a linear fit with respect to time, and apodized with a Tukey window (with  $\alpha = 0.1$ , representing the fraction of the window within the cosine-tapered region; panel a), then subjected to uneven sampling by removing 20% of the data points in four unequally spaced windows (panel b). Panels (c)-(n) present the results of various wave analysis techniques on the original data, with the exception of the Lomb-Scargle approach which was applied to the unevenly sampled signal.

The FFT, Lomb-Scargle, and Welch methods (panels c, d, and k) are able to recover the five base (dominant) oscillation frequencies (5, 12, 15, 18, and 25 Hz) and amplitudes. Notably, Welch, designed for noise reduction, exhibits a loss of frequency resolution compared to FFT (as indicated by the vertical lines on top of each frequency spectrum), highlighting the trade-off between noise reduction and resolving power. However, Welch is notably more effective at suppressing spurious signals, such as the small peak around 9.5 Hz. This advantage becomes increasingly valuable in the presence of higher noise levels, where the FFT might produce misleading peaks. Lomb-Scargle is able to handle the irregular sampling, resulting in the same identified frequencies as those found with the FFT (and Welch), validating its suitability for datasets with gaps. While none of these three techniques reliably identify the

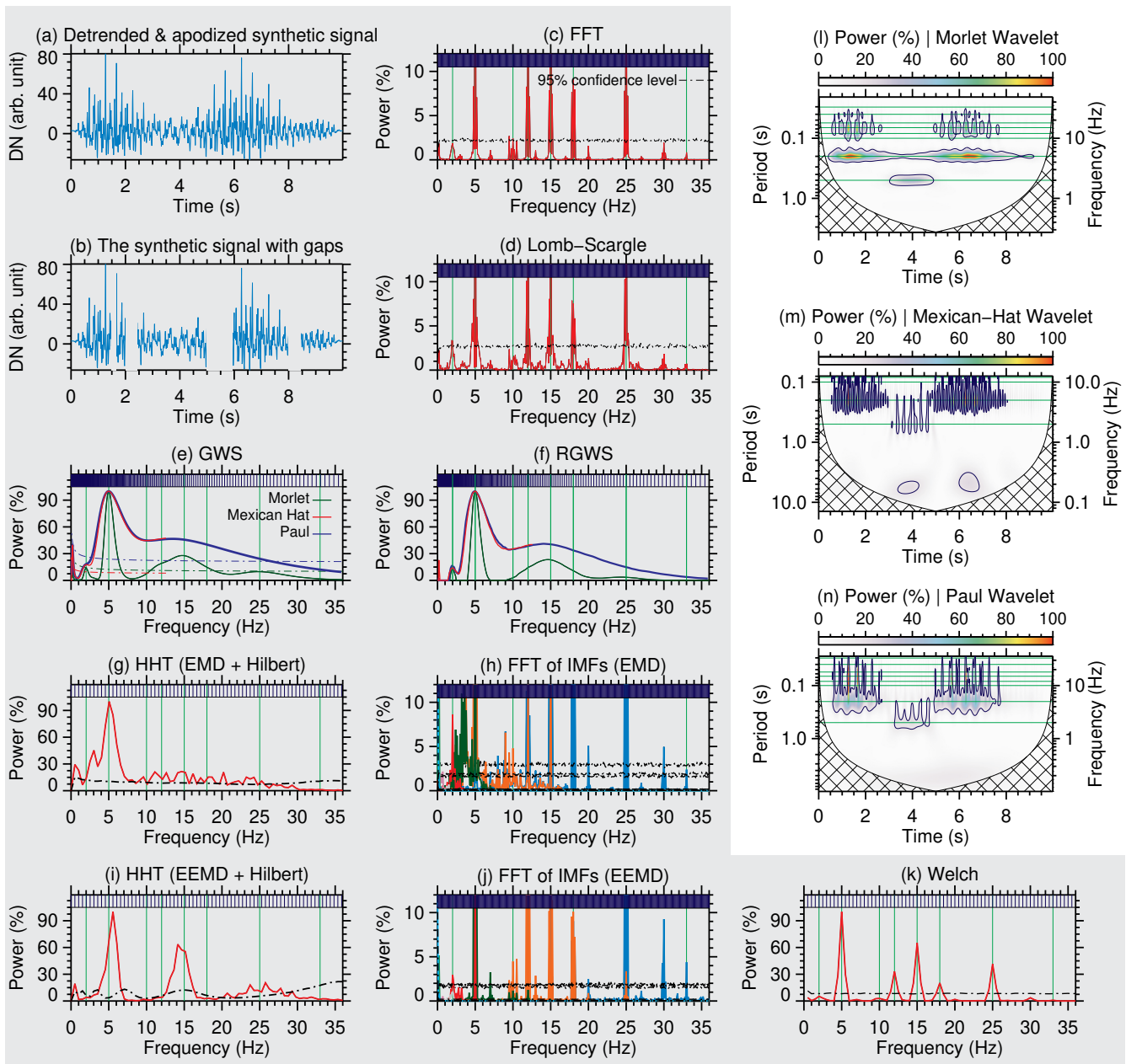


**Fig. 3 | Performance of diverse analysis methods on the intricate synthetic 1D time series described in Section 2.1.1.** This signal comprises dominant oscillations (frequencies 5, 12, 15, 18, and 25 Hz), a transient oscillation, a weak signal, a quasi-periodic signature (frequencies 2, 33, and 10 Hz), noise, and other complexities. Panel (a) shows the detrended and apodized signal. Panel (b) illustrates uneven sampling effects after removing specific data points. Panels (c)-(n) showcase the analytical results: FFT (c), Lomb-Scargle (d), and Welch (k); GWS and RGWS for three mother wavelets (e)-(f), with corresponding wavelet spectra in (l)-(n); HHT spectrum using EMD (g) and the FFT power spectra of its individual IMFs (h); HHT with EEMD (i) and the FFT power spectra of its individual IMFs (j). All powers are normalised to their maximum value and shown in percentages, with panels (c), (d), (h), and (j) zoomed in on a smaller power range for better visibility of smaller peaks. The 95% confidence levels are indicated by dot-dashed curves for 1D power spectra and solid black contours for wavelet spectra. Vertical lines above each 1D spectrum mark the frequency resolution of the 1D power spectra. Green vertical (or horizontal) lines on the frequency axes indicate the predefined frequencies used to construct the synthetic signal. See the main text for a detailed discussion of the results and insights into the strengths and limitations of each method.

weak high-frequency signal, the quasi-periodic signature, or the short-lived transient oscillation in the data, the Lomb-Scargle approach does more reliably identify the weak transient oscillation at 2 Hz.

All wavelet transforms (panels l-n) excel in detecting the transient oscillation (2 Hz frequency). This highlights their sensitivity to short-lived events that were missed by FFT, even for relatively large amplitude transients. The extremely weak 33 Hz signal remains largely undetected by the Morlet and Mexican-Hat wavelet, but is identified by the Paul wavelet. The quasi-periodic signature (10 Hz; 0.3 amplitude) is identified by all wavelet functions, but most prominently by the Mexican-Hat and Paul wavelets, emphasising the potential of specialised wavelet functions for uncovering faint or complex oscillations. Decomposition techniques (such as EMD and EEMD; see below) or filtering approaches can also be employed to detect weak signals masked by stronger components, as filtering out the dominant oscillations can reveal weaker but still significant signals.

A comparison of the three wavelet power spectra also reveals the important influence of the different wavelet functions. Each function results in a different frequency range, with the Mexican-Hat wavelet limited to frequencies below approximately 13 Hz. Furthermore, the choice of wavelet function influences the resolution in both the time and frequency domains, as well as the extent of the time-frequency space marked by the CoI. This is evident in the identification of very-low frequency spurious signals (around 0.2 Hz) by the Mexican-Hat wavelet, which are not present in the other two wavelet spectra.

While the time-frequency perspective offered by wavelets is invaluable for revealing the temporal evolution of the base and more complex oscillations in the time-frequency domain (panels l-n), their time-averaged and time-integrated spectra, the GWS and RGWS (panels e and f), result in smoother frequency spectra that lack detailed temporal information. Comparing GWS and RGWS demonstrates how excluding the CoI and low-confidence power leads to a more refined view of significant oscillatory components by the latter. Notably, while the highest frequency components (at 25 and 33 Hz) are not reliably detected by GWS (i.e., they fall below the 95% confidence levels), they are captured in the Paul-based RGWS. The latter demonstrates particular sensitivity to the quasi-periodic signature (10 Hz), as well as the transient and weak signals, whereas the Morlet-based RGWS is unable to detect the quasi-periodic and weak signatures, and the Mexican-Hat function is limited to frequencies below 13 Hz. Additionally, the Mexican-Hat-based RGWS introduces a peak at 0.2 Hz (i.e., the low frequency spurious signal). It is important to note that the frequency-dependent resolution of GWS and RGWS results in sharper peaks and artificially increased amplitudes at lower frequencies, while higher frequencies appear broader and smoothed. The smooth appearance of the GWS and RGWS, despite the relatively high frequency resolution as depicted by the vertical lines on top of the spectra (when compared to, e.g., the Welch spectrum), is primarily due to the averaging (or integrating) process over time and the properties of the wavelet used. Therefore, direct comparisons with methods like FFT require careful consideration. If one-to-one comparisons are necessary, interpolating the GWS or RGWS power onto a uniform frequency array can generate a wavelet PSD that aligns more closely with those obtained by FFT (see Box 2).

Confidence levels, estimated from 1000 randomised surrogate signals, generally distinguish genuine peaks from background fluctuations, but discrepancies between methods might arise in noisier environments, necessitating careful interpretation.

The HHT spectrum using EMD (panel g) reliably recovers only the strongest signal at 5 Hz, failing to identify other oscillatory components. To further explore the frequency content of the EMD decomposition, the FFT power spectra of the individual IMFs are shown in panel (h), with each IMF's spectrum represented by a different colour. In addition to the five base oscillations, the transient signal, and, to some extent, the quasi-periodic signature are also identified. However, several other strong peaks appear at locations where no wave signatures were introduced in the synthetic signal, demonstrating EMD's limitations in accurately decomposing and identifying all frequencies. For a more detailed discussion of the EMD results, we refer to Supplementary Section S7, where the individual IMFs and their instantaneous frequencies are also shown in Supplementary Figure S2.

Furthermore, we applied EEMD, an extension of EMD designed to mitigate mode mixing caused by noise, to the synthetic signal. The detailed results of this analysis are shown in Supplementary Figure S3. Panel (i) in Figure 3 shows the HHT marginal spectrum using EEMD, revealing two dominant frequencies of the signal at 5 and 15 Hz, and a smaller power enhancement peaked at 25 Hz. Both the EMD and EEMD HHT power spectra exhibit a

spurious frequency peak around 0.5 Hz, possibly due to residual trends in the signal. Panel (j) illustrates the FFT power spectra of the individual IMFs extracted by EEMD. These spectra show a more comprehensive recovery of the original signal’s frequency components, including the weaker wave signature, compared to the EMD results. However, although less prominent than in EMD, some additional frequencies, linked to noise and spurious signals, are still present in panel (j). See Supplementary Section S7 for a detailed discussion and comparison of EMD and EEMD.

Comparing Figure 3c and 3j highlights the value of decomposition techniques in recovering the full spectrum of frequencies. While the former spectrum was obtained by applying FFT directly to the signal with all signatures superimposed, the latter represents the results of FFT applied to the individual IMFs extracted by EEMD, showcasing the superior ability of EEMD to isolate and resolve all individual oscillatory components, even in the presence of multiple overlapping signals.

### 3.2 Synthetic spatio-temporal dataset: unveiling wave patterns

Having explored method performance on 1D time series, we now extend our analysis to the synthetic spatio-temporal dataset (introduced in Section 2.1.2). This allows us to investigate how oscillatory patterns evolve and propagate across both space and time, a crucial aspect of wave phenomena in many scientific domains. We first examine the dataset from a pixel-by-pixel perspective, applying 1D analysis techniques, such as FFT and wavelet transforms, to understand the spatial distribution of wave properties. We then delve into the application of methods specifically designed for 3D spatio-temporal data, such as  $k$ - $\omega$  and POD analyses (introduced in Section 2.3), uncovering wave modes and their interactions across both spatial and temporal dimensions.

#### 3.2.1 Dominant frequency and mean power spectra

We calculated dominant frequencies and mean power spectra of the 3D datacube using the FFT and the RGWS with both Morlet and Paul wavelet functions. This allows for a detailed comparison, showcasing the strengths and limitations of each technique.

The top panels of Figure 4 depict dominant frequency maps for the FFT (left), RGWS with Morlet (middle), and RGWS with Paul (right). While a single dominant frequency can be misleading in the presence of multiple significant spectral peaks, these maps offer a statistical overview of the spatial distribution of dominant frequencies across the observations. Notably, both FFT and Paul-based RGWS maps reveal finer spatial structures compared to the Morlet-based RGWS. This reflects the higher frequency resolution of FFT and the Paul wavelet’s enhanced sensitivity to localised features. Conversely, the Morlet-based RGWS, due to its smoothing properties, provides a more generalised view of dominant oscillations across the entire spatio-temporal domain. This is also evident in the frequency distributions, with FFT identifying frequencies up to 550 mHz (the highest frequency component in the synthetic signal). The maximum frequencies detected by Morlet- and Paul-based RGWSs are around 450 and 350 mHz, respectively. These differences highlight the caution needed when interpreting dominant frequency maps, as the results can be highly sensitive to the method employed.

We also computed normalised spatially averaged mean power spectra using FFT and both RGWS approaches (Figure 4, bottom panel). All three methods capture the full range of frequencies present in the synthetic data. The FFT mean power spectrum exhibits distinct peaks, reflecting its superior frequency resolution. In contrast, the RGWSs present broader, smoother spectral features, most notably the Paul-based RGWS.

#### 3.2.2 Spatio-temporal analysis: comparing $k$ - $\omega$ and POD filtering

Figure 5 offers a comparative analysis of wave properties derived from both  $k$ - $\omega$  filtering and POD techniques. Panel (a) presents the  $k$ - $\omega$  power diagram of the synthetic spatio-temporal datacube (introduced in Section 2.1.2), identifying regions of significant oscillatory power with all ten inserted frequencies exhibiting the strongest power. The dashed lines identify a specific frequency-wavenumber region of interest, chosen for filtering 500 mHz ( $\pm 30$  mHz) and wavenumbers between  $0.05 - 0.25 \text{ pixel}^{-1}$ . The resulting filtered datacube is shown as a sequence of the first six frames of the time series in panel (c), illustrating the evolution of the targeted wave pattern. The filtered results may provide insights into wave propagation, dispersion properties, and the identification of distinct

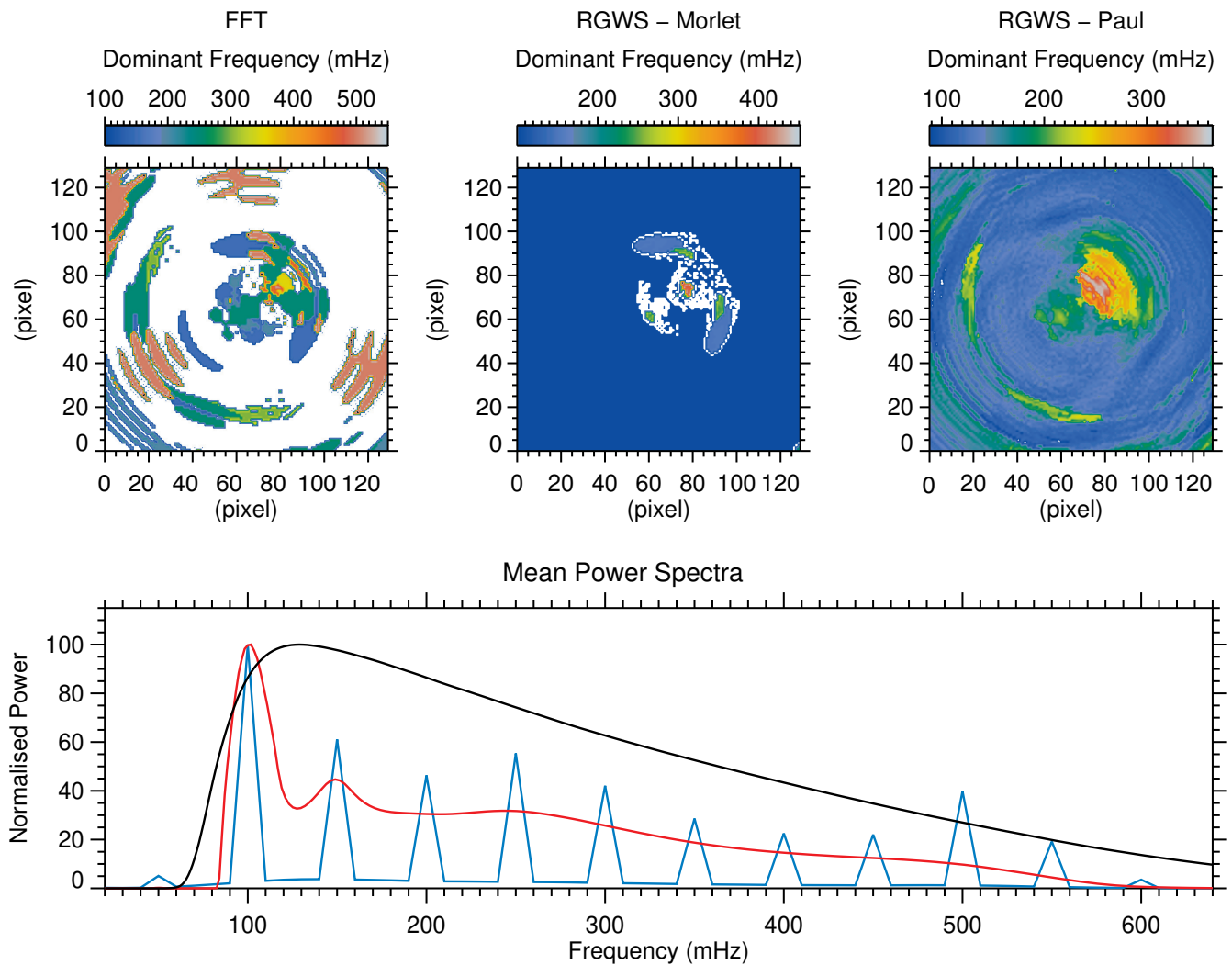


Fig. 4 | **Dominant frequency maps and mean power spectra.** Top row: Dominant frequency maps derived using FFT (left), Morlet-based RGWS (middle), and Paul-based RGWS (right). Bottom panel: Normalised mean power spectra for FFT (blue), Morlet-based RGWS (red), and Paul-based RGWS (black).

wave modes within the dataset. For details on the  $k$ - $\omega$  analysis applied to this datacube and filtering steps, see Supplementary Section S8.

Panel (b) displays the first six spatial modes derived from POD analysis applied to the mean-subtracted data using an economy-sized singular value decomposition. These modes represent the dominant, spatially coherent patterns of oscillation within the datacube (together, they contribute to 93% of the total variance of the system). For further details, including the temporal coefficients of these POD modes and their Welch power spectra, see Supplementary Figure S5. Additionally, Supplementary Figure S6 summarises the POD analysis results, including the normalised singular values (eigenvalues) of the first ten modes, their combined power spectrum, and the cumulative explained variance as a function of the number of modes included. The strongest 10 peaks of the combined power spectrum perfectly align with the base frequencies of the synthetic data, irrespective of the number of modes included. This clearly demonstrates the robustness of POD in reliably identifying dominant frequencies in the data.

While POD reveals the presence of all input frequencies, it does not isolate them individually (i.e., each mode may present multiple frequencies). To address this, we can algorithmically fit the identified, dominant ten frequencies to the temporal coefficients of these modes, creating a representation based solely on pure frequencies. For this study, we use a non-linear least-squares filter fitting to imposed sinusoids and reconstruct the data using these filtered

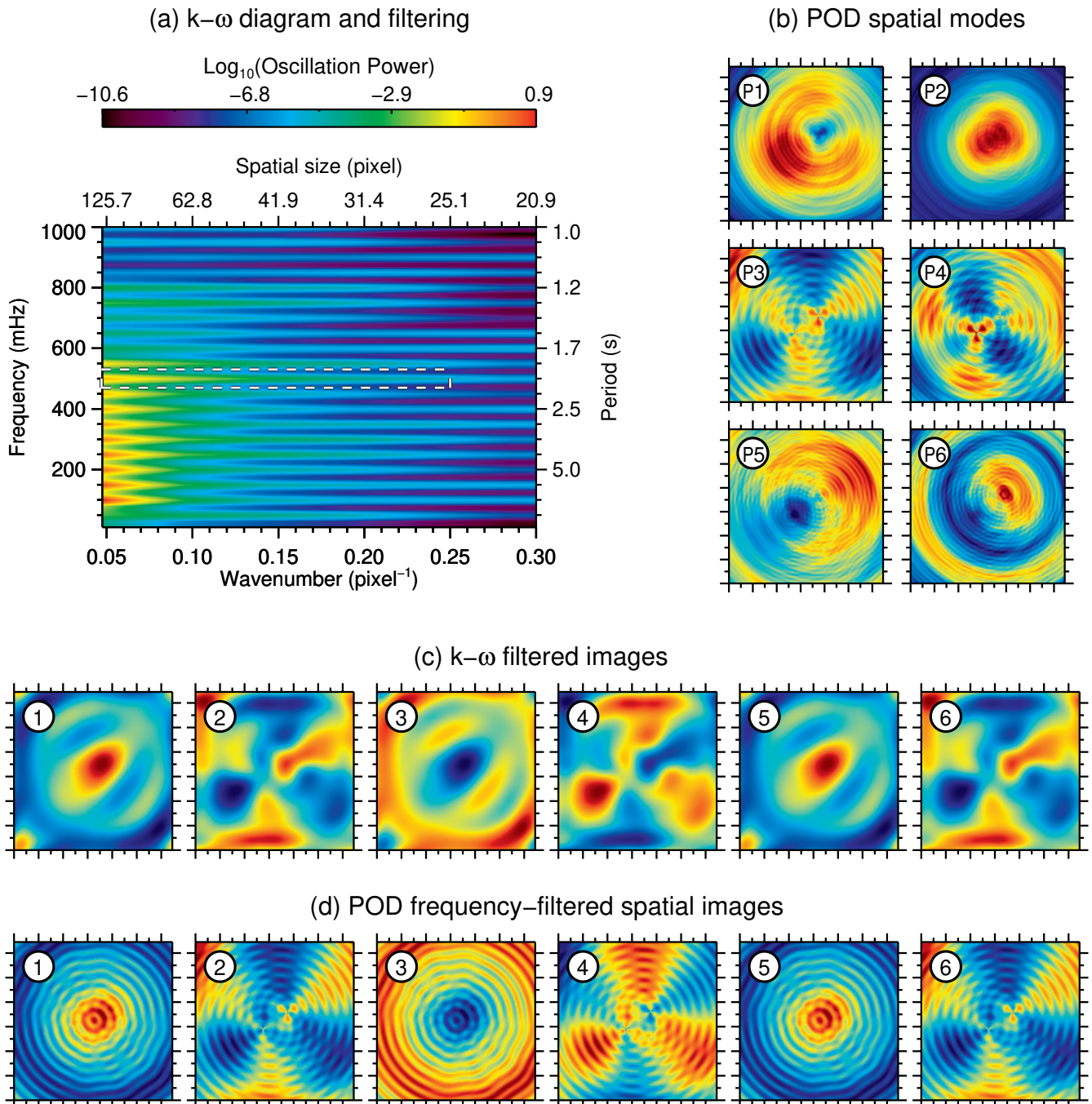


Fig. 5 | **Comparison of  $k$ - $\omega$  filtering and POD analysis.** (a)  $k$ - $\omega$  power diagram of the synthetic spatio-temporal dataset (introduced in Section 2.1.2) with a targeted filtering region (dashed lines). (b) First six spatial modes from POD analysis (each  $130 \times 130$  pixels<sup>2</sup>). (c) First six frames of the  $k$ - $\omega$  filtered datacube centred at 500 mHz ( $\pm 30$  mHz) and wavenumbers  $0.05 - 0.25$   $\text{pixel}^{-1}$ . (d) First six frames of the frequency-filtered POD reconstruction at 500 mHz using the first 22 POD modes (99% of total variance). All images and spatial modes are plotted with their own minimum and maximum values to highlight detailed structures within them. See Supplementary Section S8 and S9 for further details.

temporal coefficients and the first 22 modes (capturing 99% of the total variance). This approach creates a set of frequency-filtered spatial modes, where each mode represents the spatial pattern associated with a specific frequency over the entire time series. In panel (d), we showcase the first six frames of the reconstructed datacube after applying

frequency filtering at 500 mHz. This allows us to directly compare the spatial patterns extracted through  $k$ - $\omega$  filtering (c) and POD-based filtering (d). The POD-filtered spatial modes for the ten most dominant frequencies are presented in Supplementary Figure S7 for the first three time steps of the series, and their temporal variation for the entire time series is available as Supplementary Video 2. For more detailed discussion on POD analysis, including the identification of physically meaningful modes and a comparison with Spectral POD (SPOD), where the frequency filtering is performed before computing the eigenvalues (hence no temporal variation is obtained), please refer to Supplementary Sections S9 and S10.

The striking similarity between the filtered datacube frames in panels (c) and (d) underscores the complementarity of these two approaches. Both techniques successfully isolate the 500 mHz wave mode, revealing its spatial structure and temporal evolution. This confirms that both  $k$ - $\omega$  filtering and POD-based filtering are effective methods for extracting specific wave signatures from complex spatio-temporal datasets. Note that jumps between spatial modes may occur where multiple wave modes are superimposed, as seen in this case at 500 mHz with the concentric wave patterns and fluting-like instability superimposed (see Section 2.1.2), clearly identified through these methods, more prominently with POD.

However, subtle differences are also apparent. The  $k$ - $\omega$  filtered images appear slightly smoother, likely due to the averaging process inherent in the filtering method, particularly by filtering the spatial scales. In contrast, the POD-filtered images exhibit sharper edges and finer details, reflecting the ability of POD to capture localised spatial variations within the wave pattern due to its decomposition nature.

This comparison highlights the strengths and nuances of each method. The  $k$ - $\omega$  filtering provides a direct and intuitive way to isolate specific frequency-wavenumber combinations, while POD offers a more detailed decomposition of the spatial structure of oscillations. Choosing the most suitable approach depends on the specific research goals and the desired balance between spatial and temporal resolution, with the POD offering a more advanced analysis.

### 3.3 Cross-correlation analysis: decoding relationships

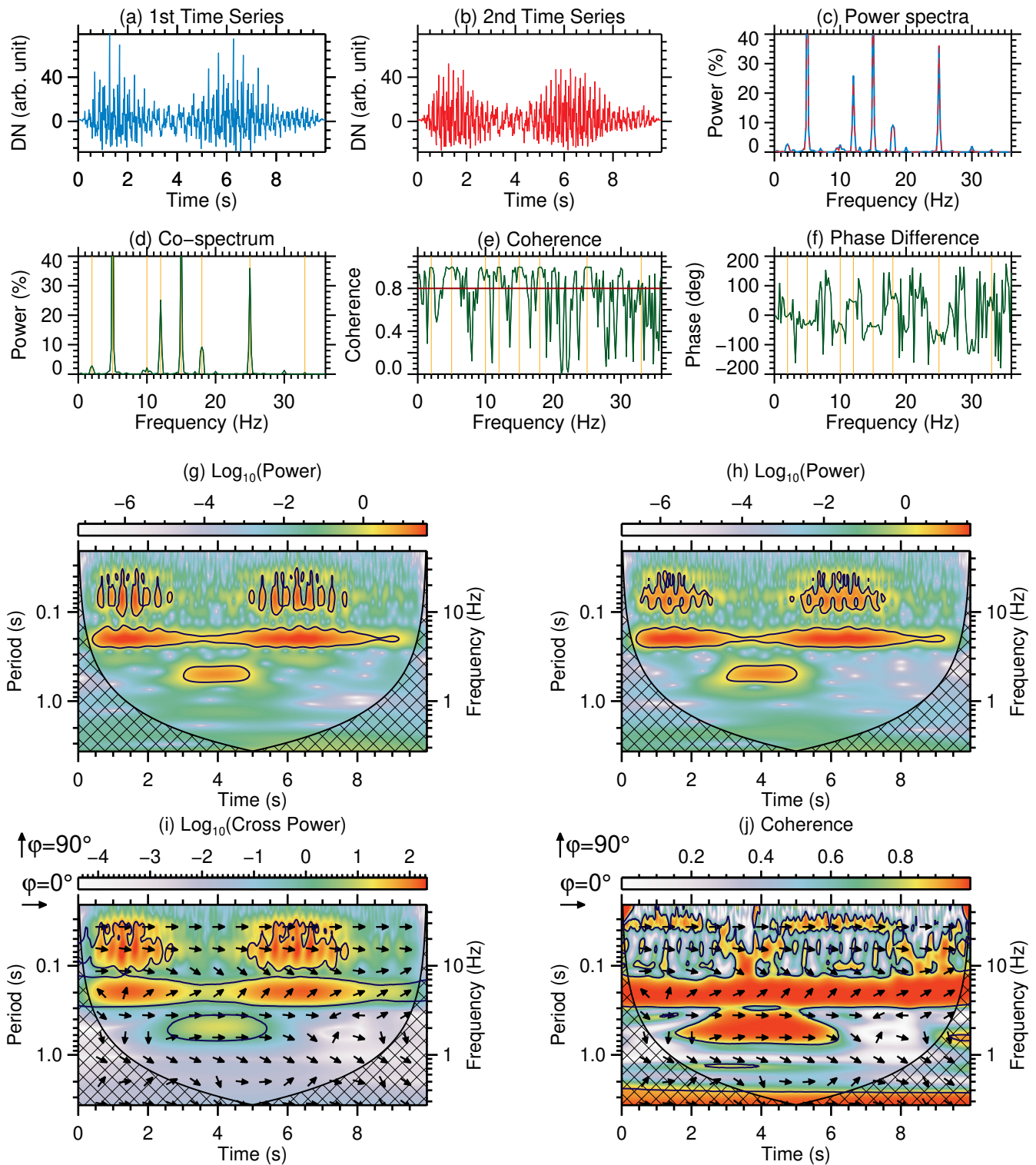
To investigate the relationships between the near-identical 1D signals (constructed as described in Section 2.1.1; see Supplementary Table S1), we applied both the FFT and wavelet-based cross-correlation techniques. These methods allow us to derive power spectra, the co-spectrum and coherence spectrum, alongside the phase shifts between the time series. This analysis simulates the scenario of observing similar wave signals at different locations or with a time delay.

Figure 6 presents a comprehensive visual comparison of the FFT and Morlet wavelet-based results. The co-spectrum clearly detects the five injected base frequencies (5, 12, 15, 18, and 25 Hz). However, as discussed in Section 3.1, the weak, transient, and quasi-periodic signals cannot be fully recovered by FFT (i.e., they fall below the noise level; see Figure 3c). The coherence spectrum varies across frequencies, with significant coherence (above 0.8, marked with a horizontal line) at specific frequencies. Interestingly, all initial waves except for the weak signal exhibit large coherence levels; the coherence of the weak signal is slightly above 0.8, thus still significant. However, there are additional large coherence levels at, e.g. 20 Hz and 30 Hz, not associated with any input frequencies in the synthetic signal's construction, rather an indication of noise (similar to those seen in Figures 3h and 3j, though the 20 Hz peak is less prominent in the latter).

The lower panels of Figure 6 display the individual Morlet wavelet power spectra, wavelet co-spectrum, and coherence. Cross-hatched regions denote the CoI, where edge effects might impact results. Phase differences in panels (i) and (j) are visualised as arrows, with rightward arrows signifying in-phase oscillations and upward arrows indicating a 90-degree phase lead in time series 1 relative to time series 2.

While the co-spectrum in both panels (d) and (i) highlights all regions where both oscillations exhibit strong power, the coherence signals reveal areas where the two time series are statistically related, regardless of power. Unlike FFT, the wavelet analysis (panels g and h) provides a 2D time-frequency representation, facilitating the identification of frequency variations across the time series.

Due to the identical nature of the signals in terms of initial frequencies and amplitudes (with phase lags introduced in the second signal), the co-spectrum would ideally recover all wave characteristics. However, the high-frequency weak signature (33 Hz), despite having relatively small power in individual and cross-power spectra, is reliably



**Fig. 6 | Cross-correlation analysis of the two synthetic 1D time series using FFT and wavelet techniques.** Panels (a) and (b) display the first and second time series, respectively. Panel (c) compares their FFT power spectra (blue: time series 1, red: time series 2). Panels (d)-(f) present the FFT-derived co-spectrum, coherence spectrum, and phase differences. Panels (g) and (h) show individual wavelet power spectra (Morlet mother wavelet). Panels (i) and (j) depict the wavelet co-spectrum and coherence map. Cross-hatched areas in wavelet panels mark the cone of influence (CoI); black contours indicate the 95% confidence level. Power is represented in log-scale in panels (g)-(i), while colours in panel (j) map coherence levels. Phase differences in (i) and (j) are visualised as arrows (right: in-phase, up: 90-degree lead for time series 1).

detected in the coherence spectrum, particularly from the wavelet. This additionally highlights the importance of combined complementary techniques in analysing oscillatory signals. Furthermore, all phase angles appearing in regions with significant power (to a 5% level) match the phase shifts introduced in the second signal relative to the first.

## 4 Applications

The methods of wave analysis detailed in this Primer find applications across a remarkably diverse range of scientific fields. From unravelling the complexities of solar oscillations to probing the dynamics of distant astrophysical objects, understanding turbulent flows in terrestrial environments, and even deciphering patterns in biological systems or financial markets, these techniques provide essential insights into the oscillatory phenomena that shape our universe and daily lives. While we explore a few representative examples in this section, the applications are far more numerous and by no means limited to those mentioned here.

### 4.1 Solar atmosphere

Wave processes are ubiquitous in the solar atmosphere and are thought to play an important role in heating the Sun's corona to millions of Kelvin – a long-standing puzzle in astrophysics<sup>167–170</sup>. Since their discovery in the 1960s, scientists have studied the creation, transportation, and energy release of these waves<sup>171–173</sup>. However, the exact ways they heat the upper solar atmosphere remain unclear<sup>174</sup>. In the solar atmosphere, multiple wave types (such as acoustic and magnetic) often interact, and these processes are further complicated by the complexities of the region where waves originate. Modern solar telescopes now provide high-resolution, multi-wavelength views of the dynamic solar atmosphere, packed with information about wave processes<sup>175,176</sup>. These waves, including Alfvén and various magnetohydrodynamic (MHD) modes, could carry enough energy to heat the solar chromosphere and corona<sup>177</sup>. To accurately measure wave properties, we need sophisticated analysis tools and must account for complex theoretical aspects, especially for the lower solar atmosphere which is governed by optically thick plasma conditions<sup>178</sup>. Recent breakthrough studies have used advanced polarimetric techniques to analyse wave-induced changes in the polarisation of light, revealing new insights about the physics of the solar atmosphere<sup>179–184</sup>. Yet, challenges remain, as the captured data is often complex, with features that evolve more quickly than our instruments can fully capture. Recently, the identification of higher-order wave modes has become possible, thanks to both the high quality of modern data and the application of advanced wave analysis methods<sup>30,40,150,185</sup>.

### 4.2 Astrophysical environments

Waves, instabilities, shocks, and turbulence mediate the conversion, transport, and dissipation of energy, governing the formation and evolution of the constituents of our Universe. Controlled lab conditions enable investigating these processes separately in different regimes. However, these phenomena are deeply coupled in astrophysics, making it difficult to disentangle them and infer the underlying physical properties via observations. Waves carry momentum and energy over vast distances before dissipating, and instabilities can profoundly alter transport, with global observable implications. Stars can act as resonant cavities for global oscillations driven by convective turbulence, which enables the study of stellar structure by carefully measuring brightness variations<sup>186–188</sup>. MHD waves turn unstable in differentially rotating accretion disks<sup>189</sup>, feeding turbulence and enabling efficient angular momentum transport and matter accretion<sup>190</sup>, powering some of the most energetic sources in the Universe<sup>191,192</sup>. Gravitational instabilities are crucial in structure formation at all scales throughout cosmic history, ranging from planets<sup>193–195</sup> to stars and stellar clusters<sup>196</sup> and galaxies to galaxy clusters<sup>197</sup>. Compact objects in binary systems can coalesce by emitting gravitational waves<sup>198,199</sup>. These signals are extremely weak and require special techniques to extract them from the background noise to infer the physical properties of black holes and neutron stars<sup>200,201</sup>. The ecosystem of wave analysis tools in this review is instrumental for acquiring and modelling astrophysical data to provide unique insights into natural phenomena that are impossible to achieve otherwise.

### 4.3 Geophysical environments

The Earth and its atmosphere resonate with a range of waves, oscillations, and instabilities, offering a rich platform for scientific investigation<sup>202–204</sup>. Geophysicists and atmospheric scientists apply advanced wave analysis techniques to understand these phenomena and their impacts on our planet<sup>205</sup>.

From seismic waves illuminating earthquake mechanics and the Earth's interior<sup>206</sup> to atmospheric waves influencing weather patterns, wave analysis drives insights across disciplines. Ocean waves and tides unveil ocean dynamics and coastal processes, while wind patterns and turbulence inform weather forecasting and climate studies. Even Earth tides offer clues about planetary elasticity and sea-level change<sup>207</sup>. These analyses are essential for natural hazard mitigation, resource management, weather prediction, and climate monitoring<sup>208</sup>. Challenges arise from complex systems and background noise<sup>209</sup>, but sophisticated analysis tools help researchers overcome them<sup>210</sup>. By carefully choosing the right analysis methods, scientists illuminate the interconnected processes that govern our planet – from its core to its turbulent atmosphere and dynamic oceans.

### 4.4 Other areas where oscillatory signals are analysed

The analysis of oscillations extends far beyond the Earth, its atmosphere, and the outer universe (including our nearest star, the Sun), playing a vital role in diverse fields across science and society. In medicine, rhythmic signals like heartbeats<sup>211</sup> and brainwaves<sup>212</sup> offer critical diagnostic information. Electrocardiograms (ECGs) track heart activity for assessing cardiovascular health<sup>213–216</sup>, while electroencephalograms (EEGs) analyse brain activity, aiding in the diagnosis of conditions like epilepsy<sup>217–220</sup> and sleep disorders<sup>221–224</sup>.

Oscillations are fundamental to the field of engineering. Analysing vibrations in structures like bridges<sup>225–227</sup>, skyscrapers<sup>228–230</sup>, aircraft<sup>231–233</sup>, and automotive engines<sup>234–236</sup> is crucial for identifying potential weaknesses and preventing failures. Similarly, electrical engineers study oscillations in circuits to design and optimise electronic systems for communication, power generation, and countless other applications<sup>237–239</sup>.

In physics, oscillatory phenomena are also ubiquitous<sup>240</sup>, from the vibrations of atoms to the behaviour of subatomic particles<sup>241,242</sup>. A notable example is the study of phonons, the quantised vibrational modes in solid-state materials<sup>243</sup>. Phonons play a crucial role in various physical properties, such as thermal conductivity, and their analysis provides insights into the microscopic behaviour of materials<sup>244–246</sup>.

Economic cycles and market fluctuations also exhibit oscillatory behaviour. Economists employ sophisticated techniques, including fundamental<sup>247–249</sup> and technical<sup>250–252</sup> analyses, to identify patterns and trends in these oscillations, facilitating forecasting and informing decision-making for businesses and governments.

These examples are just a glimpse into the ubiquity of oscillatory phenomena. Correct analysis and interpretation of these signals, which are often complex and include noise, are essential in a multitude of fields. Through understanding the hidden rhythms within these processes, we gain valuable insights leading to advancements in health, safety, technological innovation, and economic stability, to name but a few examples.

## 5 Reproducibility and data deposition

Reproducibility, the ability to independently verify research findings, is the cornerstone of reliable scientific progress<sup>253</sup>. This principle holds particular significance in wave analysis, where the study of intricate wave phenomena is inherently shaped by dataset complexities, analytical methodologies, and experimental or observational conditions.

Challenges to reproducibility in wave analysis often arise from inconsistent or non-standardised practices. Incomplete or inconsistent metadata descriptions of data origin (experimental details, simulation parameters, observational conditions), instrumentation characteristics (precision, resolution, calibration procedures), and the lack of standardised definitions for key wave properties across different subfields can hinder the interpretation, comparison, and reusability of wave data.

Transparency surrounding analysis methods is equally crucial. Beyond clearly specifying the chosen methods, researchers should explicitly acknowledge any assumptions embedded within those methods, analytical tools, or theoretical models and, whenever possible, test for sensitivities to these assumptions. Furthermore, blindly using available analysis codes (e.g., found on the web) without proper inspection poses a significant threat to reproducibility.

These codes may harbour errors or be tailored for specific scientific applications or data characteristics, leading to unreliable and irreproducible results<sup>254</sup>.

To overcome these challenges and foster a culture of reproducibility in wave analysis, researchers can adopt best practices that prioritise comprehensive and consistent metadata reporting, adhering to established standards within their respective subfields. Detailed documentation of the techniques employed, including specific code implementations, parameter selections, and the justification for those choices, is also crucial. Finally, embracing open science principles by depositing well-documented codes in accessible repositories, such as WaLSAtools (see below), allows the community to examine, validate, and build upon existing work. While open-source code sharing is a valuable practice, it is essential to critically evaluate the analysis codes. Researchers must inspect the codes, assess their suitability for their specific data and research questions, and, ideally, test the codes against established benchmarks or reference data.

The WaLSAtools repository (<https://github.com/WaLSAteam/WaLSAtools>) and its online documentation (<https://WaLSA.tools>), hosted on GitHub with its integrated version control system, represents a dynamic and expansive collection of wave analysis tools. Initiated by the Waves in the Lower Solar Atmosphere (WaLSA) Team, this open-access repository prioritises reliability and reproducibility by also providing comprehensive documentation and illustrative examples. Researchers are invited to freely access the codes and contribute to their collaborative development and advancement. The WaLSAtools repository is envisioned as a starting point, with the hope that the diverse wave analysis community will actively engage in improving and extending the existing methods and codes across various common programming languages. Code sharing not only amplifies accessibility but also sparks cross-disciplinary innovation. By adhering to these principles and embracing open science and code sharing practices, as in this code repository, the wave analysis community can strengthen reproducibility, accelerate progress in understanding intricate wave phenomena, and build upon a robust foundation of knowledge.

A selection of additional toolboxes and packages relevant to wave analysis for specific purposes are presented in Supplementary Section S12.

## 6 Limitations and optimisations

Despite their undeniable power, wave analysis methods face inherent limitations. Real-world wave data is unavoidably limited in temporal or spatial extent. This limitation influences achievable resolutions (frequency and/or wavenumber) and introduces statistical uncertainty, particularly for low-frequency wave components. The sampling frequency, which is the number of samples taken per second, directly determines the highest frequency that can be accurately represented in a discrete signal, known as the Nyquist frequency. Additionally, noise, either instrumental or inherent to the physical system, can mask true wave signatures or introduce artefacts. Techniques such as noise filtering, spectral smoothing, and robust statistical methods are essential for mitigating these effects. Establishing confidence intervals through statistical or Monte Carlo analysis can help quantify uncertainties and refine the identification of reliable features. It is crucial to remember that a signal is a noisy representation of a physical process, not the process itself. A selection of noise reduction and filtering techniques are discussed in Supplementary Section S5.

One point to consider in PSD estimation is that a simple FFT, for instance, is often a biased estimator due to the variance in each spectral bin<sup>255</sup>. This variance does not decrease with increasing length of the time series, as this alters the frequency resolution. Averaging over contiguous frequency bins or over multiple spectra of the same process can mitigate this issue<sup>163</sup>. However, the former approach inevitably reduces frequency resolution, while the latter may not always be feasible.

Non-stationary processes pose another challenge. Many techniques assume stationarity, meaning the signal's statistical properties remain constant over time. Yet, natural waves often exhibit non-stationary behaviour, with changes in frequencies, amplitudes, or propagation characteristics. Techniques like wavelet transforms or adaptive filtering are crucial for analysing them, allowing researchers to track the evolution of wave properties over time, offering insights into the time evolution of wave properties, as well as the ability to detect and characterise abrupt changes like shocks (see Supplementary Section S11).

Furthermore, wave analysis methods often rest on simplifying assumptions that might not fully capture the involved, often non-linear, dynamics of real-world systems. Advanced techniques like EEMD and HHT offer potential insights into these complexities. However, interpreting results from these methods requires careful consideration of underlying assumptions and limitations. Notably, techniques like EEMD (or EMD) primarily decompose signals into components; identifying periodicities then necessitates the application of other methods, such as FFT or wavelet analysis. Optimisation can be achieved by leveraging a combination of techniques. Addressing limitations through data preprocessing, sensitivity analysis, and the exploration of specialised wave analysis methods, [including variational methods for signal decomposition and parameter estimation](#)<sup>256</sup>, will enhance the accuracy and reliability of findings. Investments in improved instrumentation, the development of robust techniques for handling noise and non-stationarity, and the careful integration of domain expertise into the interpretation of results can provide better insights into wave phenomena.

## 7 Outlook

The study of wave phenomena holds immense potential for unlocking a deeper understanding of our world and accelerating transformative discoveries across diverse scientific fields. The increasing sophistication of analytical techniques, coupled with the continuous evolution of data acquisition and computational power, positions the scientists to tackle ever more complex challenges.

As wave analysis delves deeper into intricate natural systems, researchers will inevitably encounter challenges that demand the development and refinement of specialised techniques. While linear wave theory offers powerful tools, real-world systems often exhibit non-linear behaviours, wave-wave interactions, and complex couplings that necessitate advanced approaches. The continued development of non-linear analysis methods, integration of machine learning, and exploration of techniques tailored to specific subfields of wave analysis will be crucial for accurately modelling and interpreting these complex systems. In this regard, phase-space techniques like recurrence quantification analysis (RQA)<sup>257</sup> may offer new opportunities<sup>257–262</sup>, which may be essential in uncovering details about the origin of the underlying dynamics.

Another challenge is the increasing availability of massive and high-dimensional datasets from sophisticated instrumentation and large-scale observational campaigns. This is particularly evident in physical systems involving diverse time scales separated by orders of magnitude, which require high cadence and long time series simultaneously. This abundance of data presents both an opportunity and a challenge, as it necessitates the development of efficient algorithms, statistical methods for handling noisy or incomplete data, and dimensionality reduction techniques to extract meaningful insights. One promising example in this regard is the Incremental PCA (IPCA)<sup>263,264</sup>, formally equivalent to PCA but able to process very large batches of data. Interestingly, while designed to address a limitation of PCA, IPCA enables the additional opportunity to process time series with near-real-time data incrementally<sup>265</sup>. The detection of faint signals embedded in noise is a persistent challenge that necessitates efficient methods to separate signals from noise. Techniques like Singular Spectrum Analysis (SSA)<sup>266</sup>, PCA<sup>267</sup>, and Karhunen-Loève decomposition<sup>268,269</sup> offer potential solutions. Lastly, while waves and oscillations are ubiquitous across disciplines, terminology and analysis approaches can vary between fields. Cross-disciplinary knowledge transfer, the sharing of best practices, and the development of standardised, accessible, and reusable tools are vital to unify and accelerate progress in wave analysis.

### 7.1 Future directions

Several exciting and promising directions hold the potential to revolutionise wave analysis in the coming decade. The intelligent integration of machine learning with domain expertise could unlock new ways of analysing complex wave phenomena, identifying hidden patterns, and potentially discovering novel wave behaviours<sup>270–274</sup>. Developing robust, interpretable machine learning models, [potentially incorporating regularisation techniques to prevent overfitting and improve generalisation](#)<sup>275</sup>, remains a promising avenue of research in wave analysis<sup>276,277</sup>.

Advances in high-performance computing, cloud-based resources, and distributed systems empower researchers to analyse larger datasets, simulate intricate scenarios, and explore computationally-demanding methods, paving the way for breakthroughs in understanding involved wave phenomena.

The interconnected nature of wave phenomena calls for collaborative efforts across disciplines. International research initiatives, shared repositories of data and tools (like WaLSAtools), and interdisciplinary workshops will accelerate innovation and ensure that knowledge and expertise are accessible to the broader wave analysis community. The future of wave analysis is an evolving landscape, with the potential to transform our understanding of phenomena that shape the physical world. By actively building upon existing analysis tools, exploring novel techniques, harnessing computational advancements, and fostering a collaborative spirit, researchers are poised to unlock significant discoveries and push the boundaries of knowledge across all disciplines where waves play a fundamental role.

## Code availability

The synthetic datasets and codes used for the wave analyses presented in this Primer, including the generation of all displayed figures, are publicly available via the WaLSAtools repository on GitHub (<https://github.com/WaLSAteam/WaLSAtools>), archived at Zenodo with the DOI [TBD]. Further information and documentation are available online at <https://WaLSA.tools>.

## References

1. Shawhan, S. D. Magnetospheric plasma wave research 1975-1978. *Rev. Geophys. Space Phys.* **17**, 705–724 (1979).  
**Comprehensive framework for understanding and analysing plasma waves, paving the way for further research into their generation, propagation, and impact on particle populations.**
2. Narayanan, A. S. & Saha, S. K. *Waves and Oscillations in Nature: An Introduction* (CRC Press, 2015).  
**A seminal textbook that lays the groundwork for understanding wave propagation and energy transport across diverse mediums, offering a framework for identifying and classifying wave modes across scientific disciplines.**
3. Nakariakov, V. M. *et al.* Magnetohydrodynamic Oscillations in the Solar Corona and Earth's Magnetosphere: Towards Consolidated Understanding. *Space Sci. Rev.* **200**, 75–203 (2016).
4. Boswell, R. Plasma waves in the laboratory. *Adv. Space Res.* **1**, 331–345 (1981).
5. Hartmann, J. On a New Method for the Generation of Sound-Waves. *Phys. Rev.* **20**, 719–727 (1922).
6. Perov, P., Johnson, W. & Perova-Mello, N. The physics of guitar string vibrations. *Am. J. Phys.* **84**, 38–43 (2016).
7. Holthuijsen, L. H. *Waves in Oceanic and Coastal Waters* (Cambridge University Press, 2007).
8. Schutz, B. F. Determining the Hubble constant from gravitational wave observations. *Nature* **323**, 310–311 (1986).
9. Bogdan, T. J. Sunspot Oscillations: A Review - (Invited Review). *Sol. Phys.* **192**, 373–394 (2000).
10. Jess, D. B. *et al.* Multiwavelength Studies of MHD Waves in the Solar Chromosphere. An Overview of Recent Results. *Space Sci. Rev.* **190**, 103–161 (2015).
11. Kholenko, E. & Collados, M. Oscillations and Waves in Sunspots. *Living Rev. Sol. Phys.* **12**, 6 (2015).
12. Sheriff, R. E. & Geldart, L. P. *Exploration seismology* (Cambridge university press, 1995).
13. Shearer, P. M. *Introduction to seismology* (Cambridge university press, 2019).
14. Rost, S. & Thomas, C. Array seismology: Methods and applications. *Rev. geophysics* **40**, 2–1 (2002).
15. Jin, S., Jin, R. & Liu, X. *GNSS atmospheric seismology* (Springer, 2019).
16. Hilterman, F. J. *Seismic amplitude interpretation* (Society of Exploration Geophysicists and the European Association of Geoscientists and Engineers, 2001).
17. Gee, L. S. & Jordan, T. H. Generalized seismological data functionals. *Geophys. J. Int.* **111**, 363–390 (1992).

18. Cochard, A. *et al.* *Rotational Motions in Seismology: Theory, Observation, Simulation*, 391–411 (Springer Berlin Heidelberg, Berlin, Heidelberg, 2006).
19. Banerjee, D., Erdélyi, R., Oliver, R. & O’Shea, E. Present and Future Observing Trends in Atmospheric Magnetoseismology. *Sol. Phys.* **246**, 3–29 (2007).
20. Verth, G. & Erdélyi, R. Effect of longitudinal magnetic and density inhomogeneity on transversal coronal loop oscillations. *Astron. Astrophys.* **486**, 1015–1022 (2008).
21. Verth, G., Goossens, M. & He, J. S. Magnetoseismological Determination of Magnetic Field and Plasma Density Height Variation in a Solar Spicule. *Astrophys. J. Lett.* **733**, L15 (2011).
22. Kuridze, D. *et al.* Characteristics of Transverse Waves in Chromospheric Mottles. *Astrophys. J.* **779**, 82 (2013).
23. Jaroszewicz, L. R. *et al.* Review of the Usefulness of Various Rotational Seismometers with Laboratory Results of Fibre-Optic Ones Tested for Engineering Applications. *Sensors* **16**, 2161 (2016).
24. Lindsey, N. J. & Martin, E. R. Fiber-Optic Seismology. *Annu. Rev. Earth Planet. Sci.* **49**, 309–336 (2021).
25. Roberts, B. *MHD Waves in the Solar Atmosphere* (Cambridge University Press, 2019).  
**Comprehensive text on magnetohydrodynamic (MHD) waves in the solar atmosphere providing a detailed theoretical foundation and observational context for understanding oscillatory phenomena in this complex environment, making it essential for researchers in the field of wave studies.**
26. Bogdan, T. J. *et al.* Waves in the Magnetized Solar Atmosphere. II. Waves from Localized Sources in Magnetic Flux Concentrations. *Astrophys. J.* **599**, 626–660 (2003).
27. Cally, P. S. & Kholenko, E. Fast-to-Alfvén Mode Conversion and Ambipolar Heating in Structured Media. I. Simplified Cold Plasma Model. *Astrophys. J.* **885**, 58 (2019).
28. Fourier. Allgemeine Bemerkungen über die Temperaturen des Erdkörpers und des Raumes, in welchem sich die Planeten bewegen. *Annalen der Physik* **76**, 319–335 (1824).  
**A pioneering work laying the foundation for the mathematical theory of heat, introducing the concept of representing time series as the combination of sinusoids of varying frequency, where this powerful tool (now known as the Fourier transform) is used to analyse periodic phenomena in diverse fields.**
29. Nakariakov, V. M., Pascoe, D. J. & Arber, T. D. Short Quasi-Periodic MHD Waves in Coronal Structures. *Space Sci. Rev.* **121**, 115–125 (2005).
30. Stangalini, M. *et al.* Large scale coherent magnetohydrodynamic oscillations in a sunspot. *Nat. Commun.* **13**, 479 (2022).
31. Morlet, J., Arens, G., Fourgeau, E. & Gild, D. Wave propagation and sampling theory—part i: Complex signal and scattering in multilayered media. *Geophysics* **47**, 203–221 (1982).
32. Huang, N. E. *et al.* The empirical mode decomposition and the Hilbert spectrum for nonlinear and non-stationary time series analysis. *Proc. Royal Soc. Lond. Ser. A* **454**, 903–998 (1998).  
**A groundbreaking paper introducing the Hilbert-Huang Transform (HHT), a versatile method particularly well-suited for analysing nonlinear and non-stationary time series data common in real-world applications.**
33. Moca, V. V., Bârzan, H., Nagy-Dăbâcan, A. & Mureşan, R. C. Time-frequency super-resolution with superlets. *Nat. Commun.* **12**, 337 (2021).
34. Zhang, L. *et al.* Pacific Warming Pattern Diversity Modulated by Indo-Pacific Sea Surface Temperature Gradient. *Geophys. Res. Lett.* **48**, e95516 (2021).
35. Smith, S. W. *The Scientist and Engineer’s Guide to Digital Signal Processing* (California Technical Pub, 1997).

36. Grinsted, A., Moore, J. C. & Jevrejeva, S. Application of the cross wavelet transform and wavelet coherence to geophysical time series. *Nonlinear Process. Geophys.* **11**, 561–566 (2004).  
**A comprehensive study detailing practical tools for cross-wavelet transform and wavelet coherence analysis, expanding the capabilities of wavelet analysis for investigating relationships between two time series.**
37. Jess, D. B. *et al.* An Inside Look at Sunspot Oscillations with Higher Azimuthal Wavenumbers. *Astrophys. J.* **842**, 59 (2017).
38. Singh, P., Joshi, S. D., Patney, R. K. & Saha, K. The fourier decomposition method for nonlinear and non-stationary time series analysis. *Proc. Royal Soc. A: Math. Phys. Eng. Sci.* **473**, 20160871 (2017).
39. Stangalini, M. *et al.* A novel approach to identify resonant MHD wave modes in solar pores and sunspot umbrae:  $B - \omega$  analysis. *Astron. Astrophys.* **649**, A169 (2021).
40. Albidah, A. B. *et al.* Magnetohydrodynamic Wave Mode Identification in Circular and Elliptical Sunspot Umbrae: Evidence for High-order Modes. *Astrophys. J.* **927**, 201 (2022).
41. Ivezić, Ž., Connolly, A. J., VanderPlas, J. T. & Gray, A. *Statistics, Data Mining, and Machine Learning in Astronomy. A Practical Python Guide for the Analysis of Survey Data, Updated Edition* (2020).
42. Kantz, H. & Schreiber, T. *Nonlinear time series analysis* (Cambridge university press, 2003).
43. Donoghue, T., Schaworonkow, N. & Voytek, B. Methodological considerations for studying neural oscillations. *Eur. J. Neurosci.* (2021).
44. Hiramatsu, T., Kawasaki, M. & Saikawa, K. On the estimation of gravitational wave spectrum from cosmic domain walls. *J. Cosmol. Astropart. Phys.* **2014**, 031–031 (2014).
45. Buckheit, J. B. & Donoho, D. L. *Wavelab and reproducible research* (Springer, 1995).
46. Ivie, P. & Thain, D. Reproducibility in scientific computing. *ACM Comput. Surv. (CSUR)* **51**, 1–36 (2018).
47. Polikar, R. *et al.* The wavelet tutorial (1996).
48. Boashash, B. Estimating and interpreting the instantaneous frequency of a signal. i. fundamentals. *Proc. IEEE* **80**, 520–538 (1992).
49. Huang, N. E. New method for nonlinear and nonstationary time series analysis: empirical mode decomposition and Hilbert spectral analysis. In Szu, H. H., Vetterli, M., Campbell, W. J. & Buss, J. R. (eds.) *Wavelet Applications VII*, vol. 4056 of *Society of Photo-Optical Instrumentation Engineers (SPIE) Conference Series*, 197–209 (2000).
50. Mandic, D. P., Ur Rehman, N., Wu, Z. & Huang, N. E. Empirical mode decomposition-based time-frequency analysis of multivariate signals: The power of adaptive data analysis. *IEEE signal processing magazine* **30**, 74–86 (2013).
51. Oppenheim, A. V. & Schaffer, R. W. *Digital signal processing* (Prentice-Hall, 1975).
52. Roberts, R. A. & Mullis, C. T. *Digital signal processing* (Addison-Wesley Longman Publishing Co., Inc., 1987).
53. Hayes, M. H. *Statistical Digital Signal Processing and Modeling* (John Wiley & Sons, 1996).
54. Proakis, J. G. & Manolakis, D. G. *Digital signal processing: principles, algorithms, and applications* (1996).
55. Ifeachor, E. C. & Jervis, B. W. *Digital signal processing: a practical approach* (Pearson Education, 2002).
56. Blahut, R. E. *Fast algorithms for signal processing* (Cambridge University Press, 2010).
57. Diniz, P. S., Da Silva, E. A. & Netto, S. L. *Digital signal processing: system analysis and design* (Cambridge University Press, 2010).

58. Gold, B., Morgan, N. & Ellis, D. *Speech and audio signal processing: processing and perception of speech and music* (John Wiley & Sons, 2011).
59. Alexander, T. S. *Adaptive signal processing: theory and applications* (Springer Science & Business Media, 2012).
60. Karl, J. H. *An introduction to digital signal processing* (Elsevier, 2012).
61. Boashash, B. *Time-frequency signal analysis and processing: a comprehensive reference* (Academic press, 2015).
62. Zhang, X.-D. *Modern Signal Processing* (De Gruyter, Berlin, Boston, 2023).
63. Rangayyan, R. M. & Krishnan, S. *Biomedical signal analysis* (John Wiley & Sons, 2024).
64. Press, W. H., Teukolsky, S. A., Vetterling, W. T. & Flannery, B. P. *Numerical Recipes: The Art of Scientific Computing* (Cambridge University Press, USA, 2007), 3 edn.  
**A cornerstone resource for scientific computing, offering accessible implementations and explanations of fundamental signal processing techniques, including Fourier methods and filtering, which are crucial for wave analysis.**
65. Bevington, P. R. & Robinson, D. K. *Data reduction and error analysis for the physical sciences* (McGraw-Hill Education, 2003).
66. Hughes, P. A., Aller, H. D. & Aller, M. F. The University of Michigan Radio Astronomy Data Base. I. Structure Function Analysis and the Relation between BL Lacertae Objects and Quasi-stellar Objects. *Astrophys. J.* **396**, 469 (1992).
67. Frisch, U. *Turbulence. The legacy of A.N. Kolmogorov* (Cambridge University Press, 1995).
68. Kozłowski, S. Revisiting Stochastic Variability of AGNs with Structure Functions. *Astrophys. J.* **826**, 118 (2016).
69. Wu, Z., Huang, N., Long, S. & Peng, C. On the trend, detrending, and variability of nonlinear and nonstationary time series. *Proc. Natl. Acad. Sci. United States Am.* **104**, 14889–14894 (2007).  
**This paper proposes a novel and intrinsic definition of trend for non-stationary and non-linear time series, advocating for the use of the Empirical Mode Decomposition (EMD) technique and providing a confidence limit for its results.**
70. Alvarez-Ramirez, J., Rodriguez, E. & Carlos Echeverría, J. Detrending fluctuation analysis based on moving average filtering. *Phys. A: Stat. Mech. its Appl.* **354**, 199–219 (2005).
71. Bashan, A., Bartsch, R., Kantelhardt, J. W. & Havlin, S. Comparison of detrending methods for fluctuation analysis. *Phys. A: Stat. Mech. its Appl.* **387**, 5080–5090 (2008).
72. SHAO, Y.-H., GU, G.-F., JIANG, Z.-Q. & ZHOU, W.-X. Effects of polynomial trends on detrending moving average analysis. *Fractals* **23**, 1550034 (2015).
73. Song, P. & Russell, C. T. Time series data analyses in space physics. *Space Sci. Rev.* **87**, 387–463 (1999).
74. Misaridis, T. & Jensen, J. Use of modulated excitation signals in medical ultrasound. part ii: design and performance for medical imaging applications. *IEEE Transactions on Ultrason. Ferroelectr. Freq. Control.* **52**, 192–207 (2005).
75. Hardy, É., Levy, A., Métris, G., Rodrigues, M. & Touboul, P. Determination of the equivalence principle violation signal for the microscope space mission: Optimization of the signal processing. *Space Sci. Rev.* **180**, 177–191 (2013).
76. Prabhu, K. M. M. *Window functions and their applications in signal processing* (CRC Press, Boca Raton, 2018).  
**An in-depth exploration of window functions and their applications in various signal processing domains,**

**including digital spectral analysis, offering valuable guidance for researchers working with oscillatory signals.**

77. Coddington, I., Newbury, N. & Swann, W. Dual-comb spectroscopy. *Optica* **3**, 414–426 (2016).
78. Chen, C.-T., Chang, L.-M. & Loh, C.-H. A review of spectral analysis for low-frequency transient vibrations. *J. Low Freq. Noise, Vib. Active Control.* **40**, 656–671 (2021).  
**This study examines the impact of data length and zero-padding on spectral analysis of low-frequency vibrations, highlighting the importance of appropriate techniques and parameters for reliable and comparable results.**
79. Eriksson, A. I. Spectral Analysis. *ISSI Sci. Reports Ser.* **1**, 5–42 (1998).
80. Neild, S., McFadden, P. & Williams, M. A review of time-frequency methods for structural vibration analysis. *Eng. Struct.* **25**, 713–728 (2003).
81. Adorf, H. M. Interpolation of Irregularly Sampled Data Series—A Survey. In Shaw, R. A., Payne, H. E. & Hayes, J. J. E. (eds.) *Astronomical Data Analysis Software and Systems IV*, vol. 77 of *Astronomical Society of the Pacific Conference Series*, 460 (1995).
82. Piroddi, R. & Petrou, M. Analysis of irregularly sampled data: A review. In *Advances in Imaging and Electron Physics*, vol. 132 of *Advances in Imaging and Electron Physics*, 109–165 (Elsevier, 2004).
83. Lepot, M., Aubin, J.-B. & Clemens, F. H. Interpolation in time series: An introductory overview of existing methods, their performance criteria and uncertainty assessment. *Water* **9** (2017).  
**A review article comprehensively exploring interpolation methods for filling gaps in time series, discussing criteria for evaluating their effectiveness, and highlighting the often overlooked aspect of uncertainty quantification in interpolation and extrapolation.**
84. Groos, J., Bussat, S. & Ritter, J. Performance of different processing schemes in seismic noise cross-correlations. *Geophys. J. Int.* **188**, 498–512 (2012).
85. Kocaoğlu, A. H. & Long, L. T. A Review of Time-Frequency Analysis Techniques for Estimation of Group Velocities. *Seismol. Res. Lett.* **64**, 157–167 (1993).
86. Kreis, T. Digital holographic interference-phase measurement using the Fourier-transform method. *J. Opt. Soc. Am. A* **3**, 847–855 (1986).
87. Shynk, J. J. Frequency-domain and multirate adaptive filtering. *IEEE Signal Process. Mag.* **9**, 14–37 (1992).
88. O’Leary, S. V. Real-time image processing by degenerate four-wave mixing in polarization sensitive dye-impregnated polymer films. *Opt. Commun.* **104**, 245–250 (1994).
89. Devaux, F. & Lantz, E. Transfer function of spatial frequencies in parametric image amplification: experimental analysis and application to picosecond spatial filtering. *Opt. Commun.* **114**, 295–300 (1995).
90. Vaezi, Y. & Van der Baan, M. Comparison of the STA/LTA and power spectral density methods for microseismic event detection. *Geophys. J. Int.* **203**, 1896–1908 (2015).
91. Cooley, J. W. & Tukey, J. W. An algorithm for the machine calculation of complex fourier series. *Math. Comput.* **19**, 297–301 (1965).
92. Bracewell, R. *The Fourier Transform and its applications* (1965).
93. Brigham, E. O. *The fast Fourier transform and its applications* (Prentice-Hall, Inc., 1988).
94. Duhamel, P. & Vetterli, M. Fast fourier transforms: A tutorial review and a state of the art. *Signal Process.* **19**, 259–299 (1990).
95. Bracewell, R. N. *The Fourier transform and its applications* (2000).
96. Bloomfield, P. *Fourier analysis of time series: an introduction* (Wiley, 1976).

97. Sundararajan, D. *The discrete Fourier transform: theory, algorithms and applications* (World Scientific, 2001).
98. Lomb, N. R. Least-Squares Frequency Analysis of Unequally Spaced Data. *Astrophys. Space Sci.* **39**, 447–462 (1976).
99. Scargle, J. D. Studies in astronomical time series analysis. II. Statistical aspects of spectral analysis of unevenly spaced data. *Astrophys. J.* **263**, 835–853 (1982).
100. Ruf, T. The lomb-scargle periodogram in biological rhythm research: analysis of incomplete and unequally spaced time-series. *Biol. Rhythm. Res.* **30**, 178–201 (1999).
101. Glynn, E. F., Chen, J. & Mushegian, A. R. Detecting periodic patterns in unevenly spaced gene expression time series using lomb–scargle periodograms. *Bioinformatics* **22**, 310–316 (2006).
102. VanderPlas, J. T. Understanding the Lomb-Scargle Periodogram. *Astrophys. J. Suppl. Ser.* **236**, 16 (2018).
103. Zechmeister, M. & Kürster, M. The generalised Lomb-Scargle periodogram. A new formalism for the floating-mean and Keplerian periodograms. *Astron. Astrophys.* **496**, 577–584 (2009).
104. Bretthorst, G. L. *Bayesian Spectrum Analysis and Parameter Estimation, Lecture Notes in Statistics* (Berlin: Springer, 1998).
105. Gregory, P. C. A Bayesian revolution in spectral analysis. In Mohammad-Djafari, A. (ed.) *Bayesian Inference and Maximum Entropy Methods in Science and Engineering*, vol. 568 of *American Institute of Physics Conference Series*, 557–568 (AIP, 2001).
106. Bretthorst, G. L. Generalizing the Lomb-Scargle periodogram. In Mohammad-Djafari, A. (ed.) *Bayesian Inference and Maximum Entropy Methods in Science and Engineering*, vol. 568 of *American Institute of Physics Conference Series*, 241–245 (AIP, 2001).
107. Babu, P. & Stoica, P. Spectral analysis of nonuniformly sampled data – a review. *Digit. Signal Process.* **20**, 359–378 (2010).
108. Daubechies, I. The wavelet transform, time-frequency localization and signal analysis. *IEEE Transactions on Inf. Theory* **36**, 961–1005 (1990).
109. Lee, D. T. & Yamamoto, A. Wavelet analysis: theory and applications. *Hewlett Packard journal* **45**, 44–44 (1994).
110. Torrence, C. & Compo, G. P. A Practical Guide to Wavelet Analysis. *Bull. Am. Meteorol. Soc.* **79**, 61–78 (1998).  
**A seminal work on wavelet analysis that provides a practical guide, a step-by-step approach, accessible explanations of key concepts, and novel statistical significance tests.**
111. Walnut, D. F. *An Introduction to Wavelet Analysis* (Birkhäuser Boston, MA, 2001).
112. Starck, J.-L. & Murtagh, F. *Astronomical Image and Data Analysis* (2006).
113. Percival, D. B. & Walden, A. T. *Wavelet methods for time series analysis*, vol. 4 (Cambridge university press, 2000).
114. Aguiar-Conraria, L. & Soares, M. J. The continuous wavelet transform: Moving beyond uni- and bivariate analysis. *J. Econ. Surv.* **28**, 344–375 (2013).
115. Cohen, M. X. A better way to define and describe morlet wavelets for time-frequency analysis. *NeuroImage* **199**, 81–86 (2019).
116. Singh, A., Rawat, A. & Raghuthaman, N. Mexican hat wavelet transform and its applications. *Methods mathematical modelling computation for complex systems* 299–317 (2022).
117. Afifi, M. *et al.* Paul wavelet-based algorithm for optical phase distribution evaluation. *Opt. communications* **211**, 47–51 (2002).

118. Rowe, A. C. & Abbott, P. C. Daubechies wavelets and mathematica. *Comput. Phys.* **9**, 635–648 (1995).
119. Lepik, Ü. & Hein, H. *Haar Wavelets*, 7–20 (Springer International Publishing, Cham, 2014).
120. Ngui, W. K., Leong, M. S., Hee, L. M. & Abdelrhman, A. M. Wavelet analysis: Mother wavelet selection methods. *Appl. Mech. Mater.* **393**, 953–958 (2013).
121. Wu, S. & Liu, Q. Some problems on the global wavelet spectrum. *J. Ocean. Univ. China* **4**, 398–402 (2005). **This paper highlights potential biases in the global wavelet spectrum, demonstrating that it can overestimate the power of longer periods in certain scenarios, and advocates for careful interpretation and verification of results using complementary methods.**
122. Rilling, G., Flandrin, P., Goncalves, P. *et al.* On empirical mode decomposition and its algorithms. In *IEEE-EURASIP workshop on nonlinear signal and image processing*, vol. 3, 8–11 (Grado: IEEE, 2003).
123. Zeiler, A. *et al.* Empirical mode decomposition-an introduction. In *The 2010 international joint conference on neural networks (IJCNN)*, 1–8 (IEEE, 2010).
124. Wu, Z. & Huang, N. E. Ensemble empirical mode decomposition: a noise-assisted data analysis method. *Adv. adaptive data analysis* **1**, 1–41 (2009).
125. Huang, N. E. *et al.* A confidence limit for the empirical mode decomposition and hilbert spectral analysis. *Proc. Royal Soc. London. Ser. A: Math. Phys. Eng. Sci.* **459**, 2317–2345 (2003).
126. Huang, N. E., Shen, Z. & Long, S. R. A new view of nonlinear water waves: The Hilbert Spectrum. *Annu. Rev. Fluid Mech.* **31**, 417–457 (1999).
127. Huang, N. E. & Wu, Z. A review on Hilbert-Huang transform: Method and its applications to geophysical studies. *Rev. Geophys.* **46**, RG2006 (2008).
128. Welch, P. The use of fast fourier transform for the estimation of power spectra: A method based on time averaging over short, modified periodograms. *IEEE Transactions on Audio Electroacoustics* **15**, 70–73 (1967). **This paper introduced an influential method for power spectrum estimation using the Fast Fourier Transform (FFT) — the Welch approach — achieving computational efficiency and facilitating the analysis of non-stationary signals by segmenting the data and averaging modified periodograms.**
129. Baba, T. Time-frequency analysis using short time fourier transform. *The Open Acoust. J.* **5** (2012).
130. Jwo, D.-J., Wu, I.-H. & Chang, Y. Windowing design and performance assessment for mitigation of spectrum leakage. *E3S Web Conf.* **94**, 03001 (2019).
131. Wigner, E. On the quantum correction for thermodynamic equilibrium. *Phys. review* **40**, 749 (1932).
132. Ville, J. Theorie et application dela notion de signal analysis. *Câbles et transmissions* **2**, 61–74 (1948).
133. Claasen, T. & Mecklenbräuker, W. Time-frequency signal analysis. *Philips J. Res.* **35**, 372–389 (1980).
134. Boashash, B. & Black, P. An efficient real-time implementation of the wigner-ville distribution. *IEEE transactions on acoustics, speech, signal processing* **35**, 1611–1618 (1987).
135. Xu, C., Wang, C. & Liu, W. Nonstationary vibration signal analysis using wavelet-based time–frequency filter and wigner–ville distribution. *J. Vib. Acoust.* **138**, 051009 (2016).
136. Weinbub, J. & Ferry, D. Recent advances in wigner function approaches. *Appl. Phys. Rev.* **5** (2018).
137. Daubechies, I., Lu, J. & Wu, H.-T. Synchrosqueezed wavelet transforms: An empirical mode decomposition-like tool. *Appl. computational harmonic analysis* **30**, 243–261 (2011).
138. Daubechies, I. & Maes, S. A nonlinear squeezing of the continuous wavelet transform based on auditory nerve models. In *Wavelets in medicine and biology*, 527–546 (Routledge, 2017).
139. Bing, P. *et al.* Synchrosqueezing transform based on frequency-domain gaussian-modulated linear chirp model for seismic time–frequency analysis. *Mathematics* **11** (2023).

140. Stockwell, R. G., Mansinha, L. & Lowe, R. Localization of the complex spectrum: the s transform. *IEEE transactions on signal processing* **44**, 998–1001 (1996).
141. Gabor, D. Theory of communication. part 1: The analysis of information. *J. Inst. Electr. Eng. III: radio communication engineering* **93**, 429–441 (1946).
142. Choi, H.-I. & Williams, W. J. Improved time-frequency representation of multicomponent signals using exponential kernels. *IEEE Transactions on Acoust. Speech, Signal Process.* **37**, 862–871 (1989).
143. Zhao, Y., Atlas, L. E. & Marks, R. J. The use of cone-shaped kernels for generalized time-frequency representations of nonstationary signals. *IEEE Transactions on Acoust. Speech, Signal Process.* **38**, 1084–1091 (1990).
144. Jafarzadeh, S. *et al.* An overall view of temperature oscillations in the solar chromosphere with ALMA. *Philos. Transactions Royal Soc. Lond. Ser. A* **379**, 20200174 (2021).
145. Duvall, J., T. L., Harvey, J. W., Libbrecht, K. G., Popp, B. D. & Pomerantz, M. A. Frequencies of solar p-mode oscillations. *Astrophys. J.* **324**, 1158 (1988).
146. Krijger, J. M. *et al.* Dynamics of the solar chromosphere. III. Ultraviolet brightness oscillations from TRACE. *Astron. Astrophys.* **379**, 1052–1082 (2001).
147. Rutten, R. J. & Krijger, J. M. Dynamics of the solar chromosphere IV. Evidence for atmospheric gravity waves from TRACE. *Astron. Astrophys.* **407**, 735–740 (2003).
148. Fleck, B. *et al.* Acoustic-gravity wave propagation characteristics in three-dimensional radiation hydrodynamic simulations of the solar atmosphere. *Philos. Transactions Royal Soc. Lond. Ser. A* **379**, 20200170 (2021).
149. Lumley, J. L. The structure of inhomogeneous turbulent flows. *Atmospheric turbulence radio wave propagation* (1967).  
**A comprehensive review article that explores the application of modal decomposition techniques, including Proper Orthogonal Decomposition (POD), for analysing fluid flows and extracting coherent structures.**
150. Albidah, A. B. *et al.* Proper orthogonal and dynamic mode decomposition of sunspot data. *Philos. Transactions Royal Soc. Lond. Ser. A* **379**, 20200181 (2021).
151. Abdi, H. & Williams, L. J. Principal component analysis. *Wiley interdisciplinary reviews: computational statistics* **2**, 433–459 (2010).
152. Greenacre, M. *et al.* Principal component analysis. *Nat. Rev. Methods Primers* **2**, 100 (2022).
153. Sirovich, L. Turbulence and the dynamics of coherent structures. Part 1: Coherent structures. *Q. Appl. Math.* **45**, 561–590 (1987).
154. Stewart, G. W. On the early history of the singular value decomposition. *SIAM review* **35**, 551–566 (1993).
155. Higham, J., Brevis, W. & Keylock, C. Implications of the selection of a particular modal decomposition technique for the analysis of shallow flows. *J. Hydraul. Res.* **56**, 796–805 (2018).
156. Higham, J., Brevis, W., Keylock, C. & Safarzadeh, A. Using modal decompositions to explain the sudden expansion of the mixing layer in the wake of a groyne in a shallow flow. *Adv. Water Resour.* **107**, 451–459 (2017).
157. Liao, Z.-M. *et al.* Reduced-order variational mode decomposition to reveal transient and non-stationary dynamics in fluid flows. *J. Fluid Mech.* **966**, A7 (2023).
158. Schiavo, L. A. C. A., Wolf, W. R. & Azevedo, J. L. F. Turbulent kinetic energy budgets in wall bounded flows with pressure gradients and separation. *Phys. Fluids* **29**, 115108 (2017).
159. Rowley, C. W., Colonius, T. & Murray, R. M. Model reduction for compressible flows using pod and galerkin projection. *Phys. D: Nonlinear Phenom.* **189**, 115–129 (2004).

160. Freund, J. B. & Colonius, T. Turbulence and sound-field pod analysis of a turbulent jet. *Int. J. Aeroacoustics* **8**, 337–354 (2009).
161. Ribeiro, J. H. M. & Wolf, W. R. Identification of coherent structures in the flow past a NACA0012 airfoil via proper orthogonal decomposition. *Phys. Fluids* **29**, 085104 (2017).
162. Chao, B. F. & Chung, C. H. On Estimating the Cross Correlation and Least Squares Fit of One Data Set to Another With Time Shift. *Earth Space Sci.* **6**, 1409–1415 (2019).
163. Chatfield, C. & Xing, H. *The analysis of time series: an introduction with R* (Chapman and hall/CRC, 2019).
164. Pardo-Igúzquiza, E. & Rodríguez-Tovar, F. J. Spectral and cross-spectral analysis of uneven time series with the smoothed Lomb-Scargle periodogram and Monte Carlo evaluation of statistical significance. *Comput. Geosci.* **49**, 207–216 (2012).
165. Carter, G., Knapp, C. & Nuttall, A. Estimation of the magnitude-squared coherence function via overlapped fast fourier transform processing. *IEEE Transactions on Audio Electroacoustics* **21**, 337–344 (1973).
166. Baldocchi, D., Falge, E. & Wilson, K. A spectral analysis of biosphere–atmosphere trace gas flux densities and meteorological variables across hour to multi-year time scales. *Agric. For. Meteorol.* **107**, 1–27 (2001).
167. Fleck, B. & Deubner, F. L. Dynamics of the solar atmosphere. II - Standing waves in the solar chromosphere. *Astron. Astrophys.* **224**, 245–252 (1989).
168. Nakariakov, V. M. & Verwichte, E. Coronal Waves and Oscillations. *Living Rev. Sol. Phys.* **2**, 3 (2005).
169. Jess, D. B. *et al.* A chromospheric resonance cavity in a sunspot mapped with seismology. *Nat. Astron.* **4**, 220–227 (2020).
170. Jess, D. B., Snow, B., Fleck, B., Stangalini, M. & Jafarzadeh, S. Reply to: Signatures of sunspot oscillations and the case for chromospheric resonances. *Nat. Astron.* **5**, 5–8 (2021).
171. Leighton, R. B. In Thomas, R. N. (ed.) *Aerodynamic Phenomena in Stellar Atmospheres*, vol. 12 of *IAU Symposium*, 321–325 (1960).
172. Leighton, R. B., Noyes, R. W. & Simon, G. W. Velocity Fields in the Solar Atmosphere. I. Preliminary Report. *Astrophys. J.* **135**, 474 (1962).
173. Noyes, R. W. & Leighton, R. B. Velocity Fields in the Solar Atmosphere. II. The Oscillatory Field. *Astrophys. J.* **138**, 631 (1963).
174. Jess, D. B. *et al.* Waves in the lower solar atmosphere: the dawn of next-generation solar telescopes. *Living Rev. Sol. Phys.* **20**, 1 (2023).
175. Rouppe van der Voort, L. H. M. *et al.* High-resolution observations of the solar photosphere, chromosphere, and transition region. A database of coordinated IRIS and SST observations. *Astron. Astrophys.* **641**, A146 (2020).
176. Rast, M. P. *et al.* Critical Science Plan for the Daniel K. Inouye Solar Telescope (DKIST). *Sol. Phys.* **296**, 70 (2021).
177. Yadav, N., Keppens, R. & Popescu Braileanu, B. 3D MHD wave propagation near a coronal null point: New wave mode decomposition approach. *Astron. Astrophys.* **660**, A21 (2022).
178. Carlsson, M., De Pontieu, B. & Hansteen, V. H. New View of the Solar Chromosphere. *Annu. Rev. Astron. Astrophys.* **57**, 189–226 (2019).
179. Grant, S. D. T. *et al.* Alfvén wave dissipation in the solar chromosphere. *Nat. Phys.* **14**, 480–483 (2018).
180. Joshi, J. & de la Cruz Rodríguez, J. Magnetic field variations associated with umbral flashes and penumbral waves. *Astron. Astrophys.* **619**, A63 (2018).
181. Stangalini, M. *et al.* Propagating Spectropolarimetric Disturbances in a Large Sunspot. *Astrophys. J.* **869**, 110 (2018).

182. Baker, D. *et al.* Alfvénic Perturbations in a Sunspot Chromosphere Linked to Fractionated Plasma in the Corona. *Astrophys. J.* **907**, 16 (2021).
183. Stangalini, M. *et al.* Spectropolarimetric fluctuations in a sunspot chromosphere. *Philos. Transactions Royal Soc. Lond. Ser. A* **379**, 20200216 (2021).
184. Keys, P. H., Steiner, O. & Vigeesh, G. On the effect of oscillatory phenomena on Stokes inversion results. *Philos. Transactions Royal Soc. Lond. Ser. A* **379**, 20200182 (2021).
185. Jafarzadeh, S. *et al.* Sausage, kink, and fluting MHD wave modes identified in solar magnetic pores by Solar Orbiter/PHI. *Astron. Astrophys.* in press, DOI: 10.1051/0004-6361/202449685 (2024).
186. Christensen-Dalsgaard, J., Gough, D. O. & Thompson, M. J. The Depth of the Solar Convection Zone. *Astrophys. J.* **378**, 413 (1991).
187. Christensen-Dalsgaard, J. Helioseismology. *Rev. Mod. Phys.* **74**, 1073–1129 (2002).
188. Thompson, M. J., Christensen-Dalsgaard, J., Miesch, M. S. & Toomre, J. The Internal Rotation of the Sun. *Annu. Rev. Astron. Astrophys.* **41**, 599–643 (2003).
189. Balbus, S. A. & Hawley, J. F. A Powerful Local Shear Instability in Weakly Magnetized Disks. I. Linear Analysis. *Astrophys. J.* **376**, 214 (1991).
190. Balbus, S. A. & Hawley, J. F. Instability, turbulence, and enhanced transport in accretion disks. *Rev. Mod. Phys.* **70**, 1–53 (1998).
191. Shakura, N. I. & Sunyaev, R. A. Black holes in binary systems. Observational appearance. *Astron. Astrophys.* **24**, 337–355 (1973).
192. Pringle, J. E. Accretion discs in astrophysics. *Annu. Rev. Astron. Astrophys.* **19**, 137–162 (1981).
193. Pollack, J. B. *et al.* Formation of the Giant Planets by Concurrent Accretion of Solids and Gas. *Icarus* **124**, 62–85 (1996).
194. Boss, A. P. Giant planet formation by gravitational instability. *Science* **276**, 1836–1839 (1997).
195. Mayer, L., Quinn, T., Wadsley, J. & Stadel, J. The Evolution of Gravitationally Unstable Protoplanetary Disks: Fragmentation and Possible Giant Planet Formation. *Astrophys. J.* **609**, 1045–1064 (2004).
196. Lada, C. J. & Lada, E. A. Embedded Clusters in Molecular Clouds. *Annu. Rev. Astron. Astrophys.* **41**, 57–115 (2003).
197. Peebles, P. J. E. *The large-scale structure of the universe* (Princeton University Press, 1980).
198. Thorne, K. S. Gravitational radiation. In *Three Hundred Years of Gravitation*, 330–458 (1987).
199. Peters, P. C. & Mathews, J. Gravitational Radiation from Point Masses in a Keplerian Orbit. *Phys. Rev.* **131**, 435–440 (1963).
200. LIGO Scientific Collaboration *et al.* Advanced LIGO. *Class. Quantum Gravity* **32**, 074001 (2015).
201. Abbott, B. P. *et al.* Observation of Gravitational Waves from a Binary Black Hole Merger. *Phys. Rev. Lett.* **116**, 061102 (2016).
202. Baldwin, M. P. *et al.* The quasi-biennial oscillation. *Rev. Geophys.* **39**, 179–229 (2001).
203. Fritts, D. C. & Alexander, M. J. Gravity wave dynamics and effects in the middle atmosphere. *Rev. geophysics* **41** (2003).
204. Rhie, J. & Romanowicz, B. Excitation of earth’s continuous free oscillations by atmosphere–ocean–seafloor coupling. *Nature* **431**, 552–556 (2004).
205. Båth, B. *Spectral analysis in geophysics* (Elsevier, 2012).
206. Aki, K. & Richards, P. G. *Quantitative Seismology* (University Science Books, 2002), 2 edn.

207. Agnew, D. C. Earth Tides. In Schubert, G. (ed.) *Geodesy*, vol. 3, 163–195 (2007).
208. Rawlinson, N., Pozgay, S. & Fishwick, S. Seismic tomography: A window into deep Earth. *Phys. Earth Planet. Interiors* **178**, 101–135 (2010).
209. Tromp, J. Seismic wavefield imaging of Earth’s interior across scales. *Nat. Rev. Earth Environ.* **1**, 40–53 (2020).
210. Fichtner, A., Kennett, B. L. N., Igel, H. & Bunge, H.-P. Full seismic waveform tomography for upper-mantle structure in the Australasian region using adjoint methods. *Geophys. J. Int.* **179**, 1703–1725 (2009).
211. Shao, Z.-G. Network analysis of human heartbeat dynamics. *Appl. Phys. Lett.* **96** (2010).
212. Koudelková, Z., Strmiska, M. & Jašek, R. Analysis of brain waves according to their frequency. *Int. J. Biol. Biomed. Eng* **12**, 202–207 (2018).
213. Dzwonczyk, R., Brown, C. G. & Werman, H. A. The median frequency of the eeg during ventricular fibrillation: its use in an algorithm for estimating the duration of cardiac arrest. *IEEE Transactions on Biomed. Eng.* **37**, 640–646 (1990).
214. Strohmenger, H.-U., Lindner, K. H. & Brown, C. G. Analysis of the ventricular fibrillation eeg signal amplitude and frequency parameters as predictors of countershock success in humans. *Chest* **111**, 584–589 (1997).
215. Krasteva, V. & Jekova, I. Assessment of eeg frequency and morphology parameters for automatic classification of life-threatening cardiac arrhythmias. *Physiol. measurement* **26**, 707 (2005).
216. Christov, I. *et al.* Comparative study of morphological and time-frequency eeg descriptors for heartbeat classification. *Med. engineering & physics* **28**, 876–887 (2006).
217. Numer, M. R. Frequency analysis and topographic mapping of eeg and evoked potentials in epilepsy. *Electroencephalogr. clinical neurophysiology* **69**, 118–126 (1988).
218. Clemens, B., Szigeti, G. & Barta, Z. Eeg frequency profiles of idiopathic generalised epilepsy syndromes. *Epilepsy research* **42**, 105–115 (2000).
219. Tzallas, A. T., Tsipouras, M. G. & Fotiadis, D. I. Epileptic seizure detection in eegs using time–frequency analysis. *IEEE transactions on information technology biomedicine* **13**, 703–710 (2009).
220. Maganti, R. K. & Rutecki, P. Eeg and epilepsy monitoring. *CONTINUUM: Lifelong Learn. Neurol.* **19**, 598–622 (2013).
221. Luca, G. *et al.* Age and gender variations of sleep in subjects without sleep disorders. *Annals medicine* **47**, 482–491 (2015).
222. Siddiqui, M. M., Srivastava, G. & Saeed, S. H. Diagnosis of insomnia sleep disorder using short time frequency analysis of psd approach applied on eeg signal using channel roc-loc. *Sleep Sci.* **9**, 186–191 (2016).
223. Dimitriadis, S. I., Salis, C. I. & Liparas, D. An automatic sleep disorder detection based on eeg cross-frequency coupling and random forest model. *J. Neural Eng.* **18**, 046064 (2021).
224. Zhao, W. *et al.* Eeg spectral analysis in insomnia disorder: A systematic review and meta-analysis. *Sleep medicine reviews* **59**, 101457 (2021).
225. Yang, M.-G., Chen, Z.-Q. & Hua, X.-G. An experimental study on using mr damper to mitigate longitudinal seismic response of a suspension bridge. *Soil Dyn. Earthq. Eng.* **31**, 1171–1181 (2011).
226. Weber, F. & Mašlanka, M. Frequency and damping adaptation of a tmd with controlled mr damper. *Smart Mater. Struct.* **21**, 055011 (2012).
227. Weber, F. & Distl, H. Amplitude and frequency independent cable damping of sutong bridge and russky bridge by magnetorheological dampers. *Struct. Control. Heal. Monit.* **22**, 237–254 (2015).
228. Wada, A., Huang, Y.-H. & Iwata, M. Passive damping technology for buildings in japan. *Prog. structural engineering materials* **2**, 335–350 (2000).

229. Fujita, K., Kasagi, M., Lang, Z.-Q., Guo, P. & Takewaki, I. Optimal placement and design of nonlinear dampers for building structures in the frequency domain. *Earthq. Struct* **7**, 1025–1044 (2014).
230. Altay, O. & Klinkel, S. A semi-active tuned liquid column damper for lateral vibration control of high-rise structures: theory and experimental verification. *Struct. control health monitoring* **25**, e2270 (2018).
231. Fidell, S., Pearsons, K., Silvati, L. & Sneddon, M. Relationship between low-frequency aircraft noise and annoyance due to rattle and vibration. *The J. Acoust. Soc. Am.* **111**, 1743–1750 (2002).
232. Keye, S., Keimer, R. & Homann, S. A vibration absorber with variable eigenfrequency for turboprop aircraft. *Aerosp. Sci. Technol.* **13**, 165–171 (2009).
233. Peixin, G., Tao, Y., Zhang, Y., Jiao, W. & Jingyu, Z. Vibration analysis and control technologies of hydraulic pipeline system in aircraft: A review. *Chin. J. Aeronaut.* **34**, 83–114 (2021).
234. Warner, M. *Street Turbocharging: Design, Fabrication, Installation, and Tuning of High-Performance Street Turbocharger Systems* (Penguin, 2006).
235. Wang, L., Burger, R. & Aloe, A. Considerations of vibration fatigue for automotive components. *SAE Int. J. Commer. Veh.* **10**, 150–158 (2017).
236. Abdeltwab, M. M. & Ghazaly, N. M. A review on engine fault diagnosis through vibration analysis. *Int. J. on Recent Technol. Mech. Electr. Eng.* **9**, 01–06 (2022).
237. Senani, R., Bhaskar, D., Singh, V. K. & Sharma, R. *Sinusoidal oscillators and waveform generators using modern electronic circuit building blocks*, vol. 622 (Springer, 2016).
238. Wang, H., Du, W. *et al.* *Analysis and damping control of power system low-frequency oscillations*, vol. 1 (Springer, 2016).
239. Liu, T., Wong, T. T. & Shen, Z. J. A survey on switching oscillations in power converters. *IEEE J. Emerg. Sel. Top. Power Electron.* **8**, 893–908 (2019).
240. Main, I. G. *Vibrations and waves in physics* (Cambridge university press, 1993).
241. Wilson, E. B., Decius, J. C. & Cross, P. C. *Molecular vibrations: the theory of infrared and Raman vibrational spectra* (Courier Corporation, 1980).
242. Bernath, P. F. *Spectra of atoms and molecules* (Oxford university press, 2020).
243. Srivastava, G. P. *The physics of phonons* (CRC press, 2022).
244. Sinba, S. Phonons in semiconductors. *Critical Rev. Solid State Material Sci.* **3**, 273–334 (1973).
245. Arora, A. K., Rajalakshmi, M., Ravindran, T. & Sivasubramanian, V. Raman spectroscopy of optical phonon confinement in nanostructured materials. *J. Raman Spectrosc. An Int. J. for Orig. Work. all Aspects Raman Spectrosc. Incl. High. Order Process. also Brillouin Rayleigh Scatt.* **38**, 604–617 (2007).
246. Qian, X., Zhou, J. & Chen, G. Phonon-engineered extreme thermal conductivity materials. *Nat. Mater.* **20**, 1188–1202 (2021).
247. Greig, A. C. Fundamental analysis and subsequent stock returns. *J. Account. Econ.* **15**, 413–442 (1992).
248. Abad, C., Thore, S. A. & Laffarga, J. Fundamental analysis of stocks by two-stage dea. *Manag. Decis. Econ.* **25**, 231–241 (2004).
249. Baresa, S., Bogdan, S. & Ivanovic, Z. Strategy of stock valuation by fundamental analysis. *UTMS J. Econ.* **4**, 45–51 (2013).
250. Petrusheva, N. & Jordanoski, I. Comparative analysis between the fundamental and technical analysis of stocks. *J. Process. Manag. New Technol.* **4**, 26–31 (2016).
251. Nazário, R. T. F., e Silva, J. L., Sobreiro, V. A. & Kimura, H. A literature review of technical analysis on stock markets. *The Q. Rev. Econ. Finance* **66**, 115–126 (2017).

252. Edwards, R. D., Magee, J. & Bassetti, W. C. *Technical analysis of stock trends* (CRC press, 2018).
253. Chen, X. *et al.* Open is not enough. *Nat. Phys.* **15**, 113–119 (2019).
254. Prager, E. M. *et al.* Improving transparency and scientific rigor in academic publishing (2019).
255. Scargle, J. D. Studies in astronomical time series analysis. ii-statistical aspects of spectral analysis of unevenly spaced data. *Astrophys. Journal, Part 1, vol. 263, Dec. 15, 1982, p. 835-853.* **263**, 835–853 (1982).
256. Dragomiretskiy, K. & Zosso, D. Variational mode decomposition. *IEEE transactions on signal processing* **62**, 531–544 (2013).
257. Marwan, N. *Encounters with neighbours: current developments of concepts based on recurrence plots and their applications* (Norbert Marwan, 2003).
258. Zbilut, J. P. & Webber, C. L. Recurrence quantification analysis. *Wiley encyclopedia biomedical engineering* (2006).
259. Marwan, N., Carmen Romano, M., Thiel, M. & Kurths, J. Recurrence plots for the analysis of complex systems. *Phys. Reports* **438**, 237–329 (2007).
260. Webber Jr, C. L. & Zbilut, J. P. Recurrence quantification analysis of nonlinear dynamical systems. In Riley, M. & Van Orden, G. (eds.) *Tutorials in contemporary nonlinear methods for the behavioral sciences*, 26–94 (2005).
261. Iwanski, J. S. & Bradley, E. Recurrence plots of experimental data: To embed or not to embed? *Chaos: An Interdiscip. J. Nonlinear Sci.* **8**, 861–871 (1998).
262. Ladeira, G., Marwan, N., Destro-Filho, J.-B., Davi Ramos, C. & Lima, G. Frequency spectrum recurrence analysis. *Sci. Reports* **10**, 21241 (2020).
263. Artac, M., Jogan, M. & Leonardis, A. Incremental pca for on-line visual learning and recognition. *Object recognition supported by user interaction for service robots* **3**, 781–784 vol.3 (2002).
264. Cardot, H. & Degras, D. Online principal component analysis in high dimension: Which algorithm to choose? *Int. Stat. Rev.* **86**, 29 – 50 (2015).
265. Lippi, V. & Ceccarelli, G. Incremental Principal Component Analysis Exact implementation and continuity corrections. In *The 16th International Conference on Informatics in Control, Automation and Robotics*, 473–480 (SCITEPRESS – Science and Technology Publications, 2019).
266. Hassani, H. Singular spectrum analysis: Methodology and comparison. *J. Data Sci.* **5**, 239–257 (2022).
267. Spiegelberg, J. & Ruzs, J. Can we use pca to detect small signals in noisy data? *Ultramicroscopy* **172**, 40–46 (2017).
268. Biraud, F. SETI at the Nançay radiotelescope. *Acta Astronaut.* **10**, 759–760 (1983).
269. Trudu, M. *et al.* Performance analysis of the Karhunen–Loève Transform for artificial and astrophysical transmissions: denoizing and detection. *Mon. Notices Royal Astron. Soc.* **494**, 69–83 (2020).
270. James, S. C., Zhang, Y. & O’Donncha, F. A machine learning framework to forecast wave conditions. *Coast. Eng.* **137**, 1–10 (2018).
271. Eeltink, D. *et al.* Nonlinear wave evolution with data-driven breaking. *Nat. Commun.* **13**, 2343 (2022).
272. Shi, J. *et al.* A machine-learning approach based on attention mechanism for significant wave height forecasting. *J. Mar. Sci. Eng.* **11**, 1821 (2023).
273. Benedetto, V., Gissi, F., Ciaparrone, G. & Troiano, L. AI in gravitational wave analysis, an overview. *Appl. Sci.* **13** (2023).
274. Navas-Olive, A., Rubio, A., Abbaspoor, S., Hoffman, K. L. & de la Prida, L. M. A machine learning toolbox for the analysis of sharp-wave ripples reveals common waveform features across species. *Commun. Biol.* **7**, 211 (2024).

275. Mukhtar, H., Qaisar, S. M. & Zaguia, A. Deep convolutional neural network regularization for alcoholism detection using eeg signals. *Sensors* **21**, 5456 (2021).
276. Molnar, C. *Interpretable machine learning* (Lulu. com, 2020).
277. Kashinath, K. *et al.* Physics-informed machine learning: case studies for weather and climate modelling. *Philos. Transactions Royal Soc. A* **379**, 20200093 (2021).
278. Jess, D. B., Keys, P. H., Stangalini, M. & Jafarzadeh, S. High-resolution wave dynamics in the lower solar atmosphere. *Philos. Transactions Royal Soc. Lond. Ser. A* **379**, 20200169 (2021).
279. McAteer, R. T. J. *et al.* Long-Period Chromospheric Oscillations in Network Bright Points. *Astrophys. J. Lett.* **567**, L165–L168 (2002).
280. McAteer, R. T. J. *et al.* Observational Evidence for Mode Coupling in the Chromospheric Network. *Astrophys. J.* **587**, 806–817 (2003).
281. Méndez, F. J., Menéndez, M., Luceño, A. & Losada, I. J. Estimation of the long-term variability of extreme significant wave height using a time-dependent peak over threshold (pot) model. *J. Geophys. Res. Ocean.* **111**, C7 (2006).
282. Bello González, N., Flores Soriano, M., Kneer, F. & Okunev, O. Acoustic waves in the solar atmosphere at high spatial resolution. *Astron. Astrophys.* **508**, 941–950 (2009).
283. Thompson, R. O. R. Y. Coherence Significance Levels. *J. Atmospheric Sci.* **36**, 2020–2021 (1979).
284. Gull, S. F. & Daniell, G. J. Image reconstruction from incomplete and noisy data. *Nature* **272**, 686–690 (1978).
285. Priestley, M. *Spectral Analysis and Time Series*. No. vb. 1 in Probability and mathematical statistics : A series of monographs and textbooks (Academic Press, 1981).
286. Anderson, R. L. Distribution of the Serial Correlation Coefficient. *The Annals Math. Stat.* **13**, 1 – 13 (1942).
287. Krishna Prasad, S. *et al.* The Frequency-dependent Damping of Slow Magnetoacoustic Waves in a Sunspot Umbral Atmosphere. *Astrophys. J.* **847**, 5 (2017).
288. Box, G. E. P. & Pierce, D. A. Distribution of residual autocorrelations in autoregressive-integrated moving average time series models. *J. Amer. Stat. Assoc.* **65**, 1509–1526 (1970).
289. Kang, Y., Belušić, D. & Smith-Miles, K. Detecting and classifying events in noisy time series. *J. Atmospheric Sci.* **71**, 1090 – 1104 (2014).
290. Kasdin, N. J. Discrete simulation of colored noise and stochastic processes and  $1/f$  power law noise generation. *Proc. IEEE* **83**, 802–827 (1995).
291. Nie, X. *et al.* Noise-robust computational ghost imaging with pink noise speckle patterns. *Phys. Rev. A* **104**, 013513 (2021).
292. Zhou, J. *et al.* Pink noise: effect on complexity synchronization of brain activity and sleep consolidation. *J. theoretical biology* **306**, 68–72 (2012).
293. Morr, A. & Boers, N. Detection of approaching critical transitions in natural systems driven by red noise. *Phys. Rev. X* **14**, 021037 (2024).
294. Vaughan, S. A simple test for periodic signals in red noise. *Astron. & Astrophys.* **431**, 391–403 (2005).
295. Pont, F., Zucker, S. & Queloz, D. The effect of red noise on planetary transit detection. *Mon. Notices Royal Astron. Soc.* **373**, 231–242 (2006).
296. Rodriguez, J. B., Arce, G. R. & Lau, D. L. Blue-noise multitone dithering. *IEEE Transactions on Image Process.* **17**, 1368–1382 (2008).
297. Abdulaziz, A. S. & Kėpuska, V. Z. The short-time silence of speech signal as signal-to-noise ratio estimator. *Int. J. Eng. Res. Appl. (IJERA)* **8**, 99–103 (2016).

298. Terrell, J. Size limits on fluctuating astronomical sources. *Astrophys. J. Lett.* **213**, L93–L97 (1977).
299. Delouille, V., Chainais, P. & Hochedez, J. F. Spatial and Temporal Noise in Solar EUV Observations. *Sol. Phys.* **248**, 441–455 (2008).
300. Terzo, S. *et al.* Widespread Nanoflare Variability Detected with Hinode/X-Ray Telescope in a Solar Active Region. *Astrophys. J.* **736**, 111 (2011).
301. Jess, D. B., Mathioudakis, M. & Keys, P. H. Nanoflare Activity in the Solar Chromosphere. *Astrophys. J.* **795**, 172 (2014).
302. Jess, D. B. *et al.* Statistical Signatures of Nanoflare Activity. I. Monte Carlo Simulations and Parameter-space Exploration. *Astrophys. J.* **871**, 133 (2019).
303. Dillon, C. J. *et al.* Statistical Signatures of Nanoflare Activity. II. A Nanoflare Explanation for Periodic Brightenings in Flare Stars Observed by NGTS. *Astrophys. J.* **904**, 109 (2020).
304. Grant, S. D. T. *et al.* Statistical Signatures of Nanoflare Activity. III. Evidence of Enhanced Nanoflaring Rates in Fully Convective stars as Observed by the NGTS. *Astrophys. J.* **957**, 70 (2023).
305. Constable, C. G. Parameter estimation in non-Gaussian noise. *Geophys. J. Int.* **94**, 131–142 (1988).
306. Middleton, D. Non-gaussian noise models in signal processing for telecommunications: new methods and results for class a and class b noise models. *IEEE Transactions on Inf. Theory* **45**, 1129–1149 (1999).
307. Kassam, S. & Thomas, J. *Signal Detection in Non-Gaussian Noise*. Springer Texts in Electrical Engineering (Springer New York, 2012).
308. Dussault, D. & Hoess, P. Noise performance comparison of iccd with ccd and emccd cameras. In *Infrared Systems and Photoelectronic Technology*, vol. 5563, 195–204 (SPIE, 2004).
309. Jin, X. & Hirakawa, K. Approximations to camera sensor noise. In *Image Processing: Algorithms and Systems XI*, vol. 8655, 149–155 (SPIE, 2013).
310. Snyder, D. L., Helstrom, C. W., Lanterman, A. D., Faisal, M. & White, R. L. Compensation for readout noise in ccd images. *JOSA A* **12**, 272–283 (1995).
311. Waltham, N. Ccd and cmos sensors. *Obs. Photons Space: A Guid. to Exp. Space Astron.* 423–442 (2013).
312. Irie, K., McKinnon, A. E., Unsworth, K. & Woodhead, I. M. A technique for evaluation of ccd video-camera noise. *IEEE Transactions on Circuits Syst. for Video Technol.* **18**, 280–284 (2008).
313. Tomasi, C. & Manduchi, R. Bilateral filtering for gray and color images. In *Sixth international conference on computer vision (IEEE Cat. No. 98CH36271)*, 839–846 (IEEE, 1998).
314. Wiener, N. *Extrapolation, interpolation, and smoothing of stationary time series: with engineering applications* (The MIT press, 1949).
315. Gonzalez, R. C. *Digital image processing* (Pearson education india, 2009).
316. Buades, A., Coll, B. & Morel, J.-M. A non-local algorithm for image denoising. In *2005 IEEE computer society conference on computer vision and pattern recognition (CVPR'05)*, vol. 2, 60–65 (Ieee, 2005).
317. Dabov, K., Foi, A., Katkovnik, V. & Egiazarian, K. Image denoising by sparse 3-d transform-domain collaborative filtering. *IEEE Transactions on image processing* **16**, 2080–2095 (2007).
318. Donoho, D. L. De-noising by soft-thresholding. *IEEE transactions on information theory* **41**, 613–627 (1995).
319. Abbate, A., Koay, J., Frankel, J., Schroeder, S. C. & Das, P. Signal detection and noise suppression using a wavelet transform signal processor: application to ultrasonic flaw detection. *IEEE transactions on ultrasonics, ferroelectrics, frequency control* **44**, 14–26 (1997).
320. Wood, L. C. A review of digital pass filtering. *Rev. Geophys.* **6**, 73–97 (1968).

321. Wang, C. & Gao, R. X. Wavelet transform with spectral post-processing for enhanced feature extraction. In *IMTC/2002. Proceedings of the 19th IEEE Instrumentation and Measurement Technology Conference (IEEE Cat. No. 00CH37276)*, vol. 1, 315–320 (IEEE, 2002).
322. Higham, J. E., Brevis, W. & Keylock, C. J. A rapid non-iterative proper orthogonal decomposition based outlier detection and correction for piv data. *Meas. Sci. Technol.* **27**, 125303 (2016).
323. Dätig, M. & Schlurmann, T. Performance and limitations of the hilbert–huang transformation (hht) with an application to irregular water waves. *Ocean. Eng.* **31**, 1783–1834 (2004).
324. Sieber, M., Paschereit, C. O. & Oberleithner, K. Spectral proper orthogonal decomposition. *J. Fluid Mech.* **792**, 798–828 (2016).
325. Taira, K. *et al.* Modal analysis of fluid flows: An overview. *AIAA J.* **55**, 4013–4041 (2017).
326. Courant, R. & Friedrichs, K. O. *Supersonic flow and shock waves*, vol. 21 (Springer Science & Business Media, 1999).
327. Zel’Dovich, Y. B. & Raizer, Y. P. *Physics of shock waves and high-temperature hydrodynamic phenomena* (Courier Corporation, 2002).
328. Whitham, G. B. *Linear and nonlinear waves* (John Wiley & Sons, 2011).
329. Frigo, M. & Johnson, S. G. FFTW: An adaptive software architecture for the FFT. In *Proc. 1998 IEEE Intl. Conf. Acoustics Speech and Signal Processing*, vol. 3, 1381–1384 (IEEE, 1998).
330. Frigo, M. & Johnson, S. G. The design and implementation of FFTW3. *Proc. IEEE* **93**, 216–231 (2005). **Special issue on “Program Generation, Optimization, and Platform Adaptation”**.
331. Sanderson, C. & Curtin, R. Armadillo: a template-based c++ library for linear algebra. *J. Open Source Softw.* **1**, 26 (2016).
332. Parker, T. & Chua, L. Insite—a software toolkit for the analysis of nonlinear dynamical systems. *Proc. IEEE* **75**, 1081–1089 (1987).
333. Parker, T. S. Insite: a software toolkit for studying chaos. [1991] *Proc. 34th Midwest Symp. on Circuits Syst.* 752–755 vol.2 (1991).
334. Hegger, R., Kantz, H. & Schreiber, T. Practical implementation of nonlinear time series methods: The tisean package. *Chaos: An Interdiscip. J. Nonlinear Sci.* **9**, 413–435 (1999).
335. Ghil, M. The SSA-MTM Toolkit: applications to analysis and prediction of time series. In Bosacchi, B., Bezdek, J. C. & Fogel, D. B. (eds.) *Applications of Soft Computing*, vol. 3165, 216 – 230. International Society for Optics and Photonics (SPIE, 1997).
336. Golyandina, N., Korobeynikov, A. & Zhigljavsky, A. *Singular spectrum analysis with R* (Springer, 2018).
337. Megies, T., Beyreuther, M., Barsch, R., Krischer, L. & Wassermann, J. Obspy—what can it do for data centers and observatories? *Annals Geophys.* **54**, 47–58 (2011).
338. Krischer, L. *et al.* Obspy: A bridge for seismology into the scientific python ecosystem. *Comput. Sci. & Discov.* **8**, 014003 (2015).
339. Søndergaard, P. L., Torr sani, B. & Balazs, P. The Linear Time Frequency Analysis Toolbox. *Int. J. Wavelets, Multiresolution Analysis Inf. Process.* **10** (2012).
340. Pr ša, Z., Søndergaard, P. L., Holighaus, N., Wiesmeyr, C. & Balazs, P. The Large Time-Frequency Analysis Toolbox 2.0. In *Sound, Music, and Motion*, LNCS, 419–442 (Springer International Publishing, 2014).
341. Bota, P., Silva, R., Carreiras, C., Fred, A. & da Silva, H. P. Biosppy: A python toolbox for physiological signal processing. *SoftwareX* **26**, 101712 (2024).
342. Boashash, B. *TFSA 5.0: Time-frequency Signal Analysis Toolbox* (Queensland University of Technology, Signal Processing Research Centre, 1995).

343. Boashash, B. & Ghafoor, M. Time frequency signal analysis and processing toolbox update 6.2: An enhanced research platform with new advanced high-resolution tfds. In *2013 8th International Workshop on Systems, Signal Processing and their Applications (WoSSPA)*, 442–451 (2013).

## Acknowledgements

We wish to acknowledge scientific discussions with the Waves in the Lower Solar Atmosphere (WaLSA; [www.WaLSA.team](http://www.WaLSA.team)) team, which has been supported by the Research Council of Norway (project no. 262622), The Royal Society (award no. Hooke18b/SCTM)<sup>278</sup>, and the International Space Science Institute (ISSI Team 502). S.J. gratefully acknowledges support from the Niels Bohr International Academy (NBIA), at the Niels Bohr Institute, University of Copenhagen, Denmark, and the Rosseland Centre for Solar Physics (RoCS), University of Oslo, Norway. D.B.J. and T.D. acknowledge support from the Leverhulme Trust via the Research Project Grant RPG-2019-371. D.B.J. and S.D.T.G. wish to thank the UK Science and Technology Facilities Council (STFC) for the consolidated grants ST/T00021X/1 and ST/X000923/1. D.B.J. and S.D.T.G. also acknowledge funding from the UK Space Agency via the National Space Technology Programme (grant SSc-009). S.B. acknowledges the support from the STFC Grant ST/X000915/1. V.F., G.V. and S.S.A.S. acknowledge the support from STFC (ST/V000977/1 and ST/Y001532/1) and the Institute for Space-Earth Environmental Research (ISEE, International Joint Research Program, Nagoya University, Japan). V.F. and G.V. thank the Royal Society International Exchanges Scheme, in collaboration with Monash University, Australia (IES/R3/213012), Instituto de Astrofísica de Canarias, Spain (IES/R2/212183), National Observatory of Athens, Greece (IES/R1/221095), and the Indian Institute of Astrophysics, India (IES/R1/211123), for the support provided. R.G. acknowledges the support by Fundação para a Ciência e a Tecnologia (FCT) through the research grants UIDB/04434/2020 and UIDP/04434/2020. E.K. acknowledges the support from the European Research Council through the Consolidator Grant ERC-2017-CoG-771310-PI2FA and from the Agencia Estatal de Investigación del Ministerio de Ciencia e Innovación through grant PID2021-127487NB-I00. L.A.C.A.S. acknowledges the support from the STFC Grant ST/X001008/1. This project has received funding from the European Research Council (ERC) under the European Union's Horizon 2020 research and innovation programme (grant agreement No. 101097844 — project WINSUN). N.Y. acknowledges the support from the DST INSPIRE Faculty Grant (IF21-PH 268) and the SERB MATRICS grant (MTR/2023/001332).

## Author contributions

S.J. led the formation of the team responsible for the Primer and managed the entire writing process. S.J. and S.B. generated the initial synthetic datasets used within the Primer. S.J., D.B.J., M.S., S.D.T.G., J.E.H., L.A.C.A.S. and S.S.A.S. performed analyses of the data products and contributed to the final versions of the synthetic data that accompanies this Primer. S.J., D.B.J., M.S., S.D.T.G., J.E.H., P.H.K., T.J.D., B.F., S.M.J., E.K., O.S., G.V. and N.Y. contributed to the evolution of the analysis codes reported in the Primer. S.J., D.B.J., M.S., S.D.T.G., J.E.H., and M.P. wrote the initial draft of the manuscript, with L.A.C.A.S., S.S.A.S., and S.K.S. providing important additions that helped finalise the content. All authors provided scientific guidance throughout the project, discussed the results, helped offer recommendations for improvement, and refined the final text used within the manuscript.

## Competing interests

The majority of the authors of this Primer are members of the Waves in the Lower Solar Atmosphere (WaLSA) team (<https://WaLSA.team>), which developed and maintains the WaLSAtools repository, extensively used for all the analyses in the Primer.

## Publisher's note

Springer Nature remains neutral with regard to jurisdictional claims in published maps and institutional affiliations.

## Related Links

**WaLSAtools documentation:** <https://WaLSA.tools>

**WaLSAtools GitHub repository:** <https://github.com/WaLSAteam/WaLSAtools>

**WaLSA team:** <https://WaLSA.team>

## Glossary terms

**Oscillation:** A periodic variation of a measurable around a fixed equilibrium point.

**Wave:** A correlated collection of oscillations that propagates through a medium over time.

**Shock:** A wave propagating above the sound speed relative to the rest frame of the medium. This produces discontinuities in the medium, i.e. the '*sonic boom*' of fast aircraft.

**Harmonic:** Characteristic frequencies that an oscillation will prefer to exhibit. These are integer multiples of the natural, fundamental frequency of the oscillation.

**Non-linear waves:** Waves that deviate from the linear, sinusoidal oscillatory pattern through asymmetries or skewness, for instance shocks.

**Frequency:** The number of oscillatory cycles in a given time, typically the amount per second measured in Hertz (Hz).

**Frequency resolution:** The smallest differential in frequency that can be detected. It is linked to the rate at which the data is sampled.

**Sampling Frequency:** The number of samples taken per second from a continuous signal to create a discrete representation.

**Nyquist Frequency:** The highest frequency that can be accurately represented in a discrete signal, equal to half the sampling frequency.

**Spectral analysis:** Studying the characteristics of a range of frequencies within data.

**Wave Power:** A measure of the energy flow associated with waves. It is proportional to the square of the wave amplitude.

**Spectral Power:** The distribution of detected wave power in data as a function of frequency.

**Quasi-periodic:** An oscillation with a changing amplitude over time. They are often due to an inconsistent driver, thus can appear and vanish with time.

**Non-stationary signal:** A time series whose statistical properties, such as the mean or variance, evolve over time.

**Spectral Leakage:** Artefacts introduced to the spectral power due to sampling a non-integer number of wave cycles. Produces a 'leakage' of true wave power into adjacent frequencies.

**Wavelength:** The distance covered by one full cycle of a wave.

**Wavenumber:** The number of wavelengths per unit of distance. The angular variant describes the number of radians per unit of distance.

**Phase:** A time-dependent variable that describes the fraction of a wave encountered at a given time. Typically expressed as an angle fraction of the wave, i.e.,  $90^\circ$  or  $\frac{\pi}{2}$  radians.

**Phase Lag:** The angular difference between corresponding points on two waves of the same frequency, representing the delay of one wave relative to the other.

**Dispersion:** The separation of complex signals into discrete wave frequencies due to their differing propagation speeds. For example, white light breaking into its constituent colours when propagating through a prism.

**Magnetohydrodynamic (MHD):** Study of the interactions between a magnetic field and a fluid (gas or plasma).

**Eigenvector:** In wave analysis, an eigenvector represents a spatial pattern of oscillation that retains its shape while its amplitude might change over time.

**Eigenvalue:** A measure of the variance or energy associated with a specific eigenvector (spatial pattern of oscillation).

**Optically thick:** When a medium readily absorbs light, thus only the surface layer is typically observable.

**Transverse waves:** Oscillations that are perpendicular to the direction of wave propagation.

## Supplementary Information

This Supplementary Information provides additional details and in-depth analyses that complement the main text, offering further insights into the topics, specific methods, datasets, and results. The sections below are organised to correspond with the order in which they are referenced in the main text.

### S1 Overview of the wave analysis research cycle

Supplementary Figure S1 illustrates the cyclical and iterative nature of wave analysis research. The process begins with defining the scientific questions and understanding the characteristics of the available data. These factors guide the selection of appropriate analysis methods, which are then applied to the data. Interpretation of the results leads to insights into the underlying wave phenomena, which can, in turn, inform the refinement of scientific questions or the selection of different analysis methods, leading to a new cycle of investigation. This iterative process is crucial for ensuring robust and comprehensive wave analysis research.

### S2 Detailed parameters for synthetic datasets

The tables below provide detailed parameter specifications for the synthetic 1D time series (Supplementary Table S1) and spatio-temporal datacube (Supplementary Table S2) used in this study. These datasets serve as a controlled environment for evaluating the performance of various wave analysis techniques, as discussed in Section 2.1 (Worked Examples) of the main text.

Table S1 | Parameters for synthetic 1D time series

Parameter	Base Oscillations	Envelope	Transient	Weak	Quasi-Periodic
Frequency (Hz)	5, 12, 15, 18, 25	0.2	2	33	10
Amplitude	1.0, 0.5, 0.8, 0.3, 0.6	0.5	0.6	0.1	0.3
Phase (deg)	0, 45, 90, 135, 180	–	0	0	0
Phase shifts (deg)*	29, -45, 40, -57, 69	–	0	-46	57

\* Phase shifts for the secondary signal relative to the corresponding phase of the primary signal (see Section 2.1.1 of the main text). Positive shifts indicate the secondary signal leading the primary signal, while negative shifts indicate a lag.

Table S2 | Parameters for synthetic spatio-temporal datacube

Parameter	Base Oscillations	Transverse	Fluting	Quasi-Periodic
Frequency (Hz)	0.10, 0.15, 0.20, 0.25, 0.30, 0.35, 0.40, 0.45, 0.50, 0.55	0.25 (x), 0.25 (y)	0.5	0.55
Amplitude	1.60, 1.80, 1.90, 1.70, 1.20, 2.00, 2.40, 1.20, 1.80, 2.20	14.0 (x), 10.0 (y)	14	5.2
Phase (deg)	0, 29, 57, 86, 115, 14, 43, 72, 100, 129	–	–	29

### S3 Significance and noise in wave analysis

Statistical significance tests are crucial for distinguishing real oscillatory signals from background noise and spurious fluctuations. These tests determine confidence levels, indicating the probability that observed power could arise from random fluctuations alone. While a 95% confidence level is common<sup>279–282</sup>, the appropriate threshold depends on factors like the scientific hypothesis, signal-to-noise ratio, and the balance between sensitivity and specificity. A

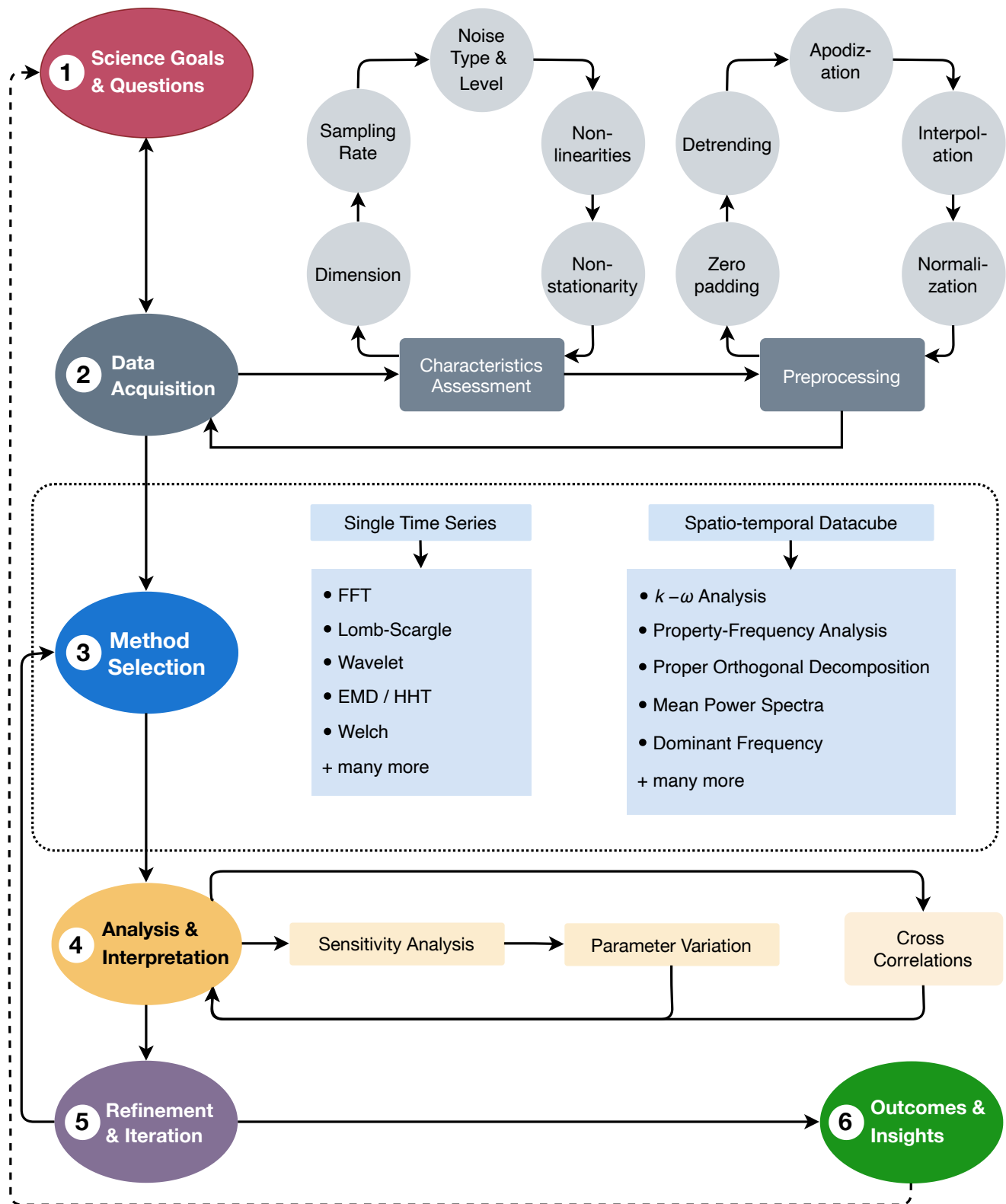


Fig. S1 | **The wave analysis research cycle.** The schematic diagram outlines the cyclical and iterative nature of wave analysis research. Careful consideration of scientific questions and data characteristics guides the selection of appropriate methods, driving the interpretation of results, and ultimately leading to deeper insights into the oscillatory phenomena under investigation.

95% confidence level indicates a 5% chance the power is due to noise, but this is only meaningful if the noise model accurately reflects the characteristics of the background fluctuations (see Supplementary Section S4 for description of various noise models).

Randomisation tests offer a flexible approach to assess significance without relying on specific noise distribution assumptions<sup>283</sup>. In these tests, statistical significance is typically assessed by comparing the observed power in the original data to the distribution of power obtained from a large number (e.g., 1000) of randomised surrogate datasets, generated by preserving certain properties of the original signal while disrupting the patterns of interest. However, understanding the noise characteristics is still valuable. The choice of noise model can influence the generation of randomised (surrogate) datasets used in the test, as different noise types (e.g., white noise vs. correlated noise) require different approaches.

Furthermore, even with randomisation tests, knowledge of the noise aids interpretation and sets appropriate confidence levels. If the noise is highly non-Gaussian or temporally correlated, a more stringent confidence level might be needed to avoid misidentifying noise artefacts as real signals. In this context, noise may refer not only to random fluctuations but also to any feature of the system that is not the primary focus of the analysis.

Therefore, understanding the noise is crucial for constructing appropriate surrogate datasets and interpreting statistical results. Exploring data at different confidence levels, guided by a well-considered noise model, leads to a more robust interpretation of wave analysis results.

## S4 Noise models

Noise, the unwanted fluctuations superimposed on measured signals, is present in some form across all data sequences in scientific domains<sup>284</sup>. Understanding the types and characteristics of noise is crucial for accurate signal processing and interpretation<sup>64</sup>. Different noise models are able to describe the origin and statistical properties of these fluctuations, each impacting subsequent data analysis in a unique way<sup>285</sup>. Importantly, since many noise models are frequency dependent, they must be treated carefully when investigating the wave and/or oscillatory behaviour of the studied system. Common noise profiles inherent to scientific observations include:

- **White noise:** This model assumes that noise has a flat PSD across all frequencies (i.e.,  $f^0$ ), meaning equal power at all frequencies<sup>286,287</sup>. White noise is often used as a baseline for assessing significance levels in wave analysis<sup>288,289</sup>.
- **Pink noise (Flicker noise):** PSD decreases with increasing frequency ( $f^{-1}$  dependence), common in electronic<sup>290,291</sup> and biological systems<sup>292</sup>.
- **Red noise (Brownian noise):** PSD decreases with increasing frequency ( $f^{-2}$  dependence), often seen in natural<sup>293</sup> and astrophysical systems<sup>294,295</sup>.
- **Blue noise:** PSD becomes larger with increasing frequency ( $f^{+1}$  dependence), resulting in less energetic low-frequency components, hence is often seen in audio acoustic signal processing<sup>296,297</sup>.
- **Poisson noise (Shot noise):** Arises from the discrete nature of events (e.g., photon arrivals in detectors<sup>298</sup>) and is characterised by its variance being proportional to the signal intensity<sup>299</sup>, which tends to a Gaussian distribution in the limit of large number statistics<sup>300-304</sup>.
- **Non-Gaussian noise:** Does not follow a normal (Gaussian) distribution and may complicate noise modelling and analysis<sup>305-307</sup>.
- **Instrumental Noise:** Inherent to the instrumentation performing the measurements, hence is affected by thermal noise<sup>308,309</sup>, readout noise<sup>310,311</sup>, and/or quantisation noise<sup>312</sup>, to name but a few examples.

The specific noise source(s) present within the data necessitate different approaches when undertaking subsequent wave analysis. For example, the presence of red noise, which exhibits stronger power at lower frequencies, may

require the application of a high-pass filter to uncover weaker high-frequency signals. Conversely, when dealing with Poisson noise, specialised techniques or averaging over multiple measurements may be advantageous to accurately estimate wave amplitudes. Additionally, non-Gaussian noise can violate the assumptions of certain statistical tests, leading to biased estimates or incorrect conclusions.

## S5 Filtering and noise reduction

While Sections S3 and S4 discussed significance levels and various noise models, it is crucial to remember that a signal is a noisy representation of a physical process, not the process itself. Without knowing the true nature of the noise (or the combination of various noises, including instrumental and other sources), there is always the risk of removing actual signal components during a de-noising process. Distinguishing between noise and signal may not always be straightforward, requiring careful considerations and potentially the exploration of different filtering techniques.

This section focuses on filtering and noise reduction techniques crucial for enhancing signal quality and preparing data for accurate wave analysis. These pre-processing techniques aim to reduce or eliminate unwanted noise or signal components while preserving the essential features of the underlying wave signals of interest. Choosing appropriate methods depends on the characteristics of the noise, the nature of the signal, and the specific goals of the analysis. It is important to note that this is not an exhaustive list of filtering and noise reduction techniques; rather, we present a selection of example methods and a few specialised approaches.

Many filtering techniques focus specifically on reducing noise while preserving the underlying signal of interest. One example is **Bilateral filtering**<sup>313</sup> which smooths images while preserving sharp edges by considering both spatial (or temporal) distances and intensity differences between neighbouring data points. This method is especially useful for images or signals where edge preservation is important. **Wiener filtering**<sup>314,315</sup> is another example of such classical methods that estimates the original signal (or image) by minimizing the mean square error between the estimated and true signals. This method relies on knowledge of the signal and noise power spectra, making it effective when such information is available or can be reliably estimated. Certain methods also utilise similar patterns, or repeated structures, within the signal for effective de-noising. For example, **Non-local means filtering**<sup>316</sup> averages similar patches within the data, making it effective for de-noising signals with repetitive patterns. A more advanced approach in this regard is **Block-Matching and 3D filtering** (BM3D)<sup>317</sup>, which groups similar patches into 3D blocks, applies a transform-domain shrinkage (e.g., wavelet shrinkage), and then aggregates the de-noised blocks. This technique is known for its strong de-noising capabilities, particularly for images. Time-frequency analysis also provided powerful tools for noise reduction. **Wavelet de-noising**<sup>318,319</sup>, for instance, separates noise from the signal by thresholding or shrinking wavelet coefficients, which is particularly effective for non-stationary signals.

Beyond noise reduction, filtering can also be used to selectively pass or remove specific frequencies or frequency bands within a signal<sup>320</sup>. This can be useful for isolating particular components of interest or removing unwanted interference. **High-pass filters** allow high frequencies to pass through while suppressing low frequencies, useful for removing low-frequency trends or drifts in the data. Similarly, **Low-pass filters** allow low frequencies to pass through while removing high frequencies, useful for, e.g., smoothing out high-frequency noise or fluctuations. As such, for isolating a specific oscillatory component of interest, or removing narrowband interference or noise, **Band-pass** or **Band-reject filters** can be used.

Filtering can also be used to enhance or isolate specific oscillatory signals of interest. This might include techniques like **Wavelet transforms**<sup>321</sup>, which can isolate signals at particular scales or frequencies, or **Synchrosqueezing**<sup>137</sup> approach which can further sharpen time-frequency representations to facilitate identification of specific oscillations. Additional specialised methods have also proven valuable for de-noising and signal enhancement. For example, in particle image velocimetry, the **POD detection and estimation method** (PODDEM)<sup>322</sup>, uses a non-iterative approach by modifying temporal coefficients from POD for efficient outlier detection and correction. **PODDEM's** ability to analyse single vector fields offers potential advantages when temporal data is limited<sup>322</sup>. Similarly, **Variational Mode Decomposition** (VMD)<sup>256</sup> decompose signals into modes that can be processed individually,

providing flexibility in handling complex signals. Furthermore, **Regularisation techniques**<sup>275</sup> can be incorporated into various de-noising algorithms to prevent over-fitting and ensure smooth solutions.

Choosing the right filtering/de-noising method requires careful consideration of data characteristics, noise properties, and analysis goals. It is often crucial to experiment with different techniques, compare their performance and effectiveness, and select the most suitable approach for the given task.

## S6 Property-frequency analysis

In this section, we introduce the concept of Property-Frequency Analysis (PFA), a versatile technique that extends the concept of frequency analysis by incorporating information about additional properties or parameters associated with the data. Although the term PFA might be new, the underlying approach of filtering oscillatory signals based on specific properties has likely been utilised in various forms across different scientific fields. However, we formalise this approach here under the term PFA to emphasise its broad applicability and highlight its potential for unifying wave analysis across disciplines. PFA can be applied to both single time series (1D data) and spatio-temporal datasets (2D or 3D data).

In PFA, the power spectrum or other frequency-domain representation of the signal is calculated for different values or ranges of a chosen property. The resulting power spectra are then compared to investigate how the frequency content of the signal varies with changes in the property. For example, in a time series of temperature fluctuations, PFA could be used to examine how the power at different frequencies changes with varying atmospheric pressure or humidity.

This approach allows for a more detailed understanding of the oscillatory behaviour within the data. By isolating and comparing frequency information based on specific properties, PFA can reveal hidden patterns and correlations that might not be apparent in traditional frequency analysis alone.

One specific example of PFA, particularly relevant in solar physics, is the  $B-\omega$  diagram<sup>39</sup>. The  $B-\omega$  diagram combines averaged FFT spectra, calculated within various magnetic field strength bins, into a single plot. Each vertical column represents the average power spectrum at a specific magnetic field strength, displayed along the horizontal axis. While  $k-\omega$  analysis works with the full 3D datacube (see Section 2.3.2 of the main text), the  $B-\omega$  method initially analyses individual pixels in the temporal domain. Power spectra from pixels within a specified magnetic field range are then averaged for each bin. This technique, which requires an associated magnetic field data, offers valuable insights into the influence of magnetic fields on oscillatory phenomena. Thus, filtering by magnetic-field strength can help us disentangle how wave behaviour varies in regions with different magnetic environments.

The principle of PFA is broadly applicable across various scientific disciplines. Depending on the field of study, the property used for filtering could be magnetic field strength, temperature, density, velocity, or any other relevant parameter. For instance, in social sciences, one could analyse fluctuations in economic indicators as a function of age or income levels. The adaptability of PFA makes it a powerful tool for unravelling complex oscillatory phenomena and their relationship with other variables of interest.

## S7 EMD and EEMD analyses

Here, we provide detailed results of the application of EMD and EEMD to the synthetic 1D signal (introduced in Section 2.1.1 of the main text) to assess their ability to resolve distinct oscillatory modes and their robustness against noise. Some of these results are discussed in Section 3.1 of the main text, in comparison with other wave analysis techniques (see Figure 3).

As shown in Supplementary Figure S2, EMD extracts eight IMFs (panels a), with their instantaneous frequencies depicted in panels (b), calculated using the Hilbert Transform. This provides insight into the time-varying frequency content of the signal, highlighting how oscillatory modes evolve over time. IMFs 4, 5, and 6 are marked as non-significant based on a statistical significance test (with 1000 randomisation). The corresponding HHT marginal spectrum (panel c) correctly identifies the strongest oscillation at 5 Hz but fails to clearly distinguish other weaker components, potentially due to the presence of noise and mode mixing. The FFT power spectra of the IMFs (panel

d) primarily recover the five base oscillations and, to a lesser extent, the transient and quasi-periodic fluctuations, but are unable to reliably detect the weak signal component present in the original signal. This indicates that the EMD decomposition can affect the frequency information content. Additionally, spurious frequencies, more prominently in the range of 2-4 mHz, are erroneously detected.

It is worth recalling that each IMF may contain more than one frequency simultaneously, and their orthogonality is only locally satisfied<sup>323</sup>. Also, in contrast to, e.g., FFT, the IMFs are not given in a closed analytical form.

Furthermore, we applied EEMD to the synthetic signal. The parameters chosen for EEMD, including a noise standard deviation of 0.2 and 1000 realisations, are critical for balancing noise influence and ensuring computational efficiency. The noise standard deviation is typically selected as a fraction of the signal standard deviation, ensuring the added noise is sufficient to resolve mode mixing without overwhelming the original signal components. The number of realisations is a trade-off between computational cost and the stability of the IMFs. More realisations generally lead to more stable IMFs by averaging out noise effects, but at the expense of increased computation time. Additionally, both EMD and EEMD utilise the same stopping criterion, ensuring that the number of zero-crossings and extrema in each IMF differ at most by one, and that the mean of the envelope is close to zero.

Supplementary Figure S3 illustrates the results of the EEMD analysis. Panels (a) display the extracted IMFs from the synthetic signal, each representing a distinct oscillatory mode. Nine IMFs are obtained, compared to eight with EMD, with IMF 1 marked as non-significant through statistical significance testing. Additionally, IMFs 7, 8, & 9 show very low frequencies likely related to residual spurious trends in the time series, or a slow evolution, so should be interpreted with caution. These characteristics are also evident in the instantaneous frequencies (panels b) and FFT power spectra of the IMFs (panel d).

The HHT marginal spectrum is presented in panel (c). This spectrum offers a comprehensive view of the energy distribution across different frequencies, integrated over time. The HHT spectrum reveals four peaks: one at very low frequencies (likely due to IMFs 7-9, thus ignored), two prominent peaks around 5 & 15 Hz, and one smaller peak at 25 Hz, corresponding to the strongest signals in the constructed time series. However, the HHT marginal spectrum does not recover the other input frequencies, indicating limitations in capturing weak or complex oscillations. Note that the HHT marginal spectrum using EMD (Figure 3g and Supplementary Figure S2c) was able to identify only the strongest signal at 5 Hz (plus the very-low frequency component), a limitation that will be further discussed below. It is worth mentioning that HHT is particularly useful for signals where the frequency content varies significantly over time, such as in biological or geophysical data.

Panel (d) illustrates the power spectra of individual IMFs, estimated using FFT. The power spectra reveal almost all input frequencies, including transient, quasi-periodic, and weak signals. Peaks corresponding to these marginal signals are considerably smaller but still above the 95% confidence level. Interestingly, a few additional frequencies appear: one at very low frequency (peaked at 0.2 Hz; linked to IMF 9 and thus disregarded), and a strong peak at 30 Hz and considerably weaker ones at 7, 10.5, 13, and 20 Hz, likely due to noise. Notably, this analysis includes both significant and non-significant IMFs. Excluding the non-significant IMF, the 30 Hz and weaker peaks disappear, confirming its noise origin, while the 33 Hz weak signal also becomes undetectable, highlighting the sensitivity of significance testing. While FFT provides a clear spectral representation, the Welch method could be employed for power spectral estimation for high noise levels, as it reduces spectral variance by averaging over segments.

Comparing these results to those obtained from traditional EMD underscores the advantages of EEMD, with EMD at its core. While EMD can decompose the signal into IMFs, it is more susceptible to mode mixing, resulting in less distinct components. EEMD's ensemble approach effectively addresses this, yielding more reliable and interpretable IMFs.

The choice of parameters in EEMD, such as noise standard deviation and the number of realisations is crucial for achieving high-quality decomposition. Similarly, the significance test for determining the relevance of IMFs is sensitive to these parameters and fitting functions. Variations in these choices can affect the determination of significant IMFs, potentially influencing the interpretation of the signal's oscillatory components.

In conclusion, EEMD of the synthetic signal demonstrates its efficacy in decomposing complicated, non-trivial signals into meaningful IMFs. Careful selection of parameters and the use of significance testing are paramount to achieving reliable results. These findings not only validate the capabilities of EEMD but also provide a robust

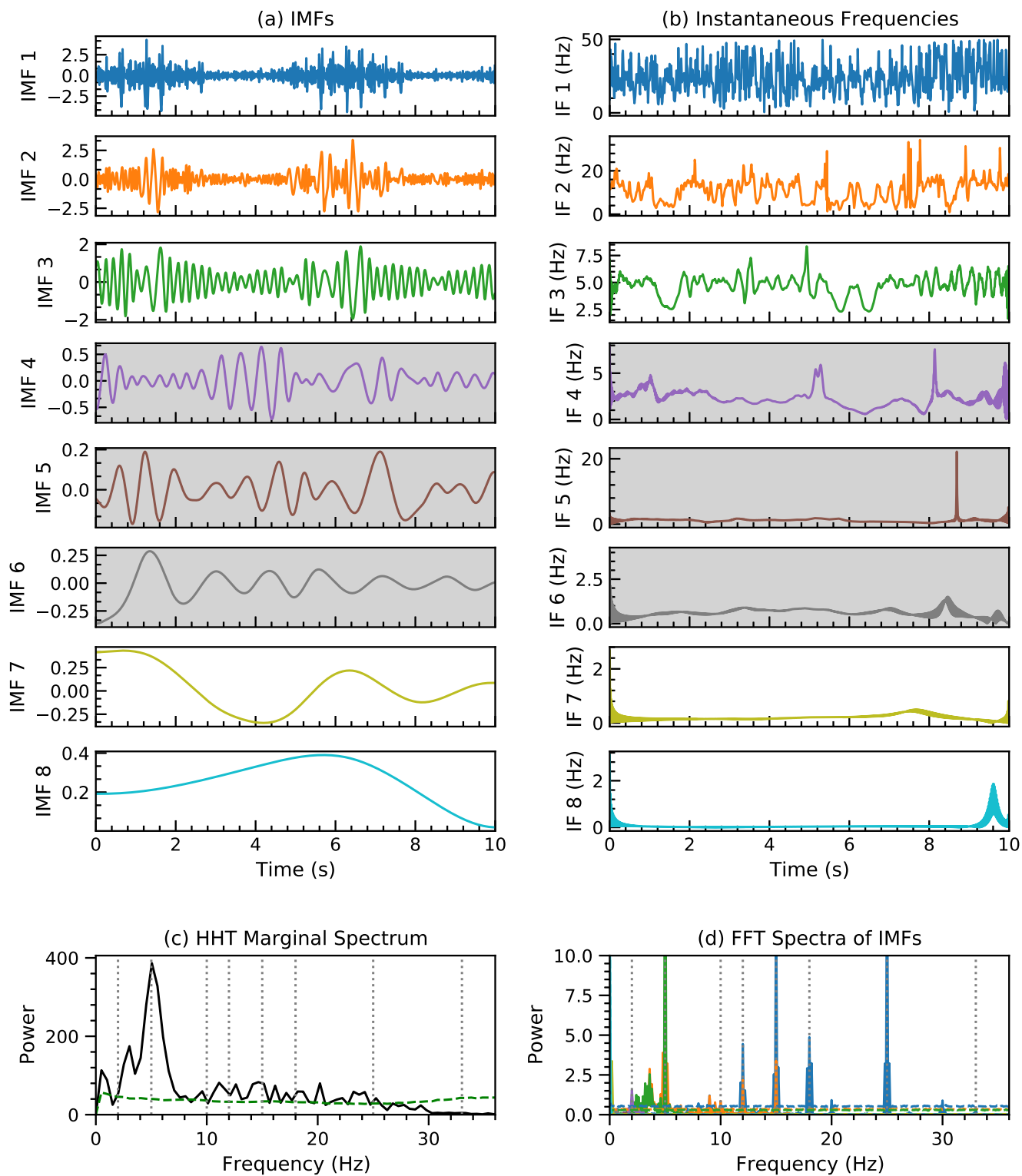


Fig. S2 | **EMD analysis of the synthetic 1D signal.** (a) IMFs extracted from the synthetic signal using EMD. IMFs 4, 5, and 6 are marked with the grey background as non-significant (at 5%) based on a significance test. (b) Instantaneous frequencies of each IMF. (c) HHT marginal spectrum. (d) FFT power spectra of individual IMFs. The dashed lines in both panels (c) and (d) indicate the 95% confidence levels. Note that the powers in panels (c) and (d) are shown in arbitrary units. The dotted vertical lines mark the oscillation frequencies of the synthetic signal.

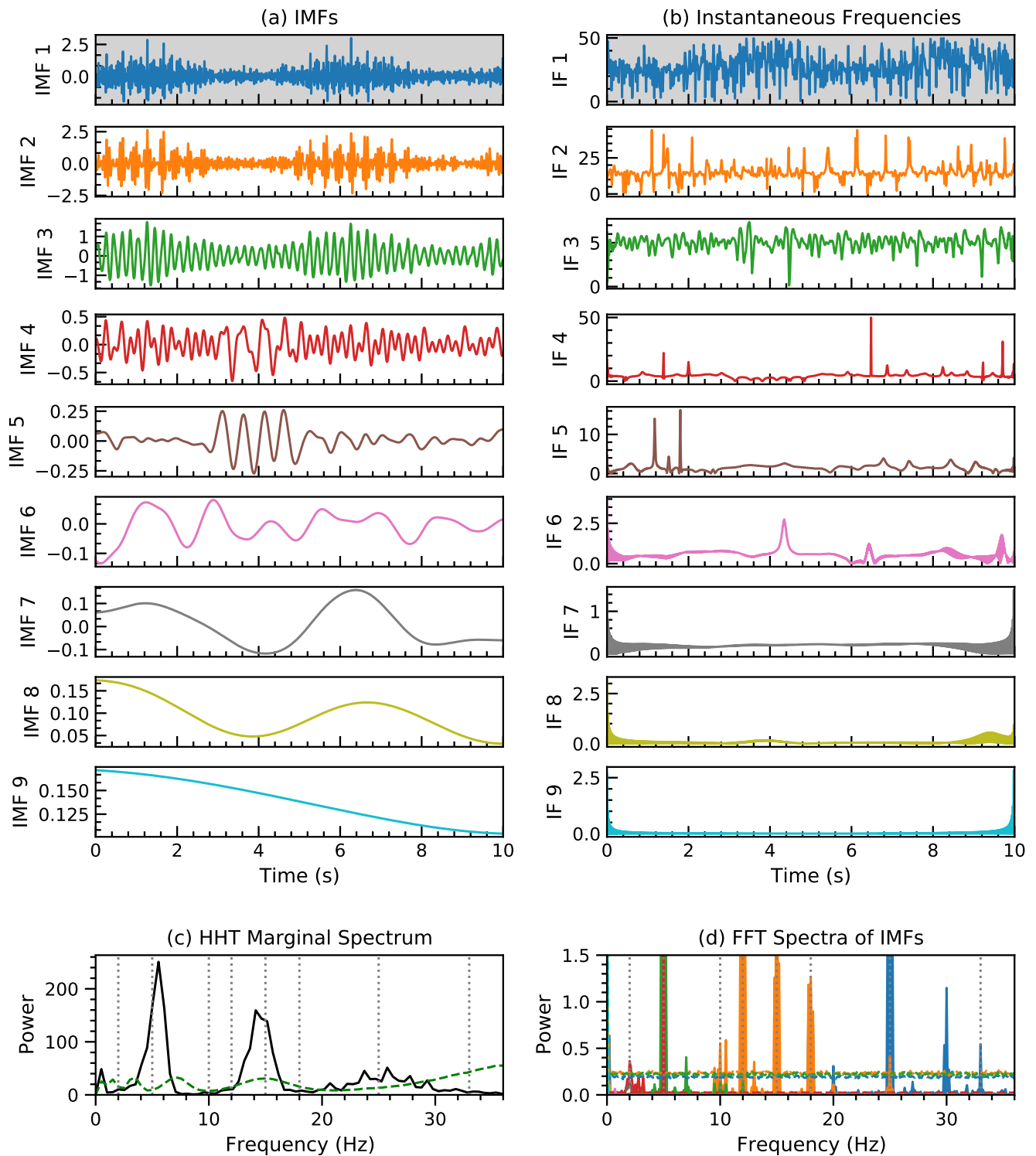


Fig. S3 | **EEMD analysis of the synthetic 1D signal.** (a) IMFs extracted from the synthetic signal using EEMD. IMF 1 is marked with the grey background as non-significant (at 5%), based on a significance test. (b) Instantaneous frequencies of each IMF in Hz, revealing time-varying frequency content. (c) HHT marginal spectrum (solid line) and its 95% confidence level (dashed line). (d) FFT power spectra of individual IMFs, with dashed lines indicating 95% confidence levels. The dotted vertical lines mark the oscillation frequencies of the synthetic signal.

framework for analysing real-world observational data, where similar complexities and noise characteristics are often encountered.

## S8 $k - \omega$ analysis and filtering

Supplementary Figure S4 provides a comprehensive look into the application of  $k - \omega$  techniques on our synthetic spatio-temporal dataset. The foundational  $k - \omega$  power diagram (panel a) maps the oscillatory power distribution, showing all 10 inserted frequencies with strong power, as it was previously demonstrated in Figure 5a. This visualisation is used to select specific regions of interest, allowing for targeted filtering. For instance, the dashed lines in panel (a) demarcated a region of interest chosen for further analysis (i.e., filtering).

Panel (b) reveals the impact of filtering by isolating specific wave features and their evolution over time (obtained by applying an inverse Fourier transform to the filtered data). Panels (c)-(e) further elucidate the filtering process, providing a step-by-step visualisation of the dataset's transformation: (c) the time-averaged spatial power spectrum of the original dataset, revealing the range of spatial scales present, (d) the mask used for spatial filtering, highlighting the selected wavenumber range, and (e) the result of applying the mask to the spatial Fourier transform, isolating the targeted spatial scales.

Finally, panel (f) focuses on the temporal filter by displaying the spatially-averaged temporal power spectrum, with the filter mask over-plotted as a dashed line. The solid red curve of the preserved Fourier power illustrates how specific temporal frequencies are enhanced while others are suppressed. This selective enhancement is vital for isolating and studying signals of interest, although it is important for the research team to ensure that the filters applied do not introduce spurious signals into the reconstructed time series.

Overall, Supplementary Figure S4 goes beyond simply visualising the filtering process. It offers a multi-faceted examination that enables us to derive insights into the waves embedded within the synthetic data. By analysing the filtered results, we can study wave propagation, dispersion properties, and potentially, identifying specific wave modes.

## S9 POD analysis

Here, we present detailed results of POD application to the spatio-temporal datacube. For complex, quasi-non-linear time series of image data, POD reveals spatially coherent patterns and their temporal evolution, ordered by their contribution to the system's variance. However, in cases with competing dynamics of similar amplitudes, POD may struggle to disentangle all temporal behaviours, resulting in higher-order modes containing multiple frequencies. On these occasions it is possible to extend the POD and further reveal spatial structure from datasets.

The POD outputs for the first six modes are presented in Supplementary Figure S5. Temporal coefficients of all spatial modes and their Welch power spectra show the repeatability of the patterns over time. These spatial modes describe dominant, coherent patterns propagating through the spatio-temporal domain. The Welch method balances frequency resolution and statistical reliability through a segment length of 150, a segment overlap of 25, an FFT length of  $2^{14}$  points (i.e., zero padded FFT), and a sampling frequency of 2 Hz.

Supplementary Figure S6 summarises the POD analysis results further. The top-left panel shows the square of singular values (Eigenvalues) of the first ten modes, normalised to the total Eigenvalues and shown in percentages. The power spectrum of these modes (top-middle panel) reveals their dominant frequencies. The strongest 10 peaks of this spectrum align with the base frequencies of the synthetic data, while additional weaker peaks (lying below the 95% confidence level) are likely due to noise. Importantly, these 10 strongest (significant) peaks remain consistent as the number of modes included in the combined power spectrum changes, demonstrating the robustness of POD in identifying dominant frequencies.

The top-right panel of Supplementary Figure S6 shows the total Eigenvalues captured as a function of the number of POD modes included. The blue, green, and red vertical lines mark the cumulative variance captured by the first 2, 10, and 22 modes, respectively, revealing that these subsets account for 84%, 96%, and 99% of the total variance. Notably, even with just the first three modes, POD captures approximately 88% of the total variance, indicating that these modes are sufficient to reconstruct a significant portion of the original signal's energy. Using only these first

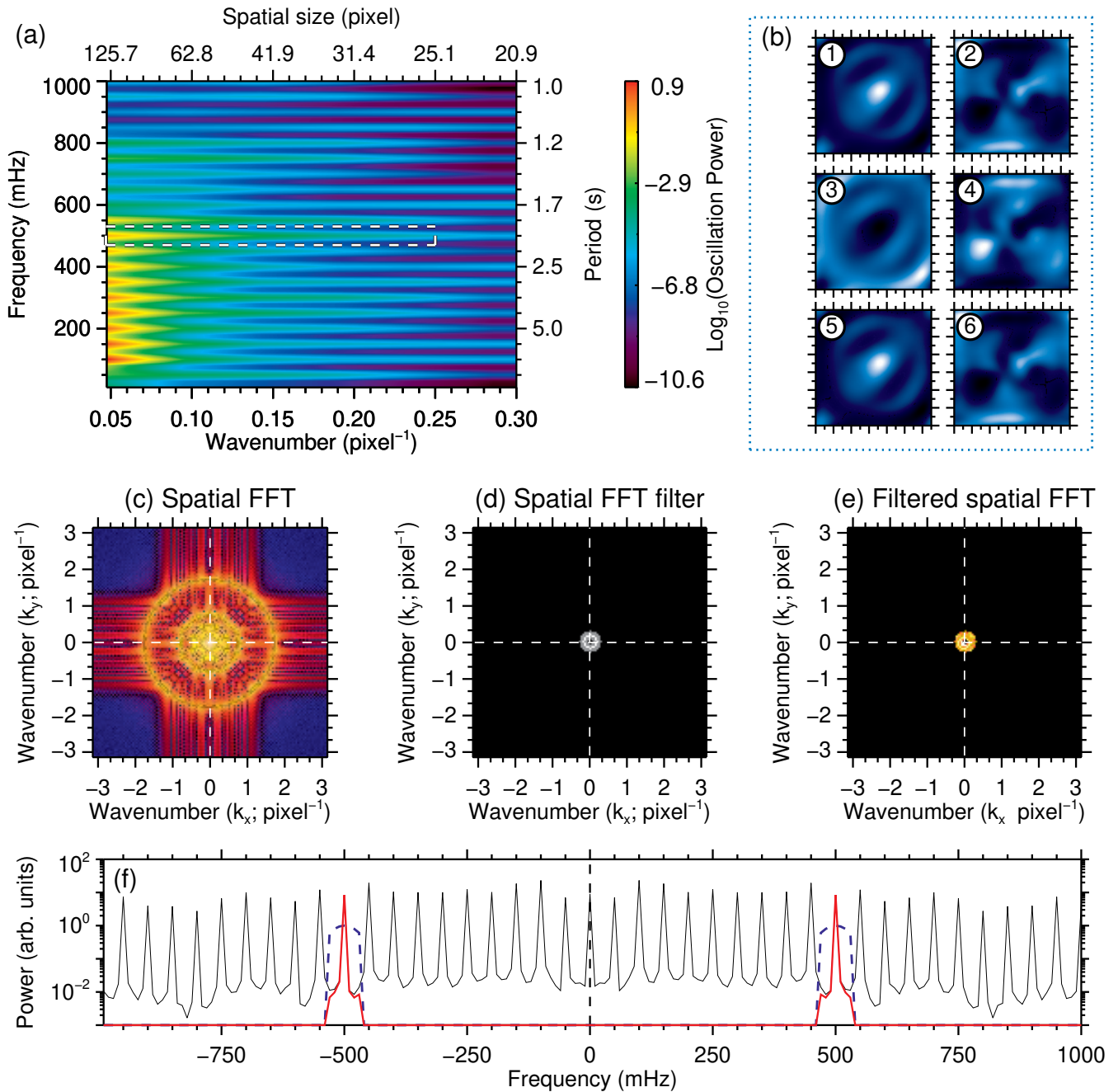


Fig. S4 | **Illustration of  $k-\omega$  analysis and filtering applied to the synthetic spatio-temporal dataset of Figure 2 and Table S2.** Panel (a) displays the  $k-\omega$  power diagram, with the dashed lines outlining the targeted filtering region. Panel (b) presents a six-frame sequence from the filtered datacube, showcasing the spatial and temporal evolution of the isolated wave features. Panels (c)-(e) provide a step-by-step visualisation of the filtering process: first, the time-averaged spatial power spectrum of the original dataset, followed by the spatial filter mask, and finally, the result of applying the mask to the spatial Fourier transform, highlighting the spatial scales preserved in the filtered dataset. Panel (f) shows the spatially-averaged temporal power spectrum. The temporal filter masks are indicated by dashed lines, while the preserved oscillatory power within the filtered data is depicted by the solid red curves.

three modes for reconstruction yields a combined power spectrum free of noise-related peaks. We note that POD results in as many modes as are in the input snapshots (i.e., 200 modes in this example), but not all POD modes

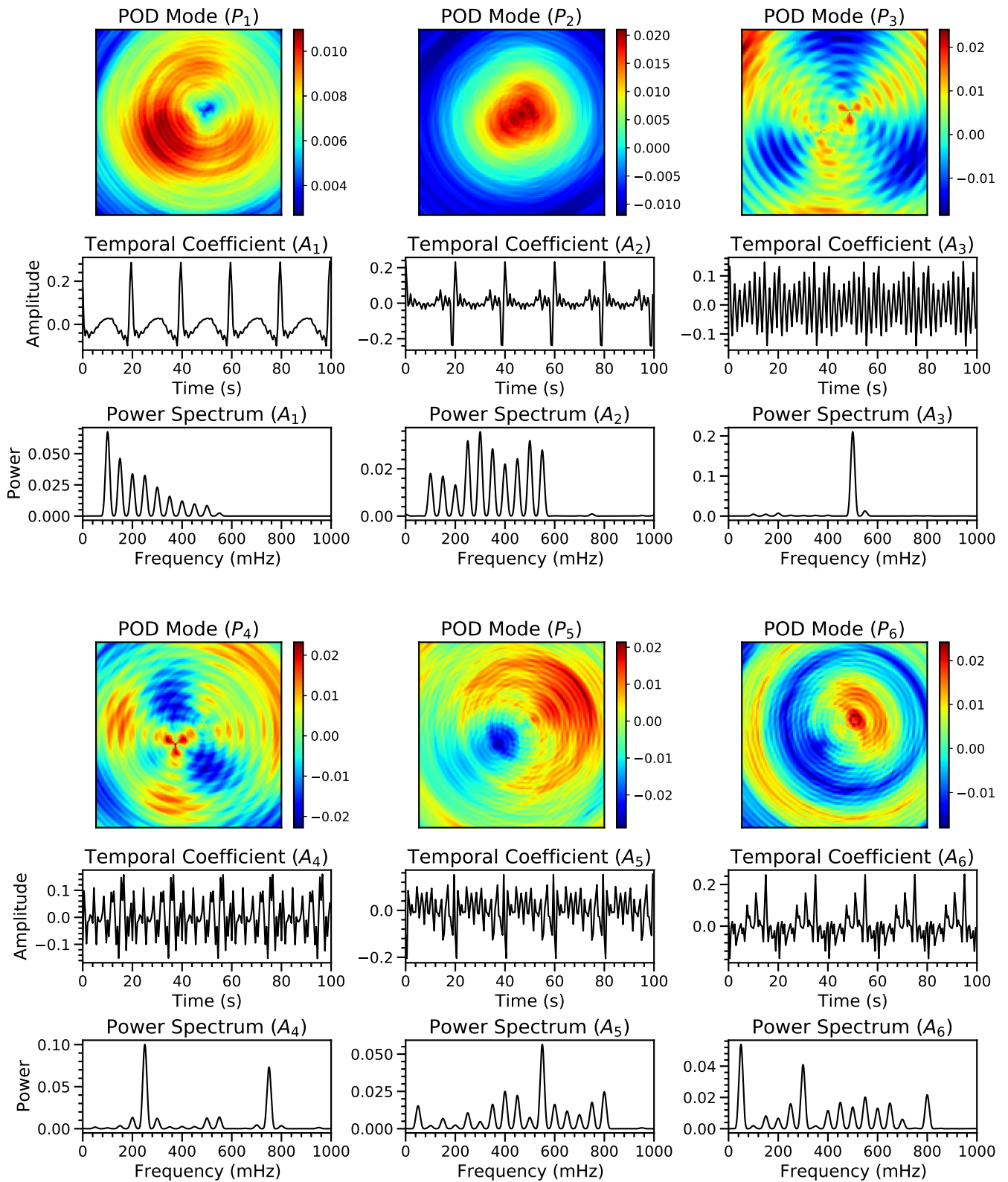


Fig. S5 | **POD analysis results.** The first six spatial modes ( $130 \times 130$  pixels<sup>2</sup> each), along with their temporal modes and Welch power spectra of the temporal coefficients.

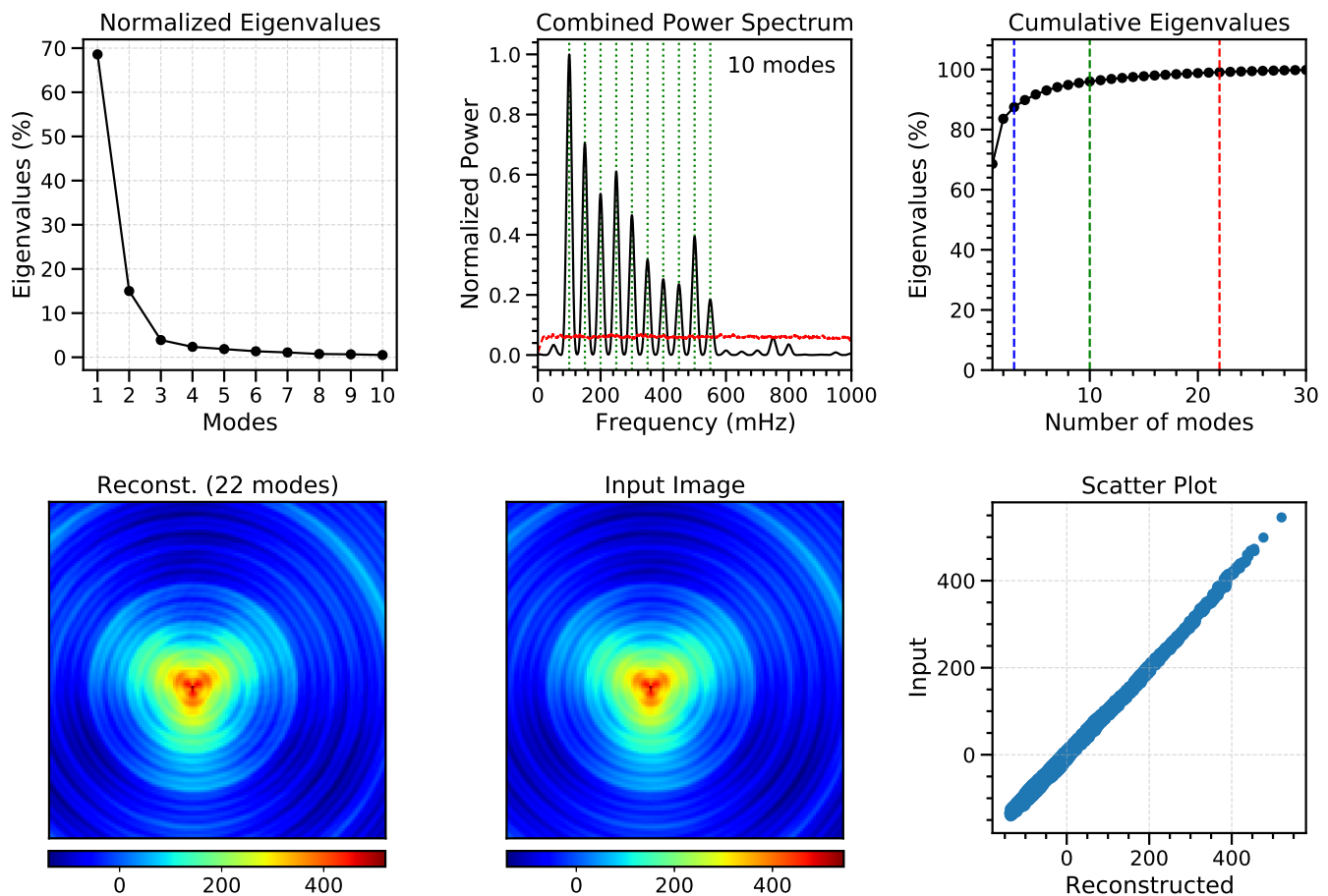


Fig. S6 | **POD mode analysis.** Top left: Normalised squared singular values (Eigenvalues) of the first ten POD modes, demonstrating their relative contributions to the total variance. Top middle: Combined power spectrum of the first ten POD modes, revealing the dominant frequencies captured by these ten modes. The vertical dotted lines mark the ten base frequencies used to construct the synthetic data; the red dashed line identifies the 95% confidence level (estimated from 1000 bootstrap resamples). A movie of this panel showing the combined power spectrum as a result of various numbers of modes included is shown in [Supplementary Video 3](#). Top right: Cumulative explained variance as a function of the number of POD modes included, with vertical lines indicating the cumulative variance captured by 2 (blue), 10 (green), and 22 (red) modes. Bottom left: Reconstructed image ( $130 \times 130$  pixels<sup>2</sup>) of the first frame of the time series using 22 first modes. Bottom middle: Original image ( $130 \times 130$  pixels<sup>2</sup>; first frame) of the datacube. Bottom right: Scatter plot of the reconstructed and original image.

are physically meaningful, as many might be due to noise and spurious signals in the data. Identifying physical modes requires detailed information about the system being analysed. In the worked example we presented here, we reconstruct the original image by adding the first 22 modes (as they capture 99% of the total variance), shown in the bottom-left panel of Supplementary Figure S6, for the first frame of the time series. The original image from the input data, alongside a scatter plot of the reconstructed and original images are also illustrated in the bottom-middle and bottom-right panels of Supplementary Figure S6, respectively, showing a near-perfect match.

While these modes identify all ten base frequencies, their amplitudes may not fully reflect the original input values. This is likely due to the superposition of frequencies propagating into higher-order modes and/or the exclusion of noise-dominated modes. As such, the amplitudes obtained from the combined power spectrum may depend on the number of modes included.

While POD reveals the presence of all base frequencies, it does not visually isolate them individually. To address this, we can algorithmically fit the ten identified dominant frequencies to the temporal coefficients of these modes, creating a representation based solely on pure frequencies. For this study, we use a non-linear least-squares fitting

approach to imposed sinusoids and reconstruct the data using these filtered temporal coefficients and the first 22 modes (capturing 99% of the total variance). This approach creates a set of frequency-filtered spatial modes, where each mode represents the spatial pattern associated with a specific frequency over the entire time series.

Supplementary Figure S7 presents these POD-filtered spatial modes for the ten most dominant frequencies at the first three time steps of the series. This method can be particularly useful in identifying patterns in a signal that are otherwise occluded by other superimposed frequencies. The temporal variation of these spatial modes is available as Supplementary Video 2, providing insights into the dominant dynamical features of the system. It is worth noting that jumps between spatial modes may be observed at frequencies where two or more different wave modes are superimposed. One example of such spatial variation occurs at 500 mHz, where both concentric waves and fluting-like instability were constructed in the synthetic datacube.

Another method for extracting spatial modes associated with specific frequencies, but without capturing temporal variations of the reconstructed data, is to apply the filtering before computing the eigenvalues, known as Spectral POD (SPOD)<sup>324</sup>, as discussed below, in Supplementary Section S10.

## S10 Spectral Proper Orthogonal Decomposition

Spectral POD (SPOD) is an extension of the traditional POD using snapshot method<sup>153</sup>. While both snapshot and SVD approaches yield identical POD results<sup>325</sup> the snapshot method can be better suited for large datasets. To properly introduce SPOD, we first briefly recap the mathematical formulation of the snapshot method.

A dataset  $q(\mathbf{x}, t)$  can be decomposed into a time average and a fluctuation field, with the fluctuation field further decomposed into POD modes:

$$q(\mathbf{x}, t) = \langle q(\mathbf{x}) \rangle + q'(\mathbf{x}, t) = \langle q(\mathbf{x}) \rangle + \sum_{n=1}^N a^{(n)}(t) \phi^{(n)}(\mathbf{x}), \quad (2)$$

where  $\phi^{(n)}$  represents a set of space-dependent orthonormal modes,  $a^{(n)}$  is a time-dependent mode amplitude,  $N$  is the number of snapshots and  $n$  is the mode index. Here  $\langle \rangle$  denotes a time average and the  $( )'$  indicates a fluctuation. A reconstructed fluctuation field can then be approximated by,

$$\tilde{q}'(\mathbf{x}, t) \approx \sum_{n=1}^M a^{(n)}(t) \phi^{(n)}(\mathbf{x}), \quad (3)$$

where  $M$  is the number of modes used in the reconstruction. Using the snapshots method<sup>153</sup>, the modal basis is constructed from a covariance matrix of the fluctuation field:

$$C_{t_1, t_2} = \frac{1}{N} \int_{\Omega} q'(\mathbf{x}, t_1) q'(\mathbf{x}, t_2) d\mathbf{x}. \quad (4)$$

Since this matrix is symmetric, positive, and semi-definite, we can compute its eigenvalues and eigenvectors using SVD. Thus, the POD spatial modes can be computed by a linear combination of the snapshots into an orthonormal set of basis functions:

$$\phi^{(n)}(\mathbf{x}) = \frac{1}{\lambda_n N} \sum_{k=1}^N \xi_{k,n} r'(\mathbf{x}, t_k), \quad (5)$$

where  $\lambda_n$  are the eigenvalues, and  $\xi_{k,n}$  are the eigenvectors of the covariance matrix  $C$ . The term  $k$  corresponds to the  $k$ th column of  $\xi$  in the eigenvalue problem  $C\xi = \lambda\xi$ . Finally, the time-dependent mode amplitude is given by:

$$a^{(n)}(t_k) = \sqrt{N\lambda_n} \xi_{k,n}. \quad (6)$$

SPOD<sup>324</sup> introduces a filtering step to the covariance matrix  $C$  before computing eigenvalue, resulting in a filtered matrix  $S$ :

$$S_{i,j} = \sum_{k=-N_f}^{N_f} g_k C_{i+k, j+k}. \quad (7)$$

where  $g_k$  is a filter kernel<sup>161,324</sup> (here we employ a Gaussian filter kernel<sup>161</sup>). The filtering limits the frequencies per mode, where the SPOD filter allows for a continuous fading from the energetic optimality of POD to the spectral purity of DFT<sup>324</sup>.

To summarise the entire process, it begins by computing the fluctuation field, obtained by subtracting the time average from each snapshot of the data. This fluctuation field is crucial for constructing the correlation matrix using the snapshot method, capturing relationships between different time snapshots.

To implement SPOD, a periodic boundary condition is applied to the correlation matrix to account for the periodic nature of the data. This correlation matrix is then filtered using a Gaussian function to create the spectral matrix, which is subsequently decomposed into eigenvalues and eigenvectors via SVD.

Examination of the resulting spatial and temporal modes, along with their power spectra (Figure S5, illustrating the first six SPOD modes; see [Supplementary Video 4](#) for all SPOD modes), reveals that the modes often form pairs with the same frequency. For instance, modes (1, 2), (3, 4), (5, 6), and so on, exhibit similar frequencies and spatial structures, a characteristic feature of the SPOD method. However, where two dominant waves coexist at the same frequency, the pair modes display distinct structures, revealing the two underlying wave modes. Examples include the sinusoidal wave and fluting-like instability at 500 mHz, and the concurrent sinusoidal and transverse waves at 250 mHz. This correlation is confirmed by analysing the temporal coefficients in phase space<sup>161</sup>. In such cases, analysing the corresponding mode pair together is crucial for a complete understanding of the waves.

Analysis of all SPOD modes (see [Supplementary Video 4](#)) reveals that the first twenty modes represent the ten base frequencies used to construct the synthetic signal, effectively capturing the primary features of the data. Beyond the 20th mode, the power drops significantly, suggesting that the remaining modes likely represent noise and spurious signals. This drop-off underscores SPOD's effectiveness in isolating important frequencies and filtering out less relevant information.

## S11 Shock analysis: capturing abrupt changes

Shocks, characterised by sudden, often discontinuous changes in physical properties of a system (e.g. pressure, density, temperature)<sup>326</sup> can arise from the steepening of non-linear waves, collisions, explosions, or other dynamic processes<sup>327</sup>. These abrupt transitions present challenges in wave analysis due to their distinct characteristics. Shocks are inherently non-stationary events, introducing rapid changes in a signal's properties over time. The sharp transitions at the shock front also pose challenges for techniques designed for smooth, continuous signals. Furthermore, shocks often contain significant high-frequency energy, requiring methods with sufficient time resolution to capture the details of the shock front. Several techniques are particularly well-suited for analysing shocks, including:

- Wavelet transforms: The time-frequency localisation of wavelets can allow the identification of both the time and spatial location of shock arrivals, in addition to the analysis of the evolution of their frequency content.
- HHT: The adaptive decomposition of HHT can isolate shock signatures within a signal and track their evolution through instantaneous frequency analysis.
- Time-domain methods: Techniques like the shock-fitting method, which focuses on the shape of the shock front, can be used to directly estimate shock parameters (e.g., speed, strength)<sup>328</sup>.

The results of shock analysis can provide valuable insights into the shock location and timing, pinpointing the arrival time of a shock front and its spatial position in multi-dimensional data. They can also estimate the shock's strength and speed, as well as analyse how the shock's properties (e.g., frequency content) change as it propagates. Additionally, shock analysis can help understand how energy is released and transferred during the shock process.

## S12 Specialised toolboxes for wave analysis

While this Primer has focused on a core set of fundamental wave analysis methods, a wealth of specialised toolboxes and packages are available to researchers, often offering optimised implementations, advanced features, or tailored

functionalities for specific applications. All analyses presented in this Primer were performed using the WaLSAtools repository (see Section 5 of the Primer). This section provides a brief overview of some additional toolboxes and packages, highlighting their potential value in complementing the techniques discussed in this Primer.

Table S3 lists a selection of toolboxes and packages relevant to wave analysis. These resources offer a wide range of functionalities, from optimised implementations of fundamental techniques to specialised methods for analysing specific signals.

Table S3 | **Overview of specialised toolboxes and packages for wave analysis.**

Toolbox	Description/Language	Key Features/Applications
FFTW <sup>329,330</sup>	Fastest Fourier Transform in the West. Highly optimised FFT library for various platforms. (C, Fortran)	Widely used in scientific computing and signal processing. Provides high-performance FFT routines. URL: <a href="https://www.fftw.org">https://www.fftw.org</a>
SigPack	Signal Processing toolbox. A collection of signal processing tools, using the Armadillo library <sup>331</sup> as a base (C++)	Implement fundamental signal processing algorithms. URL: <a href="https://sigpack.sourceforge.net">https://sigpack.sourceforge.net</a>
INSITE <sup>332,333</sup>	Software toolkit for studying non-linear dynamical and chaotic systems.	Includes algorithms for, e.g., periodic solutions, dimension estimation, and Lyapunov exponents.
TISEAN <sup>334</sup>	Non-linear time series analysis package. (Fortran, C)	Offers a wide range of algorithms for analysing non-linear and chaotic systems. URL: <a href="https://www.pks.mpg.de/tisean">https://www.pks.mpg.de/tisean</a>
TFTB	Time-Frequency Toolbox. Wide range of time-frequency analysis techniques. (GNU Octave, MATLAB, R; also in Python)	Developed for the analysing non-stationary signals using time-frequency distributions. URL: <a href="https://tftb.nongnu.org">https://tftb.nongnu.org</a>
SSA-MTM Toolkit <sup>335</sup>	Singular Spectrum Analysis - Multi-Taper Method Toolkit for analysing short, noisy time series, and multivariate data. (Fortran)	Offers tools for noise reduction, trend extraction, and spectral analysis. URL: <a href="https://research.atmos.ucla.edu/tcd/ssa/">https://research.atmos.ucla.edu/tcd/ssa/</a>
Rssa <sup>336</sup>	R package for SSA. Implements Singular Spectrum Analysis (SSA) for time series decomposition and forecasting. (R)	A collection of methods for singular spectrum analysis. URL: <a href="https://github.com/asl/rssa">https://github.com/asl/rssa</a>
Obspy <sup>337,338</sup>	Python toolbox for seismology. Primarily used for processing seismological data, but includes many general-purpose signal processing tools. (Python)	Contains FFT, wavelet transform, and spectral analysis methods. URL: <a href="https://docs.obspy.org">https://docs.obspy.org</a>
LTFAT <sup>339,340</sup>	The Large Time-Frequency Analysis Toolbox. A modern library for time-frequency analysis, including Gabor and wavelet transforms. (MATLAB, Octave)	Offers high-resolution time-frequency representations. Useful in, e.g., audio signal processing and biomedical applications. URL: <a href="https://ltfat.org">https://ltfat.org</a>
Biosppy <sup>341</sup>	Bio-signal processing library. Focused on analysis of bio-signals such as EEG and ECG, including filtering and clustering. (Python)	Includes wavelet and Fourier analysis, spectral analysis, and feature extraction tools. URL: <a href="https://biosppy.readthedocs.io">https://biosppy.readthedocs.io</a>

It is important to note that this table is by no means comprehensive and represents only a small fraction of the available online resources. Many other specialised toolboxes and packages, such as TFSA<sup>342,343</sup>, have also been

developed for specific scientific domains or analysis tasks. Researchers are encouraged to explore these tools and consider their suitability for their specific needs and research questions. However, it is crucial to critically evaluate any toolbox or package before applying it to research data. This includes carefully examining the references and documentation, understanding the underlying assumptions and limitations of the implemented methods, and validating the code's performance against known benchmarks or synthetic datasets.

**Important Disclaimer:** The inclusion of a toolbox or package in this list (including their URLs) does not imply endorsement or guarantee its accuracy or reliability. Researchers are responsible for conducting their own careful checks and validation before utilising any of these tools in their research.

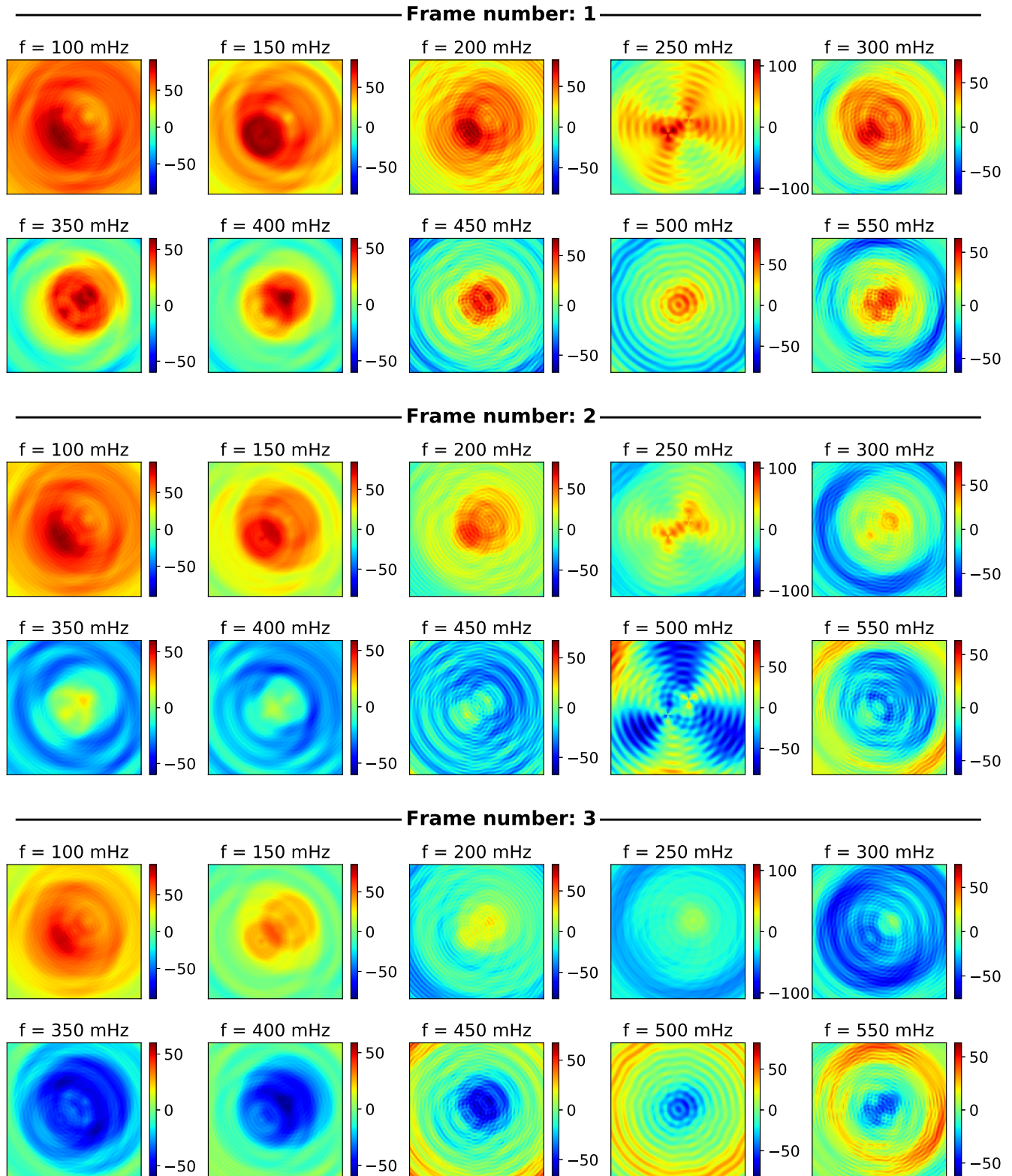


Fig. S7 | **Frequency-filtered spatial modes for the ten dominant frequencies.** The spatial patterns associated with each frequency are shown for the first three time steps of the series, with each image covering  $130 \times 130$  pixels<sup>2</sup>. A movie of the time series, showing the temporal evolution of each frequency-filtered mode, is shown in [Supplementary Video 2](#).

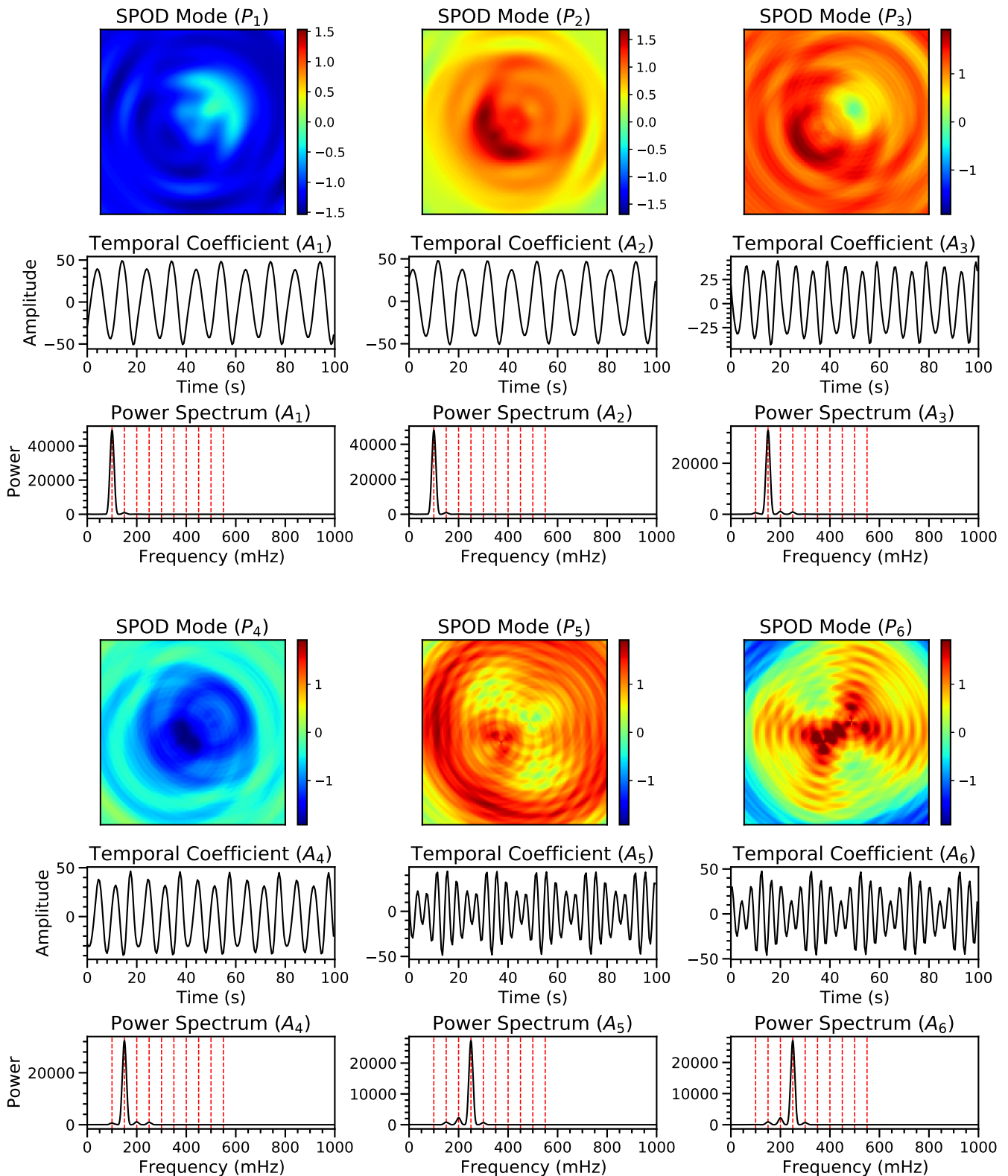


Fig. S8 | **SPOD analysis.** Spatial modes ( $130 \times 130$  pixels<sup>2</sup> each), temporal coefficients, and Welch power spectra of the first six SPOD modes. The SPOD analysis was performed with a Gaussian filter kernel, illustrating the frequency pairing phenomenon, where each frequency is associated with two distinct spatial modes with corresponding temporal coefficients. The shared frequency content is evident in the Welch power spectra. The ten base frequencies are marked with vertical dashed lines. A movie of all 200 SPOD modes is available as [Supplementary Video 4](#).